ENERGY TRAPPED RESONANCES IN SOLID STRUCTURES

by

PETER JOHN KALMARCZIE

Submitted for the Degree of Doctor of Philosophy

at

The University of Aston in Birmingham

October 1976

SUMMARY

The end resonant modes of vibration in solid and hollow cylinders, strips and plates are considered. Experimental results presented for solid cylinders, made of various materials, establish not only the position of cylindrical end modes, within the frequency spectrum, but also their dependance upon Poisson's Ratio. Additional experimental results, obtained for hollow cylinders of various wall thicknesses, indicate how the antisymmetric end resonant modes of solid cylinders are influenced by the presence of a concentric hole.

Numerical solutions have been found, for the end resonant modes in plates and strips, by the method of summation of stresses associated with real and complex modes of propagation. In all, results have been obtained for eleven different values of Poisson's Ratio in the range 0.1 to 0.5. The modulus and phase of the amplitude coefficients for real and complex modes are presented in graphical form.

A general method of obtaining expressions for the impedance of mechanical resonators is discussed. The technique, based on the principal of virtual work, makes use of normal mode expansions. Three examples are considered in detail, with special attention being given to the application, of the obtained impedance expressions, to an existing acoustic transmission line theory, as a means of analysing the echo technique used for the experimental work.

An empirical equation is derived, which enables the

calculation of the natural frequencies of a pair of dynamically clamped rectangular plates to be carried out. The equation, obtained by comparing experimental results with theoretical solutions for the corresponding statically clamped plate, relates the resonant frequency to plate dimensions and the known frequency factors for the static case.

ACKNOWLEDGMENTS

The author wishes to express his gratitude to his supervisor, Dr. J. F. W. Bell for his guidance and encouragement during this study, his appreciation to Mr. A. E. Sutton, of the University Mathematics Department, and Mr. R. W. Davey of the Electrical Engineering Department, for their helpful comments, and his thanks to Dr. J. Zemanek Jr., for permission to reproduce figures from his paper (reference 9), and Professor J. E. Flood, Head of Electrical Engineering Department in which the work was carried out.

Acknowledgment is also due to the Science Research Council for the studentship provided.

CONTENTS

CHAPTER 1

GENERAL INTRODUCTION

The contents of this thesis can be divided into two principal subjects, trapped or end resonances of structures and experimental investigations of the resonant vibrations of dynamically clamped plates. For many years the resonant behaviour of structures has attracted a great deal of attention. As far back as 1789 mathematicians were making attempts to secure theoretical explanations for the experimental results obtained by Chladni, regarding the nodal patterns of vibrating plates. The topic has since gained momentum and with the increasing maturity of the industrial age it has reached great importance in the area of design. Problems associated with vibrations have become more dominant as the size and velocity of devices have increased and therefore the demand for information, experimental and theoretical has expanded accordingly.

Another area which has precipitated the desire to obtain more information about vibrating bodies is that of measurements. More and more frequently, mechanical resonators are being applied to the field of measurements, either as a means of measuring the properties of the resonator or the change in these properties created by environment.

The subject of end resonances has received only a modest proportion of the attention and effort given to

this topic. There are two major reasons for this. Firstly the phenomenon does not appear to have been observed until as late as 1957. Secondly, an adequate means of exciting and identifying such modes of vibration was not readily available. The later problem has been overcome by the use of acoustic transmission lines to transport energy to and from the resonator. This is the method used to obtain the results of this thesis. The line forms part of an echo system which operates on the principle of sending a burst of stress waves, via the line, to the resonator and observing the character of the returning echo. Resonance of the resonator is well defined because of the shape of echo it produces. Identification of the modes is achieved by the use of a second line, which is placed in contact with the vibrating body at various points. Displacement of the body produces stress waves in the line. These are ultimately processed by a receiver which gives information about the amplitude and phase of the displacement at different points on the body. Therefore a picture can be built up of the nodal pattern of the mode vibration. A discussion of the echo technique used is given in chapter three.

End resonance, as the name suggests, is a natural mode of vibration, that a structure possesses, where all the motion is confined to one or both of its ends. For example, a finite solid cylinder can be made to resonate at one end only, most of the displacement taking place within the first one or two diameters of

length. The structures considered are solid and hollow cylinders, rectangular bars and strips. All have been found to have similar characteristics and parallels can be drawn between these modes of vibration and those of other structures such as discs and rings. An exact theory for end resonances is not known and therefore related discussions are usually kept within the framework of the general analysis of wave propagation in extended bodies.

The analysis of stress wave propagation through extended isotropic solids takes account of the existance of two types of wave, waves of dilatation and distortion. They travel with velocities having different dependances on the elastic properties of the medium. In general neither wave can exist by itself, if any part of a boundary is free of stress, for on arrival at a boundary a wave of either type will result in the reflection of both types of wave.

These features are responsible for the inherent complexities associated with the theory of vibrations of many systems, particularly those of end resonances.

In addition to the dilatational and distortional waves, propagation on the surface of a solid may also take place. These surface waves decay exponentially with depth and, of all three types of wave, have the lowest velocity of propagation. Waves of this type were first investigated by Lord Rayleigh and are closely related to seismology. It was observed that an earthquake consisted of three tremors, two early rather

minor disturbances corresponding to the arrivals of dilatational and distortional waves, followed by a tremor of much greater magnitude capable of creating significant damage. This it was considered suggested that the insignificance of the early tremors was a result of their energy being dissipated in the interior of the earth; therefore the third tremor must be produced by a wave whose energy dispersion was less rapid. This could only be accounted for by assuming that the disturbance took place mainly on the surface. It has since been found that waves of this type can propagate on the surface of most solids.

The phenomenon of end resonance exhibits a character which is very similar in nature to that of surface waves. However it is also true to say that it could be described equally as well by modes that propagate into the body with complex propagation constants. Modes of this type have been indicated by complex solutions to the classical frequency equations, and have been used with good effect to locate the frequency of an end resonant mode of solid cylinders. A discussion of complex propagation is given in chapter two.

The concept of dynamic clamping, considered in chapter seven is predominantly associated with the theory of flexural vibrations of plates. Two plates, joined together, are used to obtain the required clamping effect. The whole system is constructed in such a way that the net

momentum, of the two vibrating plates, is zero. Typical of dynamic clamping is the tuning fork which can be regarded as two plates vibrating in anti-phase. The effect of two plates vibrating in anti-phase at the end of a bar, as in the case of a tuning fork, is the induction of a propagating mode in the bar. If the frequency of vibration is below the cut-off frequency of the propagating mode, propagation can only take place with a complex or imaginary propagation constant. This has the effect of increasing the effective length of the vibrating plates. Comparison with results obtained from the classical theory for clamped vibrating plates gives support to this argument.

CHAPTER 2

PROPAGATION OF ELASTIC WAVES IN SOLID CYLINDERS

CHAPTER 2

PROPAGATION OF WAVES IN SOLID CYLINDERS

2.1 Introduction

It is essential to the understanding of end resonances, where propagation may be of a complex nature, that the mechanism of propagation in solids is understood. The contents of this chapter forms a necessary part of that understanding.

Exact theories exist for the propagation of waves in both infinite plates and infinite cylinders and, because of their similarities in terminology and dispersion curves, a discussion on either would suffice. A majority of the experimental work of this thesis was however carried out on cylinders, and because the echo technique used is based on the propagation of waves in cylindrical wires the contents of this chapter is confined to the later of these theories.

The motion of elastic waves in infinite cylindrical rods can be described exactly by the equations developed by both Pochhammer (1) and Chree (2). By satisfying the boundary conditions, of zero stress, on the curved surface both authors arrived at a frequency equation which, at that time, would have appeared somewhat formidable. In fact, even though this work was executed in the second half of the 1800's very little advancement was made until the middle part of this century. Bancroft (3) (1941) is attributed as being

the first to make a detailed exploration of this frequency equation, confining his area of interest to the lowest axisymmetric mode.

A year later Hudson (4) carried out a similar examination presenting dispersion curves for the lowest symmetric and antisymmetric modes, illustrating their behaviour at high frequencies. These results consolidated the conclusion by Bancroft that as the wavelength of the vibrations became smaller their phase velocity approach the velocity of Rayleigh surface waves. While being aware of the existance of higher modes neither author undertook a study of their character.

The 1950's saw an increased interest in the higher modes. This was probably stimulated by the availability of high speed computers. Holden (5) (1951) studied the spectrum of phase velocities of rods, but only considered modes with real propagation constants. Onoe (6) extended this in 1955 by obtaining solutions with imaginary propagation constants. It would appear that this was simultaneously achieved by Adem (7), who also found an infinity of roots of a complex nature.

A comprehensive study of the frequency spectrum, with illustrations of the dispersion curves for the axisymmetric modes has been given by Onoe, McNiven and Mindlin (8) (1962). More recently (1972) results published by Zemanek (9) include the antisymmetric modes in addition to the ones showing axial symmetry.

A great deal of effort has been directed to the

study of wave propagation in cylindrical rods and a great deal of accompanying literature published; some of these are given in references (10) to (20).

2.2 Elastic Constant, and Velocity Relationships

The study of the elastic properties of solids can be divided into two main categories. Firstly, if the deformations of the body are small the stress will be linearly related to the strain; under these conditions the body is said to obey Hooke's law. Secondly, if the deformations are increased elastic relationships still exist but cease to be linear, and therefore we have a region of nonlinear elastic deformation. Beyond this, elastic relationships no longer apply and the body undergoes plastic deformation.

In the discussions that follow the strains are considered to be small and therefore Hook's law is applied.

Generalizing, Hooke's law may be written as

$$\sigma_{ij} = C_{ijk\ell} \quad \varepsilon_{k\ell} \qquad 2.1$$

in cylindircal co-ordinates $i,j,k,\ell = r,\theta, z$. The coefficients C_{abcd} are the elastic constants of the material and since 2.1 represents nine equations with nine terms in each there will be 81 coefficients in all. However, $\sigma_{ij} = \sigma_{ji}$ which leads to the conclusion $C_{ijk\ell} = C_{jik\ell}$ and therefore only 36 remain. Love (p99) has shown that $C_{ijk\ell} = C_{ij\ell k}$; consequently the number of

independent constants is reduced to 21. Because of these conditions four subscripts are no longer required to describe the stress-strain relationships and so 2.1 may be rewritten as

$$\sigma_n = C_{nm}\,\varepsilon_m \qquad 2.2$$

$$n,m = 1,\ 2,\ 3,\ 4,\ 5,\ 6$$

The number of elastic constants required to describe a material will depend upon its axis of symmetry. In the case of materials which are isotropic in nature, and symmetry exists around any axis, the number of independent constants required is two. Love has shown this to be so by considering the strain energy function to be invarient to changes in co-ordinate axis. It is usual in the case of isotropic materials to use Lamé's constants (μ ,λ), these are related thus

$$\begin{aligned} C_{11} &= C_{22} = C_{33} = \lambda + 2\mu \\ C_{44} &= C_{55} = C_{66} = \mu \\ C_{12} &= C_{13} = C_{23} = \lambda \end{aligned} \qquad 2.3$$

All other terms in C_{nm} being equal to zero. Therefore for an isotropic solid equations 2.2 are

$$\begin{vmatrix} \sigma_1 \\ \sigma_2 \\ \sigma_3 \\ \sigma_4 \\ \sigma_5 \\ \sigma_6 \end{vmatrix} = \begin{vmatrix} \lambda+2\mu & \lambda & \lambda & 0 & 0 & 0 \\ \lambda & \lambda+2\mu & \lambda & 0 & 0 & 0 \\ \lambda & \lambda & \lambda+2\mu & 0 & 0 & 0 \\ 0 & 0 & 0 & \mu & 0 & 0 \\ 0 & 0 & 0 & 0 & \mu & 0 \\ 0 & 0 & 0 & 0 & 0 & \mu \end{vmatrix} X \begin{vmatrix} \varepsilon_1 \\ \varepsilon_2 \\ \varepsilon_3 \\ \varepsilon_4 \\ \varepsilon_5 \\ \varepsilon_6 \end{vmatrix} \qquad 2.4$$

It is sometimes found more desirable to use the constants Young's modulus 'E' and Poisson's ratio 'σ' , the relationship between these and Lamé's constants are obtained as follows. By definition $E = \sigma_1/\varepsilon_1$ with stresses σ_2 and σ_3 equal to zero. Therefore by solving the first three equations of 2.4 simultaneously one obtains

$$E = \mu(3\lambda + 2\mu)/(\lambda + \mu) \qquad 2.5$$

and similarly for $\sigma = -\varepsilon_2/\varepsilon_1$ we have

$$\sigma = \lambda/2(\lambda + \mu) \qquad 2.6$$

Solving equations 2.5 and 2.6 for λ and μ gives

$$\mu = E/2(1 + \sigma) \qquad 2.7$$

and

$$\lambda = \sigma E/(1 + \sigma)(1 - 2\sigma) \qquad 2.8$$

The above relationships hold for any extended isotropic medium.

In the case of thin plates, where the assumption of zero stress and strain normal to the plane of the plate is made, a different set of relationships apply. Following the same procedure as before we have

$$E = 4\mu(\mu + \lambda)/(\lambda + 2\mu) \qquad 2.9$$

and

$$\sigma = \lambda/(\lambda + 2\mu) \qquad 2.10$$

In terms of λ and μ

$$\mu = E/2(1 + \sigma) \qquad \text{as before} \qquad 2.11$$

and

$$\lambda = \sigma E/(1 - \sigma^2) \qquad 2.12$$

As already stated there are two basic types of wave, dilatational and distortional, that can propagate in elastic media, each being characterised by a specific velocity. If the medium is of infinite extent each wave may exist independently. In the practical case however where the body has finite dimensions these waves are usually coupled. The relationship between these velocities and the elastic constants are fixed and may be written down directly as:-

$$\begin{aligned} &\text{dilatational velocity} \quad c^2_d = (\lambda + 2\mu)/\rho \\ &\text{distortional velocity} = \quad c^2_s = \mu/\rho \end{aligned} \qquad 2.13$$

From equations 2.7 and 2.11 it can be seen that the distortional velocity is the same for a two dimensional as for a three dimensional system, namely,

$$c^2_s = E/2\rho(1 + \sigma) \qquad 2.14$$

This is not so for the dilatational wave as can be observed from the relationships of equations 2.8 and 2.12 and therefore we have for unbounded media

$$c^2_d = E(1 - \sigma)/\rho(1 + \sigma)(1 - 2\sigma) \qquad 2.15$$

and for plates

$$C^2_{dp} = E/\rho(1 - \sigma^2) \qquad 2.16$$

It is usual to drop the 'd' subscript from equation 2.16 and refer to this velocity as the plate velocity C_p.

These relationships will be valid for any linearly elastic media, that is, for any body which obeys Hook's law. However this law has no mechanism which allows for energy losses due to internal friction, and as such does not truly represent the physical situation. For a great number of solids the internal energy losses are so small that for many purposes it can be assumed that they obey the elastic rules.

If the foregoing equations are adjusted so that losses due to internal friction are represented the stress-strain relationship is said to be visco-elastic. Due to the structural complexities of internal friction an exact theory is difficult to obtain and consequently numerous models have been presented in am attempt to describe the nature of this damping. Detailed accounts of this topic can be found in Kolsky (21) Campbell and Sherwood (22).

One way of treating internal friction is by assuming that the damping stress is proportional to the rate of change of strain, this can be incorporated in equation 2.2 thus.

$$\sigma_n = C_{nm}\,\varepsilon_m + \eta_{nm}\,\frac{\partial \varepsilon_m}{\partial t} \qquad 2.17$$

A medium displaying this relationship is referred to as a Voigt solid. Voigt (23) being one of the originators of the model. If the body performs sinusoidal vibrations $\frac{\partial}{\partial t}$ may be replaced by $j\omega$. Therefore we have

$$\sigma_n = C^*_{nm}\, \varepsilon_m \qquad 2.18$$

where C^*_{nm} is complex and given by

$$C^*_{nm} = C_{nm} + j\omega\, \eta_{nm} \qquad 2.19$$

It may be noted that in this situation the stress and strain are not in phase, and that the magnitude of this phase shift is dependent upon both the loss constant η and the frequency ω.

2.3 Equations of Motion

The vector differential equation of motion for small deformations in elastic media can be written as

$$(\lambda + 2\mu)\nabla\Delta - 2\mu\nabla \times \bar{\omega} = \rho\ddot{\bar{u}} \qquad 2.20$$

Equation 2.20 gives some indication of the influence of dilatation and distortion, as represented by the terms containing $C^2_d\Delta$ and $C^2_s\bar{\omega}$ respectively, Where Δ is the dilatation and $\bar{\omega}$ is the rotational vector. A solution of this equation was obtained by Pochhammer and Chree, a discussion of which can be found in Love. The method used, by these authors, was to obtain four Bessels equations from 2.20 in favour of the dilatation and

three rotational components. Relationships for the displacements were then obtained by simultaneously satisfying the solutions of the Bessels equations. A more elegant means of acquiring a solution is to describe the displacement vector in terms of potential functions. The resolution of a vector field in this way is part of a theorem by Helmholtz (see Morse and Feshback (25) p.52). Writing the displacement in this manner gives

$$\bar{u} = \nabla\phi + \nabla \times \bar{H}, \quad \nabla.\bar{H} = 0 \qquad 2.21$$

where ϕ and $\bar{H}$ are scalar and vector potentials. It can be shown (Appendix A.2.3) that 2.21 is a solution of 2.20 if ϕ and $\bar{H}$ are solutions of the equations

$$c_d^2 \nabla^2\phi = \frac{\partial^2\phi}{\partial t^2} \qquad 2.22$$

$$c_s^2 \nabla^2 \bar{H} = \frac{\partial^2\bar{H}}{\partial t^2} \qquad 2.23$$

Inserting the solutions of 2.22 and 2.23 into 2.21 gives the required displacement vector, the three components being of the form

$$\begin{aligned} u_r &= U(r)\ \text{Cos}\ n\theta \exp j(\gamma z - \omega t) \\ u_\theta &= V(r)\ \text{Sin}\ n\theta \exp j(\gamma z - \omega t) \\ u_z &= W(r)\ \text{Cos}\ n\theta \exp j(\gamma z - \omega t) \end{aligned} \qquad 2.24$$

where t is the time dimension, γ is the propagation constant for the z direction, ω is the angular frequency and n the number of wavelengths in the θ direction, which may be equal to zero or an integer. The accompanying

functions of r are,

$$U(r) = A\,J_n'(hr) + \gamma B\,J_n'(kr)/k + nC\,J_n(kr)/r$$

$$V(r) = nA\,J_n(hr)/r - \gamma Bn\,J_n(kr)/kr - C\,J_n'(kr) \qquad 2.25$$

$$W(r) = j\gamma\,A\,J_n(hr) - j\,Bk\,J_n(kr)$$

where $J_n'(xr) = \frac{\partial}{\partial r} J_n(xr)$ and

$$k^2 = (\omega^2/C_s^2) - \gamma^2 \qquad h^2 = (\omega^2/C_d^2) - \gamma^2 \qquad 2.26$$

2.4 Frequency Equations

The constants A, B and C in equation 2.25 are obtained by satisfying boundary conditions. For a free infinite cylinder the relevant conditions are that the stresses on the curved surface should be zero. The stresses are given by equation 2.2 where the subscripts for a cylindrical co-ordinate system should be substituted thus.

$$\begin{aligned} 1 &\rightarrow rr \\ 2 &\rightarrow \theta\theta \\ 3 &\rightarrow zz \\ 4 &\rightarrow \theta z \\ 5 &\rightarrow zr \\ 6 &\rightarrow r\theta \end{aligned} \qquad 2.27$$

On the cylindrical surface only three stresses are present, one plane stress σ_{rr} and two shear stresses σ_{zr} and $\sigma_{r\theta}$. These are obatined from 2.4 and can be

written as

$$\sigma_{rr} = \rho((C_d^2 - 2C_s^2)\Delta + 2C_s^2\,\varepsilon_{rr})$$

$$\sigma_{zr} = \rho C_s^2\,\varepsilon_{zr}$$

$$\sigma_{r\theta} = \rho C_s^2\,\varepsilon_{r\theta}$$

Here the substitution Δ has been made for the dilatation $\varepsilon_{rr} + \varepsilon_{\theta\theta} + \varepsilon_{zz}$ and the relationships 2.13 inserted to give some physical meaning to the constants. The strains are related to the derivitives of the displacement components by

$$\varepsilon_{rr} = \frac{\partial u_r}{\partial r} \qquad \varepsilon_{\theta\theta} = \frac{1}{r}\frac{\partial u_\theta}{\partial \theta} + \frac{U_r}{r}$$

$$\varepsilon_{r\theta} = \tfrac{1}{2}\left(\frac{1}{r}\frac{\partial u_r}{\partial \theta} + \frac{\partial u_\theta}{\partial r} - \frac{u_\theta}{r}\right) \qquad \varepsilon_{zz} = \frac{\partial u_z}{\partial z} \qquad 2.31$$

$$\varepsilon_{zr} = \tfrac{1}{2}\left(\frac{\partial u_z}{\partial r} + \frac{\partial u_r}{\partial z}\right) \qquad \varepsilon_{\theta z} = \tfrac{1}{2}\left(\frac{\partial u_\theta}{\partial z} + \frac{1}{r}\frac{\partial u_z}{\partial \theta}\right)$$

For a cylinder of radius 'a' the boundary conditions will be

$$\sigma_{rr} = \sigma_{zr} = \sigma_{r\theta} = 0 \quad \text{at} \quad r = a \qquad 2.32$$

Therefore, to obtain the frequency equation, 2.24 are substituted in 2.31 which in turn are implanted in equations 2.28 to 2.30. The resulting stress relationships are evaluated at the boundary to give three homogeneous equations in terms of the constants A, B and C. These can be represented in matrix form as

$$\begin{vmatrix} a_{11} & a_{12} & a_{13} \\ a_{21} & a_{22} & a_{23} \\ a_{31} & a_{32} & a_{33} \end{vmatrix} \begin{vmatrix} A \\ B \\ C \end{vmatrix} = 0 \qquad 2.33$$

where the elements a_{nm} as given by Zemanek can be found in Appendix A.2.4. Non-trivial solutions of these equations are obtained when the determinant

$$|a_{nm}| = 0 \quad n, m = 1, 2, 3 \qquad 2.34$$

Expanding this leads to the required frequency equation.

2.5 Axisymmetric Modes

If n takes the value zero in 2.33 (see Appendix A.2.4) elements $a_{33} = 0$ and $a_{23} = a_{13}$. The determinant can then be simplified by subtracting line two from line one. On doing this we have

$$\begin{vmatrix} (a_{11} - a_{21}) & (a_{12} - a_{22}) \\ a_{31} & a_{32} \end{vmatrix} a_{23} = 0 \qquad 2.35$$

The condition implied by putting n equal to zero can be best understood by considering equations 2.24 and 2.25. The choice of the trigonometric terms in 2.24 is arbitrary and with no loss of generality one may replace the sine terms with cosine terms and vice versa. Hence it can be seen from these equations that when n is zero the displacements cease to be functions of θ and therefore the motions are

symmetric about the z axis. With this value of n imposed on equation 2.25 it is obvious that V(r) becomes uncoupled from U(r) and W(r). So we have two types of axisymmetric modes, one set which has displacement in the θ dierection only, known as the torsional modes, and one set in which the motions take place in the r and z directions only, known as the longitudinal modes. Each family of modes have their own frequency equation, resulting from the factoring of 2.35. These are, for the torsional modes.

$$a_{23} = 0 \qquad 2.36$$

and for the longitudinal modes.

$$\begin{vmatrix} (a_{11} - a_{21}) & (a_{12} - a_{22}) \\ a_{31} & a_{32} \end{vmatrix} = 0 \qquad 2.37$$

The first of these two equations is a function of two dimensionless variables Ω and γa, where Ω is given by $\omega a/C_s$. The roots of this equation are not dependent upon Poisson's Ratio σ, although the freuqency will be, because of the presence of C_s in Ω. These modes (torsional) have no significance in the following chapters; therefore any further reference to "axisymmetric modes" applies to the longitudinal family only.

The roots of equation 2.37 depend on σ in addition

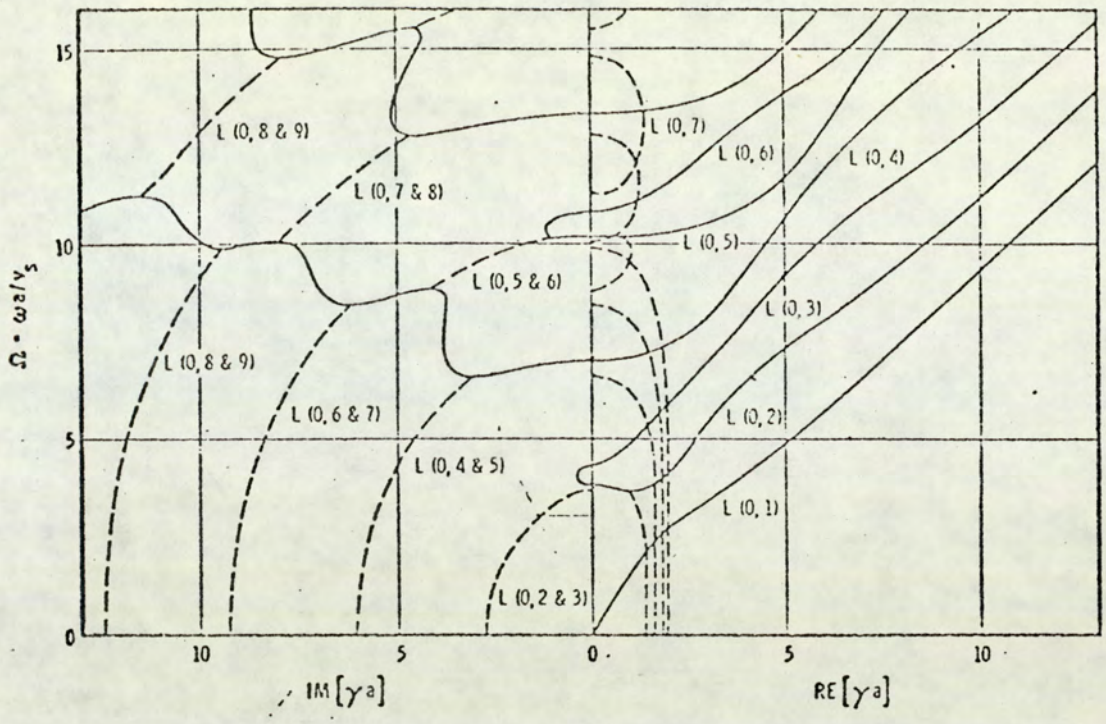

Fig. 2.1 Dispersion curves for the symmetric modes of wave propagation in a solid cylinder. (——): real or imaginary modes; (---): complex modes. $\sigma = 0.3317$

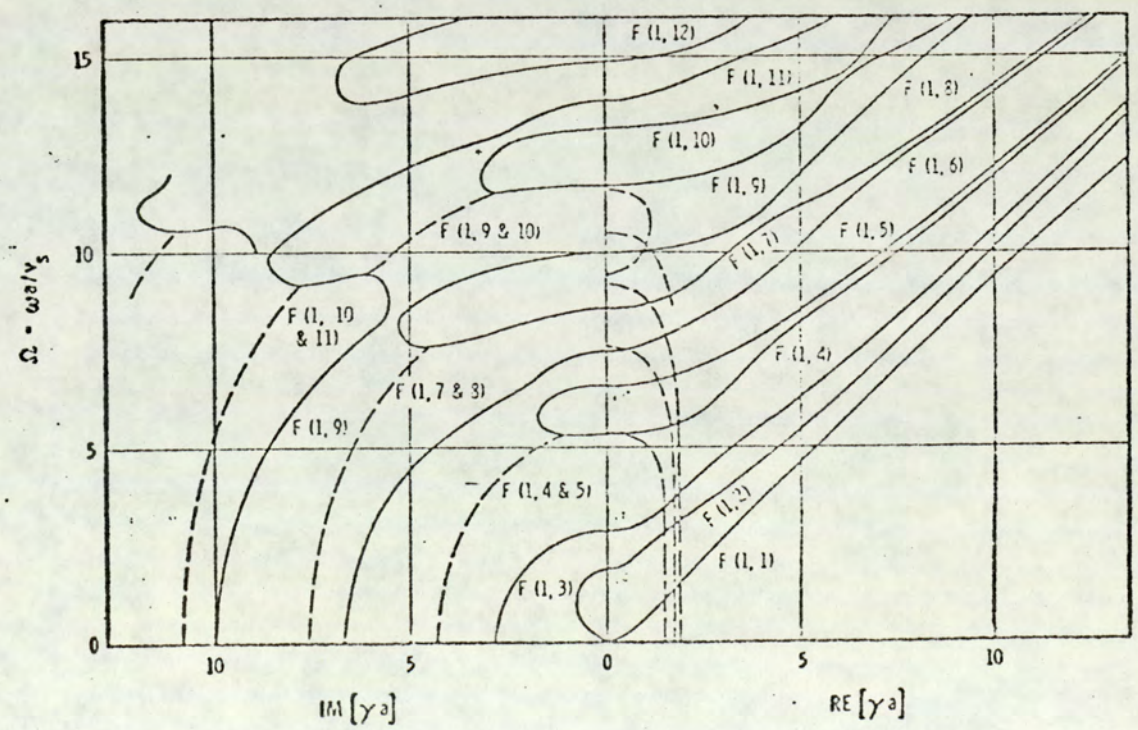

Fig. 2.2 Dispersion curves for the first anti-symmetric modes of wave propagation in a solid cylinder. (——): real or inaginary modes; (---): complex modes. $\sigma = 0.3317$.

to Ω and γa; dispersion curves for σ=.33 showing the relationship between Ω and γa are shown in Fig.2.1. It can be seen that the frequency spectrum occupies two planes, real and imaginary. Imaginary roots of equation 2.37 are shown as continuous lines in the imaginary plane. The dashed lines represent the complex roots; these are discussed later.

Solutions for an infinite number of axisymmetric modes are contained within this equation and a method of labelling is required. A convenient method is that used by Meitzler (25) and Zemanek; the notation numbers the modes in the order of which there dispersion curves occur in the frequency spectrum. Thus the first mode will be labelled L(O, 1) and the second L(O,2) where O represents n = O and L that it is a longitudinal mode.

2.6 Antisymmetric Modes

When n has a value other than O (i.e. $n \geq 1$) equations 2.24 show that the displacements become dependent on θ and as such indicate the antisymmetric property that these modes exhibit. The term flexural is often applied to this type of propagation, but this tends to be misleading, since it is only the values of n = 1 and 2 that satisfy the basic hypothesis of the Bernoulli-Euler theory for flextural motion of beams: That is that any plane cross-section initially perpendicular to the neutral surface remains so after deformation. Therefore the term 'compound' has been used, in this thesis, to describe all modes with $n \geq 1$. The word compound

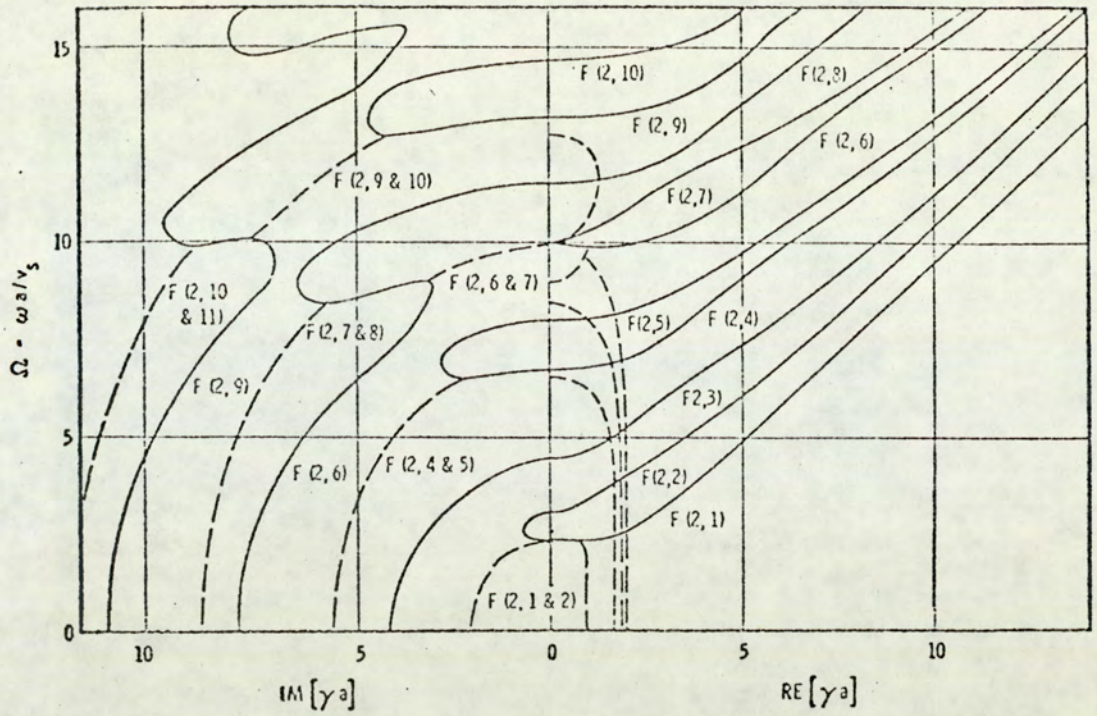

Fig. 2.3 Dispersion curves for the second anti-symmetric modes of wave propagation in a solid cylinder. (——): real or imaginary modes; (---): complex modes. σ = 0.3317.

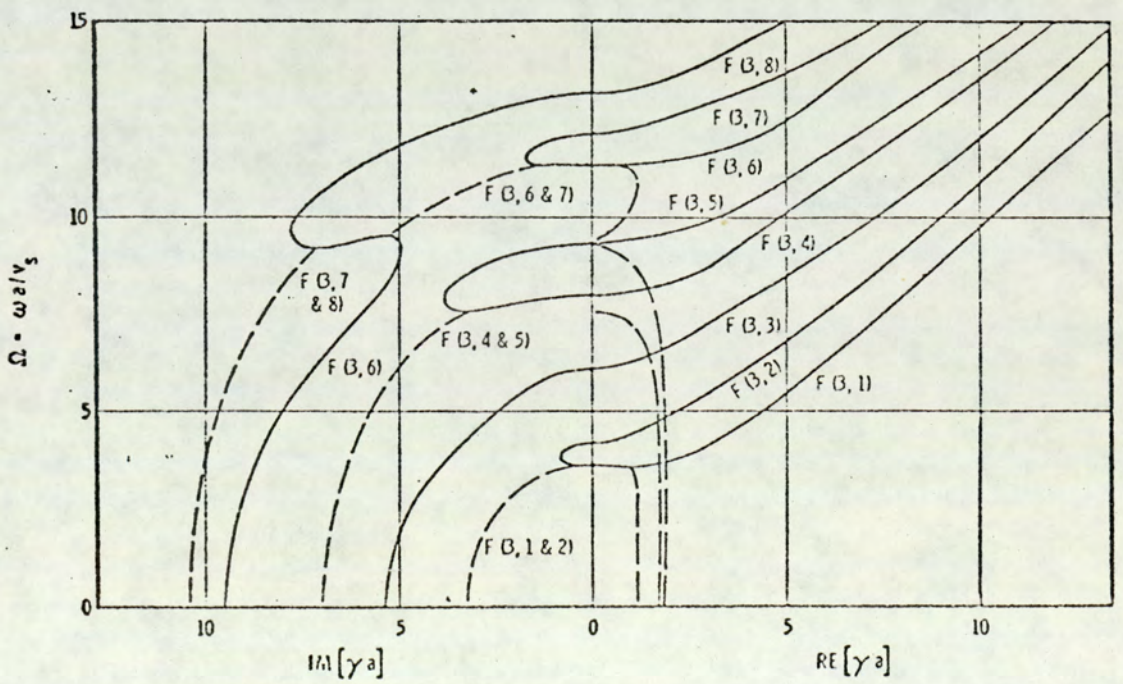

Fig. 2.4 Dispersion curves for the third anti-symmetric modes of the wave propagation in a solid cylinder. (——):real or imagnary modes; (---): complex modes. σ = 0.3317

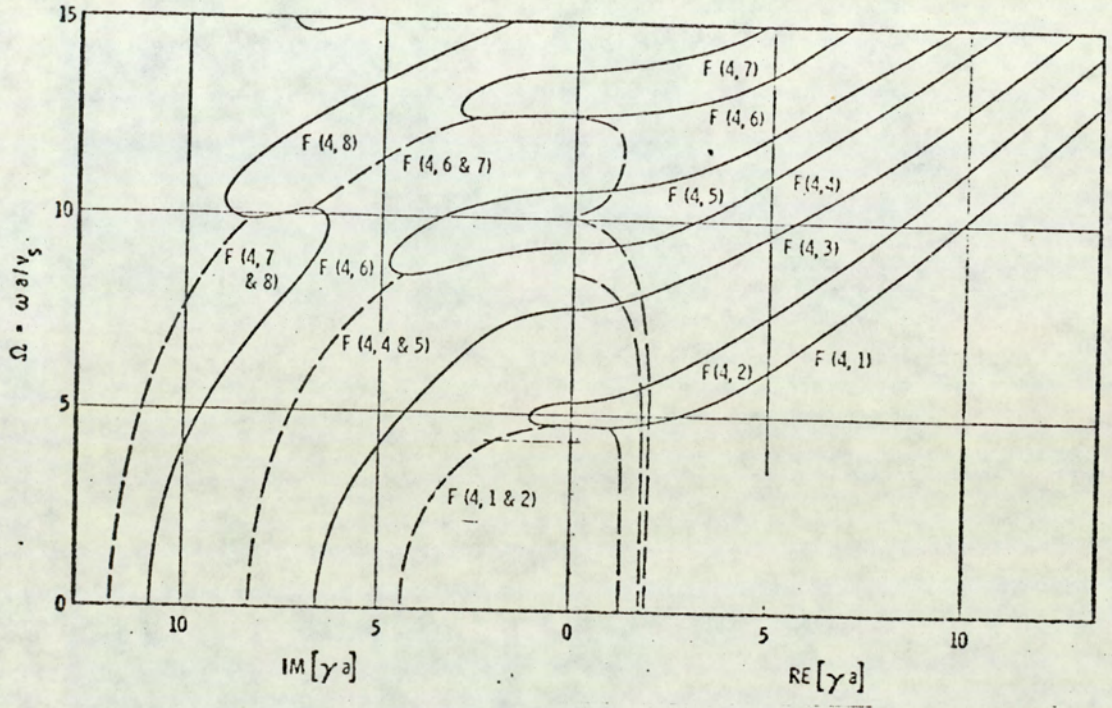

Fig. 2.5 Dispersion curves for the fourth anti-symmetric modes of wave propagation in a solid cylinder. (——): real or imaginary modes; (---): complex modes. σ = 0.3317.

indicating that the displacement vector is a function of all three co-ordinate axis.

The method of labelling these modes is similar to that of the longitudinal case. For example, the lowest mode for the n = 1 family is labelled F(1, 1) and for n = 2 F(2, 1) etc., this is in accordance with references (9) and (25).

An examination of the elements in 2.33 will show that, for $n \geq 1$, all are required to obtain the frequency equation for these modes. Figures 2.2,2.3,2.4 and 2.5, show dispersion curves as obtained by Zemanek from equation 2.33. These curves, like those of the longitudinal modes, extend into the imaginary plane representing imaginary and complex propagation constants γ.

2.7 Cut Off Frequencies

The presentation of results in the manner shown in Figures (1) to (5) has numerous advantages. A feature of particular usefulness is that it provides simultaneous information about group and phase velocities. If any point on the curve is taken, for example, the group velocity is given by the slope at the point multiplied by the shear velocity. e.g.

$$C_g = C_s \frac{\partial \Omega}{\partial (\gamma a)} \qquad 2.38$$

The product of the shear velocity and the ratio of the ordinate to abscissa for the same point will give

the phase velocity thus

$$C_{ph} = C_s \frac{\Omega}{(\gamma a)} \qquad 2.39$$

Considering Fig. 2.1 it can be seen that by applying the conditions of 2.38 and 2.39, the curves display some interesting characteristics; for instance on curve L(O, 1) close to the origin there is the situation

$$\frac{\partial \Omega}{\partial (\gamma a)} \simeq \frac{\Omega}{(\gamma a)}$$

and therefore the group and phase velocities have the same value. This condition is an essential part of the discussion in Chapter 3. Another point that is presented particularly well by Fig. 2.1 is the existance of a phenomenon described as backward wave motion. In essence this is a situation that arises when the group and phase velocities have opposite sign. Inspection of Fig. 2.1 shows that this occurs on the curve L(O, 2) between its point of minimum frequency in the real plane and the frequency axis. Experimental observations of this phenomena together with discussion are presented by Meitzler (26).

The feature displayed by these curves, that is of particular interest in this part of the discussion, is the existance of cut-off. This is the term used to describe the event where propagation of a mode ceases. Mathematically this would be represented by a zero propagation constant γ. Graphically we see that when γ goes to zero the dispersion curves intersect the

frequency axis; the points at which this occurs gives the cut off frequencies for their respective modes. All modes, except the lowest in each family, have two common characteristics at γ equal to zero, that are often used to define this phenomenon. Firstly, the group velocity goes to zero and secondly, the phase velocity goes to infinity; this becomes apparent when the conditions of 2.38 and 2.39 are applied to Figs. 2.1 to 2.5

If γa is allowed to go to zero in the preceeding frequency equations a modified set of equations are obtained. The procedure is as follows. Considering the axisymmetric modes first, equation 2.35 reduces to

$$(a'_{11} - a'_{21})\, a'_{32}\, a_{23} = 0 \qquad 2.40$$

where the primes indicate modification of the elements a_{nm} by putting $\gamma a = 0$. The element a_{23} is unaffected by imposing this condition on it, and so all the foregoing comments about it are still valid (i.e. modes represented by the frequency equation $a_{23} = 0$ have an uncoupled displacement in the θ direction). When the roots of the equation $a'_{32} = 0$ are substituted into the displacement equations 2.25 the resulting partical displacement is entirely axial. For similar treatment of the roots from the equation $(a'_{11} - a'_{21}) = 0$ all the displacement takes place in the radial direction. The modes associated with these cut off frequencies are therefore called axial and radial shear modes respectively. Therefore

with reference to Appendix A.2.4 the cut off frequency equations become

$$\Omega J_o(\Omega) - 2J_1(\Omega) = 0 \quad \text{for torsional modes} \qquad 2.41$$

$$(\alpha\Omega)J_o(\alpha\Omega) - 2\alpha^2 J_1(\alpha\Omega) = 0 \quad \text{for radial shear modes} \qquad 2.42$$

$$J_1(\Omega) = 0 \quad \text{for axial shear modes} \qquad 2.43$$

Following the same procedure for the compound modes, reduces equation 2.33 to

$$\begin{vmatrix} a'_{11} & a_{13} \\ a_{21} & a_{23} \end{vmatrix} \; a'_{32} = 0 \qquad 2.44$$

writing these equations in full

$$a'_{32} = 0$$

becomes $\Omega J_{n-1}(\Omega) - nJ_n(\Omega) = 0$ 2.45

and

$$\begin{vmatrix} a'_{11} & a_{13} \\ a_{21} & a_{23} \end{vmatrix} = 0$$

becomes

$$b_1 b_2 - b_3 b_4 = 0 \qquad 2.46$$

where

$$b_1 = |2(n^2-1)|\Omega J_{n-1}(\Omega) - nJ_n(\Omega)| - \Omega^2 J_n(\Omega)|$$

$$b_2 = |\alpha\Omega J_{n-1}(\alpha\Omega) - (n+1)J_n(\alpha\Omega)|$$

$$b_3 = J_n(\alpha\Omega)|n^2 - 1 - \Omega^2/2|$$

$$b_4 = |(2n^2 + 2n - \Omega^2)J_n(\Omega) - 2\Omega J_{n-1}(\Omega)|$$

For n = 0 equation 2.45 is the same as 2.43 and equation 2.46 is the product of 2.41 and 2.42.

2.8 Complex Propagation

It can be seen from the dispersion spectrum that all modes have curves which terminate at the zero frequency plane. The path these curves take to reach the point $\Omega = 0$ depends on the mode. In general all modes except the L(0, 1) and the F(0, 1) will have made the journey by going into the complex plane, either by direct route from the real plane, or by passing through the imaginary plane first. The curves in the complex plane, shown as broken lines, represent the complex roots of equation 2.33. Fig.2.6 shows the three dimensional plot given by reference 8 for the axisymmetric modes. It can be seen from this plot how each curve makes its way to the zero frequency plane. Because of the complex and somewhat confusing appearance of this figure the correct interpretation requires some

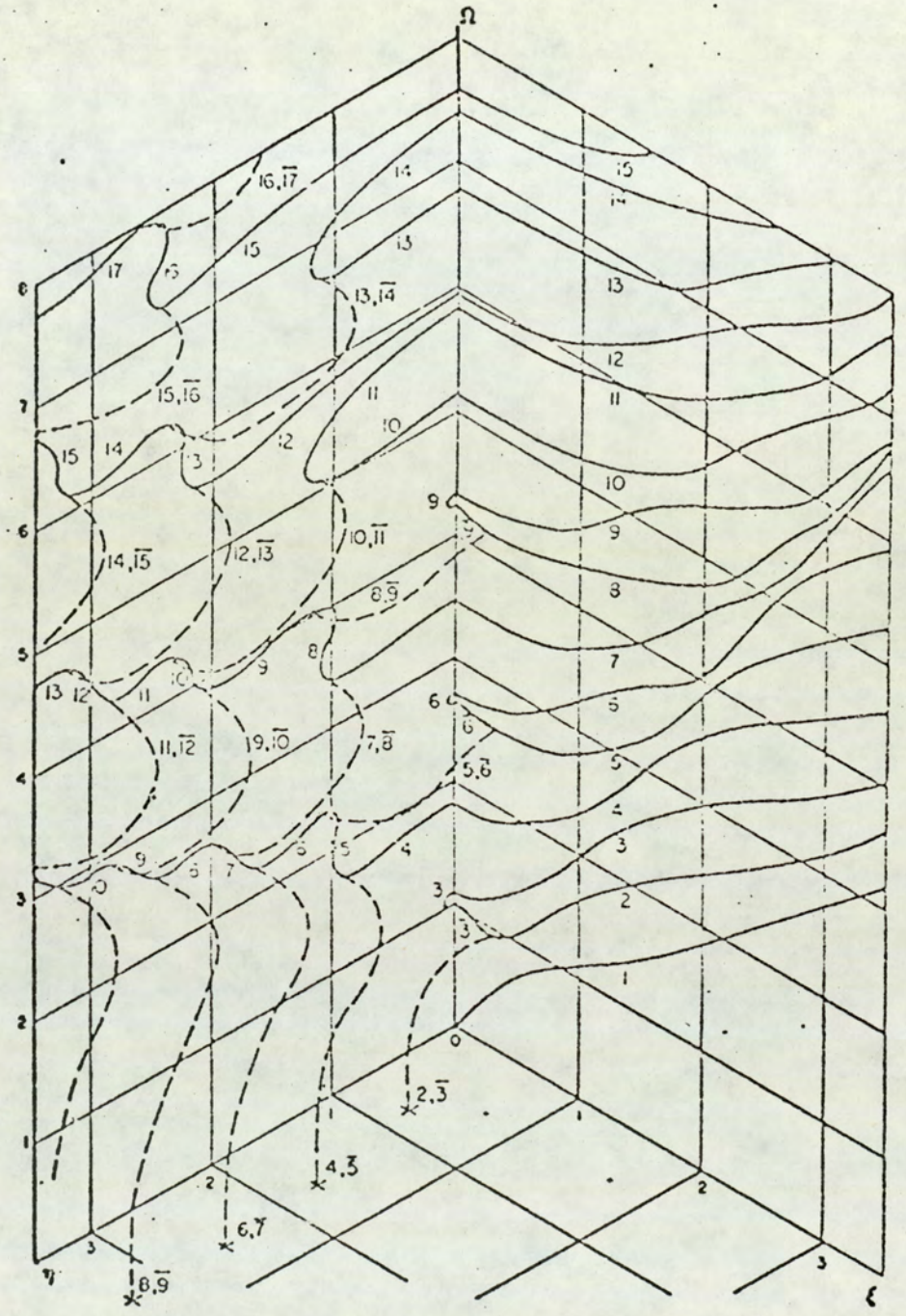

Fig. 2.6 Three dimensional plot of frequency spectrum for symmetric modes of propagation in a solid cylinder. (——): real or imaginary modes; (---): complex modes. $\sigma = 0.31$
(Reproduced from reference 8).

discussion.

When examining this frequency spectrum it is most important to appreciate the way in which the roots emerge from equation 2.35. Real and imaginary roots occur in pairs while the complex roots occur in groups of four. Each real and imaginary solution has its negative counter-part and therefore a complete plot of the roots of this equation would take up four quadrants. The complex roots also have positive and negative solutions but in addition to this each has its conjugate; hence there is a complex curve in each of the four quadrants. Because of the limits set by nature any involvement with the negative imaginary plane would create a violation of the physical problems that exist. In accordance with this the frequency spectrum can only have any meaning in the two remaining quadrants. Therefore when examining Fig.2.6 it should be realised that there exists a real plane in the negative direction which is a mirror image of the one drawn. This now brings us to the point where some meaning can be given to the method of labelling.

The numbering of the curves in the real plane is in the order in which these modes occur. A bar over a number in the real plane indicates that this portion of the curve extends into the negative real plane. The barred numbers on the complex curves have similar meaning in that they imply the existance of the negative conjugates, of the curves drawn, in the second quadrant.

As an example therefore, if one tracks the behaviour of the curve labelled 9 in the real plane as it makes its way to the zero frequency plane it can be seen that, in all, this mode has three segments in the imaginary plane, one in the negative real plane, one complex segment in the quadrant shown and two complex segments in the second quadrant. The physical significants of this can only be described in terms of a finite or semi-infinite elastic cylinder, where a wave may emanate or be reflected from an end boundary. The imaginary propagation constants represent a non-oscillatory motion decaying exponentially from this boundary, while the complex constant gives an oscillatory motion which also decays spatially. It can be seen from Fig.2.6that the non-real segments only occur below cut off and if these modes are excited by an externally applied force, the character of the motion will change as the frequency of this force goes from that of cut off to zero.

2.9 Displacement Distributions

The displacement pattern produced when any one mode is propogating in a bar is dependent upon the frequency, and therefore no general pattern can be associated with any mode. This is in contrast to the theory of thin discs where, because each mode has a discrete frequency, the pattern associated with that

frequency will identify the mode. For instance the inplane compound modes of discs are usually labelled, as the (m, n) mode. Here as in the case of rods n refers to the integer number of wave lengths by which the circumference is divided, and m the order that modes occur on the frequency spectrum for a given value of n. That is for n = 2 say, the modes are labelled as (1, 2), (2, 2), (3, 2) etc. The feature of disc modes that makes them easy to identify, by their displacements, is that for the (m, n) mode there will be n nodal diameters and m nodal circles.

It has already been stated that the displacement vector for an elastic rod can be written in terms of scalar and vector potentials (equation 2.21). Considering the axisymmetric modes (because of the relative simplicity of the equations) the r dependent displacement components are, from equation 2.25.

$$U(r) = A(J_o'(hr) + M\gamma J_o'(kr)/k) \qquad 2.47$$

$$W(r) = jA(\gamma J_o(hr) - MkJ_o(kr)) \qquad 2.48$$

where M = B/A; the value of this ratio is obtained by satisfying one of the boundary conditions 2.32. Making the necessary substitutions between equations 2.47, 2.48, 2.24 and 2.32 the following relationship is obtained

$$M = \frac{2\gamma^2 a^2}{(\Omega^2 - 2\gamma^2 a^2)\alpha^2} \cdot \frac{J_o'(ha)}{J_o'(ka)} \qquad 2.49$$

where

$$J_o'(xa) = \frac{\partial J_o(xa)}{\partial a} \qquad \text{and } \alpha = C_s/C_d$$

From this it can be seen that M is frequency dependent. The implications of this are that, since the first terms of equations 2.47 and 2.48 represent a displacement contribution from a dilatational wave and the second terms from a rotational wave, the displacement vector must itself be frequency dependent.

A possible method of defining a mode by its displacement pattern can be obtained by taking a special solution of equation 2.49. If the value $\Omega^2 = 2\gamma^2 a^2$ is substituted, M becomes infinite and for the displacements to remain finite A must equal zero. Therefore equations 2.47 and 2.48 become

$$U(r) = -K\gamma J_1(\gamma a \frac{r}{a})$$

$$W(r) = -jK\gamma J_o(\gamma a \frac{r}{a}) \qquad 2.50$$

The point to notice about these relationships is that they make the displacement vector a function of the vector potential only and as such can only describe a shear (distortional) wave. If 2.5 is now substituted into a permissible boundary condition of 2.32 the characteristic equation

$$J_1'(\gamma a) = 0 \qquad 2.51$$

is obtained. Here, as one might expect for a shear

wave, the roots are independent of Poisson's Ratio. The solutions of equation 2.51 together with the relationship $\Omega = \sqrt{2}\ (\gamma a)$ gives the frequencies of Lamb's (27) distortional modes. Writing the roots of 2.51 as $\gamma_n a$ the displacements for any mode will be

$$U_n(r) = -K_n \gamma_n J_1(\gamma_n a \frac{r}{a})$$

$$W_n(r) = -jK_n \gamma_n J_o(\gamma_n a \frac{r}{a}) \qquad 2.52$$

From these equations it is now possible to obtain a relationship between mode and displacement.

The relationships that exist are:-
For the nth mode there will be n circles at which the displacement $U_n(r)$ is zero. The smallest of these circles always having zero radius. At r = a $W_n(r)$ will be only a few percent of its maximum value at r = 0 and for the present discussion can be considered as being a node. This being the case, at the nth mode the axial displacement $W_n(r)$ will also have n nodal circles.

The practical usefullness of defining modes in this way is limited because of the problems involved in exciting a single mode in isolation. However it does help give a physical picture of the various modes. One redeeming aspect of the method is that it is immune to any variation in Poisson's Ratio and therefore the relationships just stated are true for all isotropic materials.

The equations given in this chapter represent the

exact analysis of wave propagation in infinite cylinders. Boundary conditions, on the curved surface, and equations of motion are satisfied by displacement relationships given. When a second boundary exists, as in the case of a semi-infinite cylinder, approximations have to be made to satisfy the condition of zero stress, at this boundary. The problems involved in trying to obtain an exact solution result from having to satisfy three zero stress conditions simultaneously. These boundary conditions are that

$$\sigma_{zz} = \sigma_{rz} = \sigma_{z\theta} = 0$$

It can be shown that if one of these conditions is satisfied the remainder can not be. The physical explanation for this is that when an incident mode is reflected at an end boundary other modes are generated. Therefore a traction-free boundary will only occur when the resultant of all the stresses produced by these modes is zero. The boundary conditions must therefore be written as

$$\sum_{m=0}^{\infty} \sigma_{zzm} = \sum_{m=0}^{\infty} \sigma_{rzm} = \sum_{m=0}^{\infty} \sigma_{z\theta m} = 0$$

Where, for a given frequency, σ_m is the stress produced by the mth generated mode. The limits of the summation indicate the need for approximation.

Support for this explanation is given by Zemanek,

who by considering the first nine (four complex and their conjugates and one real) axisymmetric modes obtained within 0.5% the frequency of the end resonance for this family of modes.

This illustrates the important role that this chapter plays in further discussions on end resonances.

CHAPTER 3

THE ECHO TECHNIQUE

CHAPTER 3

THE ECHO TECHNIQUE

3.1 Introduction

The idea of using an echo to obtain information at a remote observation point, is implemented in a wide variety of situations. The complexities of the system involved, in using this technique, range from those of say radar or sonar to those of a system as rudimentary as that of measuring the time lapse between dropping a stone into a well and the returning sound of it hitting the bottom. In each of these systems the basic principle is the same, and is one of transmitting energy to a target so that an echo containing information about it's characteristics can be obtained. The medium used to transport the energy will depend on the system, which in general will be designed to suit a given set of environmental circumstances.

The echo technique used to obtain the results discussed in the following chapters employs this principle. Fig. (3.1) is a block diagram of the system used. A magnetostrictive launcher is used to transmit and receive a burst of high frequency stress waves. The burst transmitted takes the form of a pulse which acts as an envelope for the high frequency carrier wave, the number of oscillations contained being selected to allow sufficient information to be

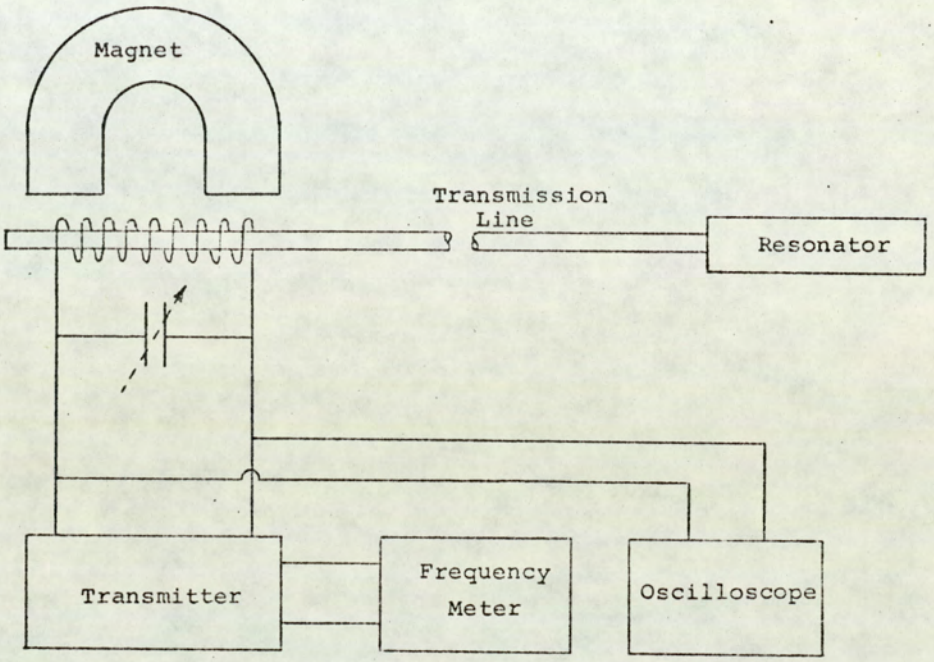

Fig. 3.1 Basic layout for the echo technique used to obtain the results of this thesis.

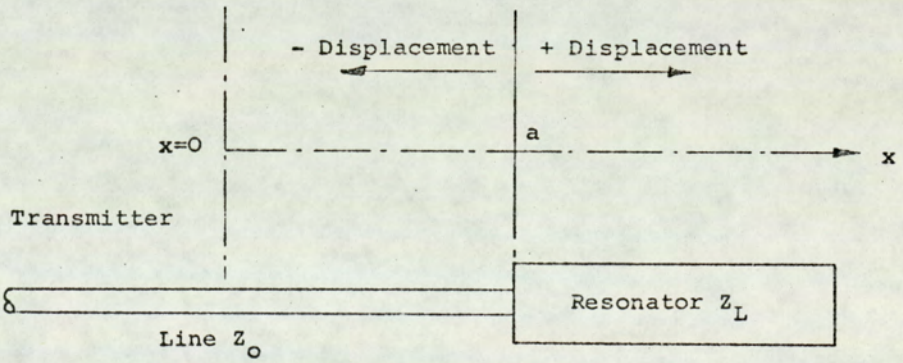

Fig. 3.2 If $Z_L > Z_o$ a positive displacement will reflect as a negative displacement $Z_L = Z_o$ no reflection and for $Z_L < Z_o$ incident and reflected waves will have the same signal.

echoed. An acoustic line is used to carry these pulses to and from the resonator. Unlike the radar and sonar cases there is no spreading and the only attenuation arises from absorption in the material of the line and scattering from grain boundaries, supports and other impedance discontinuities. The line and launcher are very often constructed of the same material, thereby eliminating all of the problems associated with the discontinuities produced by jointing. Line lengths are not important providing they are long enough to contain half the pulse length e.g. for a pulse of duration T the length ℓ of the line will be given by

$$\ell > CT/2 \qquad 3.1$$

where C is the velocity of propagation in the line. At the other extreme the length should not be such that the overall attenuation produced by the line becomes a dominant problem. Within these limits the line length can be tailored to suit the physical environment for which it is intended.

The resonator can have a variety of geometrical forms, and to a greater extent the structure chosen will depend upon the parameter to be measured. This constraint is one of necessity rather than convenience and will be determined by the availability of empirical or theoretical solutions for the parameters involved.

The method of taking measurements is to vary the transmitter frequency until it coincides with a natural

frequency of the resonator. At this instant resonance will occur. The echo that this situation produces is quite distinct having a phase sensitive null and therefore facilitates a method of measuring resonator parameters. In general, when resonance occurs, information can be obtained in two forms; either by way of the resonant frequency, or of the Q factor, a particular mode may exhibit. The type of information required will determine its source. As one might expect measurements involving energy loss will lend themselves more readily to the method of observing Q's, whereas information relating to elastic constants of the resonator, or any parameter that may have an effect on them, can best be obtained by measuring the frequency.

3.2 Transmission Line Theory

Analogies may be drawn between the acoustic line and the electric transmission line provided only one mode is considered to be propagating. This mode, sometimes referred to as "Young's modulus" mode, is the lowest axisymmetric mode to propagate in a cylindrical rod. The torsional mode, which in general is not excited by the method of drive, would propagate at the much lower shear velocity. With reference to figure (2.1) it can be seen that this mode, labelled L(0,1), has no cut off frequency, and that for $\gamma a<1$ there exists a linear relationship between Ω and (γa). If this relationship is written as $\Omega \doteq k\gamma a$

and the substitutions $\omega a/C_s$ and $2\pi a/\lambda_1$ are made for Ω and γa respectively the frequency equation

$$\lambda_1 f \doteq kC_s \qquad 3.2$$

is obtained. The value of k can be obtained by imposing the restriction $\gamma a<1$ on the frequency equation for the axisymmetric modes (equation 2.37). By replacing the Bessel functions with their series expansion and retaining only the low order terms the equation

$$\lambda_1 f \doteq C_o \qquad 3.3$$

is obtained. Where C_o the velocity of longitudinal waves of infinite wavelength in a bar is equal to $\sqrt{E/\rho}$. The steps taken to acquire this result can be found in Love p.289. Therefore from equations 3.2, 3.3, 2.38 and 2.39 it can be seen that for $\gamma a<1$

$$C_g \doteq C_{ph} \doteq C_o \doteq \sqrt{E/\rho} \qquad 3.4$$

If the radius 'a' of the line is small (i.e. $a<\lambda/2\pi$) the usual procedure may be adopted in that all displacements and hence their derivitives, except those in the axial direction, are assumed zero. This reduces the stress strain relationships of Hook's law to

$$\sigma_{zz} = (\lambda + 2\mu)\ \varepsilon_{zz}, \qquad 3.5$$

which by definition gives $E = (\lambda + 2\mu)$. Also the

rotational vector $\bar{\omega}$ (see Appendix A.3.2) will be zero. Therefore the equation of motion 2.20 becomes

$$\frac{\partial^2 u_z}{\partial z^2} = \frac{1}{C_o^2} \ddot{u}_z \qquad 3.6$$

The dilatational velocity for a one dimensional system is from equations 2.13 and 3.5

$$C_d = C_o \qquad 3.7$$

If we use this relationship in equation 2.26 it is seen that h for a thin rod is zero. Putting h = 0 in equation 2.49 gives M = 0 which ultimately leads to the displacement components 2.47 and 2.48 being reduced to

$$u(r) = 0$$

$$w(r) = jA\gamma$$

giving consistency to the assumptions previously made.

The transmission line theory can therefore be built up around equation 3.6 providing $a<\lambda/2\pi$. If losses are taken into account, as represented by 2.18, equation 3.6 becomes

$$\frac{\partial^2 u}{\partial z^2} + \frac{\eta}{E} \frac{\partial^2 \dot{u}}{\partial z^2} = \frac{\ddot{u}}{C_o^2} \qquad 3.7$$

which has a solution of the form

$$u(z) = (B \exp j(-qz) + B' \exp j(qz)) \exp j\omega t \qquad 3.8$$

As with the electrical transmission line theory this wave has two components, representing two waves travelling in opposite directions. B and B' are the complex amplitudes of the waves travelling in the positive and negative z directions respectively. The propagation constant q is also complex and is given by

$$q^2 = -\omega^2/(C_o^2 + j\omega\eta/\rho) \qquad 3.9$$

To make comparisons between the acoustic and electric transmission line theories one must give analogies between the respective parameters. The most convenient and most often used, is that of current/velocity and voltage/force. This therefore gives the acoustic (or mechanical) impedance as the force divided by the velocity. Using these analogies Pollard (29) obtained equations for input and transfer impedances, and the reflection coefficient showing that each has a structure identical to those of the electrical theory.

The reflection coefficient is given as

$$R = B'/B = (Z_o - Z_L)/(Z_o + Z_L) \qquad 3.10$$

where Z_o the characteristic impedance is equal to $\rho A(C_o^2 + j\omega\eta/\rho)^{\frac{1}{2}}$, and Z_L the load impedance at the end of the line $z = 0$. Equation 3.10 will therefore give

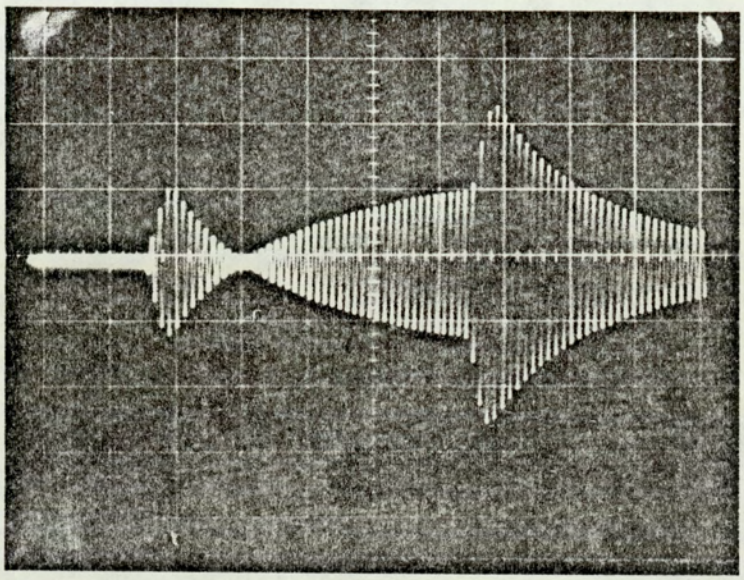

Fig. 3.3 Oscilloscope trace showing echo from a Brass line resonator at its fundamental mode. Frequency = 25.06 KHz. Resonator length = 7 cm.

the echo in terms of the system impedances and the input signal. The input impedance for a finite length ℓ of line, given by reference (29) is

$$Z = Z_o \tan hjk\ell \qquad 3.11$$

where k has the same function as q in 3.8. If this is substituted for Z_L in equation 3.10, the resulting expression gives the reflection coefficient for a line terminated with a line resonator. Using this, Sharp (30) obtained an expression for the echo resulting from a sinusoidal input. The results obtained give good support to the theory.

3.3 The Echo

The echo system shown in Figure (3.1) was originally developed for resonant ultrasonic thermometry by Bell (31), (32). However it has since been used for many other applications, one being the type of work covered in this thesis. The input used is sinusoidal; this gives, at resonance, the form of echo shown in figure (3.3). Although the method has been used in numerous experimental works over the last few years no completely satisfactory explanation has been given of why an echo of this shape is obtained. The computer plots obtained by Sharp are in excellent agreement with experiments, but because of the complexities of the equations involved one cannot obtain a physical picture of what is happening.

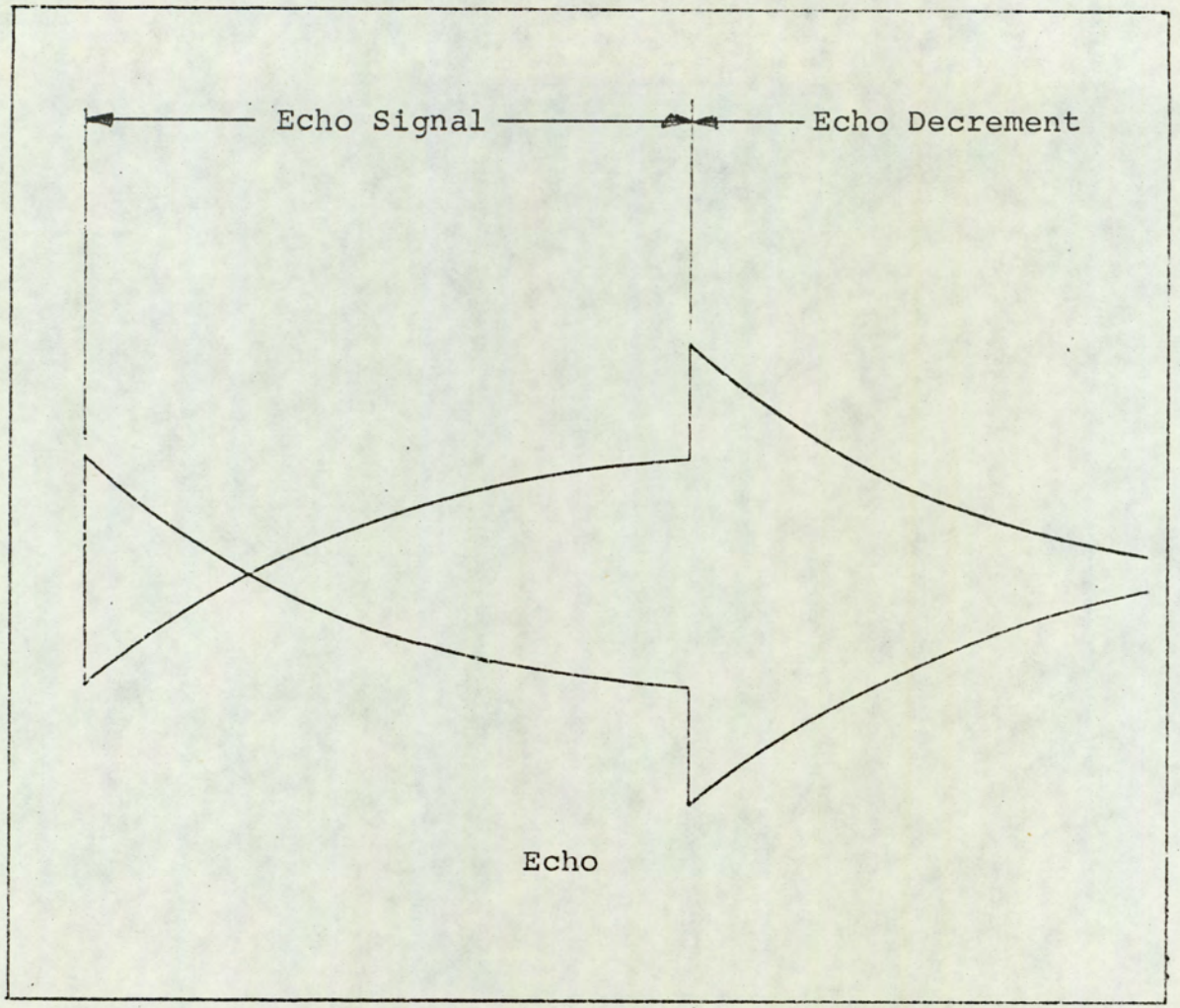

Fig. 3.4 The echo has two main components; the echo signal, representing the reflection from the line resonator junction, and the echo decrement a signal transmitted by the resonator.

Fig. (3.4) shows a sketch of the echo together with the terminology used to describe its two major components. The echo signal is the same length as the input burst and therefore the echo decrement occurs after the last cycle has reflected off the resonator. To give some physical meaining to this picture the following simple analysis is given.

If it is considered that the line is terminated by a lossless impedance Z_L, such that it has the form Ms+k/s where M and k are parameters of the body and s is the Laplace operator, equation 3.10 becomes.

$$R(s) = -1 + 2Z_o s/(Ms^2 + Z_o s + k) \qquad 3.12$$

This assumes that the losses in the line are zero and therefore that Z_o is real. The echo will be given by

$$f(s) = g(s)\ R(s) \qquad 3.13$$

g(s) the incident wave ususally consist of a burst of sinusoidally varying displacement. Shortening the burst length so that it contains only one half cycle will give an insight into how the system responds to the first cycle of the burst and how the echo is built up when a series of similar negative and positive disturbances follow. Therefore the forcing function will be

$$g(t) = H(t)A \sin \omega t + H(t-\pi/\omega)A \sin \omega(t-\pi/\omega) \qquad 3.13$$

Using Laplace transforms the solution of 3.12 is obtained by substituting equation 3.13. On inverting back into the time domain, and assuming that the natural frequency ω_n of the resonator is given by $\sqrt{k/M}$. The following equation is obtained for the echo at resonance:

$$f(t) = |H(t)A \sin\omega_n t + H(t-\pi/\omega)A \sin\omega_n(t-\pi/\omega)|$$
$$- |H(t)2A \exp(-Z_o/2M)t \sin(\omega_n^2 - Z_o^2/4M^2)^{\frac{1}{2}}t|$$
$$- |H(t-\pi/\omega)2A \exp(-Z_o/2M)(t-\pi/\omega)$$
$$\sin(\omega_n^2 - Z_o^2/4M^2)^{\frac{1}{2}}(t-\pi/\omega)| \qquad 3.14$$

This equation can be simplified further to give a more readable solution, but there is one important point that would be missed if this was carried out without comment. The first bracketed term of this equation is seen to have a frequency identical to the launched frequency. This is not so with the remaining terms which, because of their exponential character, must represent the natural decay of a body due to an initial disturbance. If a comparison is made between these terms and the example given by Kolsky (p. 101) it is seen that Z_o has the same function as a damping factor. Hence it is apparent that the line introduces damping to the system. Therefore the echo decrement will not in general be at the natural frequency of the resonator. However $Z_o^2 << 4M^2\omega_n^2$ so for this discussion the decrement frequency will be assumed

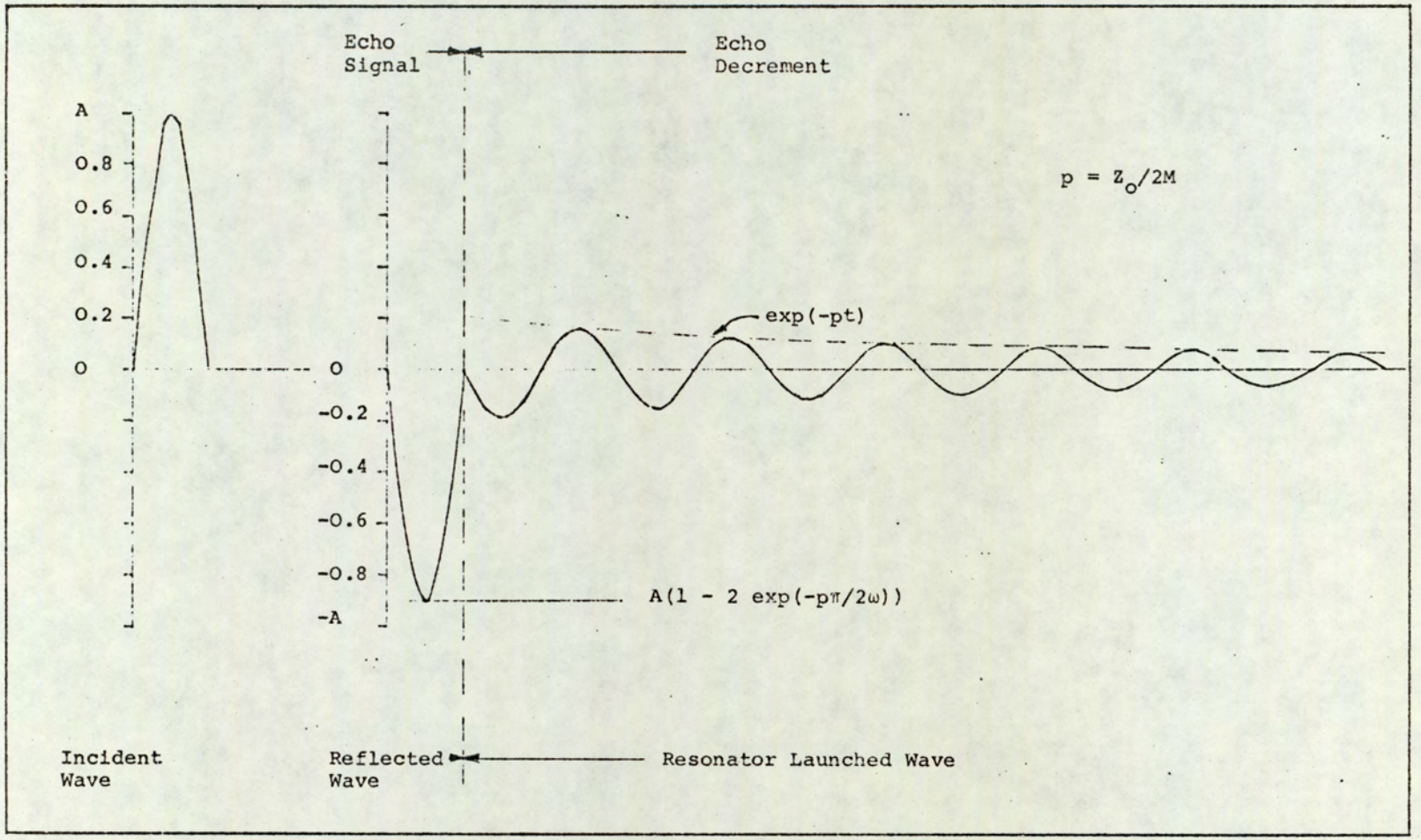

Fig. 3.5 Theoretical echo produced when a wave of half cycle impinges on the line resonator boundary.

to be ω_n; therefore equation 3.14 becomes

$$f(t) = H(t)A(1 - 2\exp(-Z_o/2M)t)\sin \omega_n t$$

$$+ H(t - \pi/\omega_n)A(1 - 2\exp(-Z_o/2M)(t - \pi/\omega_n))$$

$$\sin\omega_n(t - \pi/\omega_n) \qquad 3.14$$

A plot of this function is shown in figure (3.5).

With the aid of this plot it will now be possible to explain why the echo has its characteristic shape at resonance. The first half cycle is the reflection, of the input, from the interface between the line and resonator. It is inverted because the condition $Z_o << 2M\omega_n$ implies that the load impedance Z_L is greater than Z_o which, from equation 3.10, gives a negative reflection coefficient. Its amplitude is reduced because part of the energy, contained in the incident wave will have been used in setting the resonator in motion. The following part of the echo represents a wave being transmitted from the resonator which, by now has stored enough energy to enable it to perform in the same way as the launcher. When the incident wave hits the resonator they must both move in phase, and therefore the transmitted wave from the resonator has the same phase as the incident wave. This is shown to be the case in figure (3.5). To make this a little clearer consider the sketch in figure (3.2). At rest, the line-resonator junction is a distance x=a from some reference x=0, also a displacement that increases

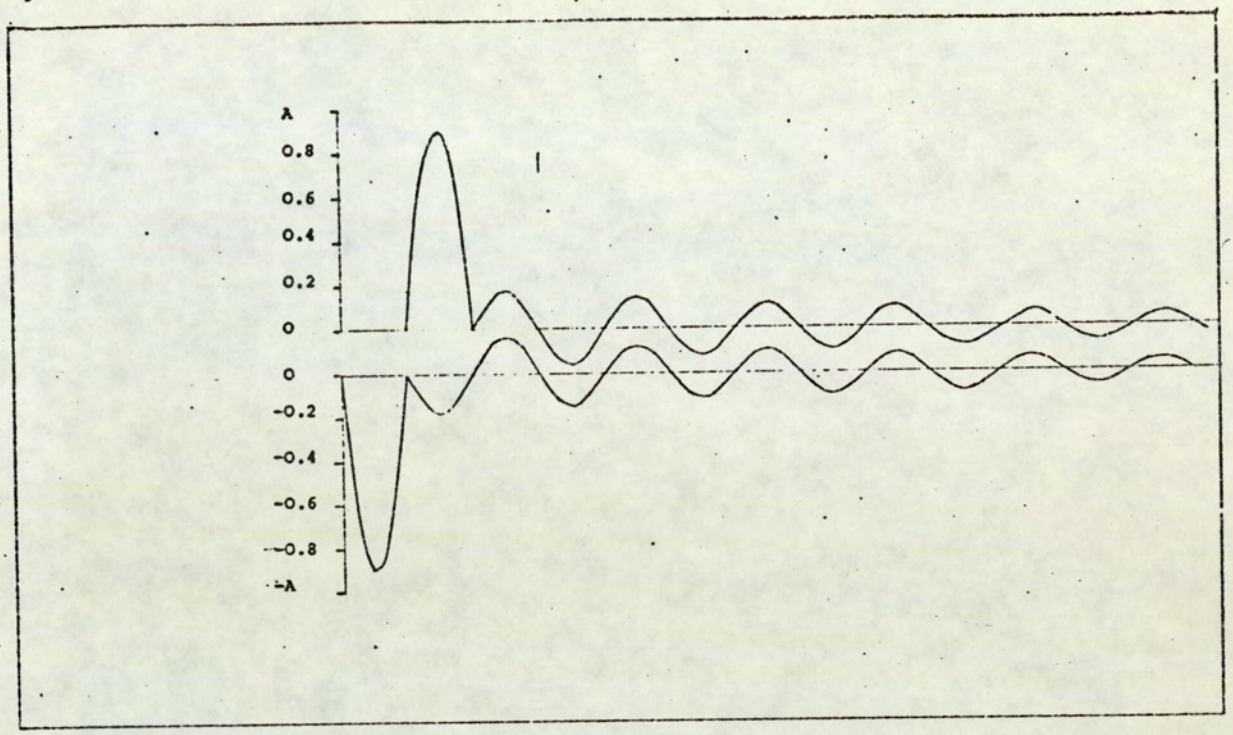

Fig. 3.6 (a) The addition of a second half cycle shows how the amplitude of the echo signal decreases with time and how the amplitude of the echo decrement increases with cycles in the burst.

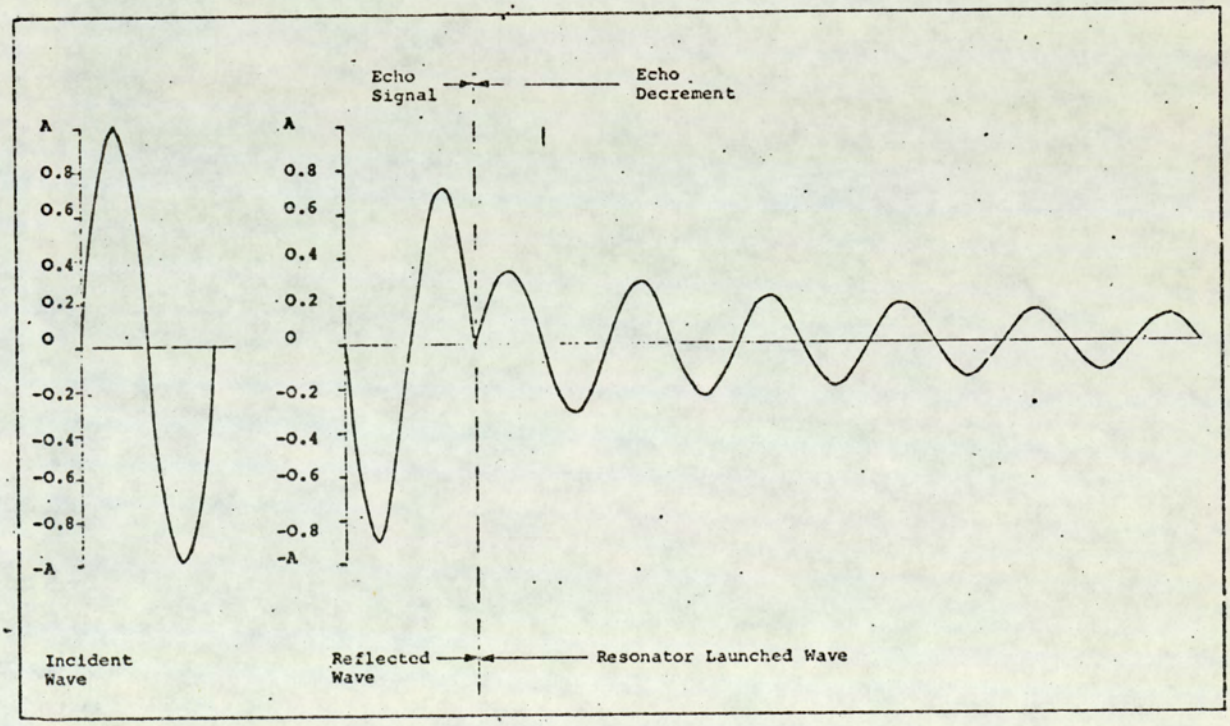

Fig. 3.6 (b) The echo produced by a wave of one cycle. As more half cycles are added the echo decrement becomes larger than the incident wave. At the point of equal amplitude the phase of the echo changes from that of the echo signal to that of the echo decrement.

x is positive and a displacement that decreases x is negative. Therefore if a positive half cycle, representing a positive displacement, impinges on this junction it will tend to increase x. If the impedance Z_L is infinite there will be no displacement; for this to happen a wave representing a negative displacement of the same amplitude must be reflected so that the resultant at the boundary is zero. Reducing the impedance will allow a displacement to take place; however if its amplitude is less than that of the wave producing it, a negative displacement wave will still be reflected but with diminished amplitude. This is represented by the first half cycle of the echo plotted in figure (3.5). Displacing the junction through half a cycle brings it back to the point x=a , but the portion of Z_L adjacent to the junction will now contain kinetic energy and therefore it will continue to move toward the reference launching a negative displacement wave, of half a cycle, back down the line. The process is repeated but next time the displacement is positive, and so it continues until the energy contained in Z_L is zero. This action is one of exponential decay, as one might expect from a system containing losses (i.e. the line), and is indicated thus in figure (3.5).

The effect of transmitting a burst containing one whole cylce can be obtained by superposition as shown in figure (3.6a). Waves that are launched from the resonator are seen to reinforce, hence increasing their amplitude. On the other hand the reflected wave from the junction is

cancelled by a wave that would have already been in the line due to the previous half cycle. The net effect is shown in figure (3.6b). What this means physically can be best understood by reconsidering figure (3.5) and the condition that existed after the first half cycle. That is that the junction was at the point a and moving towards the reference x=O. Therefore when the negative half cycle, representing a negative displacement, arrives at the junction the wave and junction are moving in the same direction. Hence the impedance Z_L presented to the line is reduced and so is the amplitude of the reflected wave. Increasing the burst length will further reduce Z_L and the amplitude of the reflection from the junction. If the burst length is increased such that its period is five times the time constant of the system (i.e. $5 \times 2M/Z_o$) a steady state condition will be approached. At this point the impedance Z_L, because it is assumed lossless, becomes zero, and the line resonator junction will appear as if it were a free boundary. On reflection from a free boundary a displacement wave does not change phase and therefore the resultant displacement at the boundary is twice that of the wave. The stress wave is, of course, of reverse polarity fulfilling the stress free end condition. This is dealt with in some detail in reference (33) p.81. With the steady state condition reached the echo will continue to be the total reflection, without inversion, of the transmitted wave. Since it has gone from an impedance greater than that of the line, at rest, to zero impedance

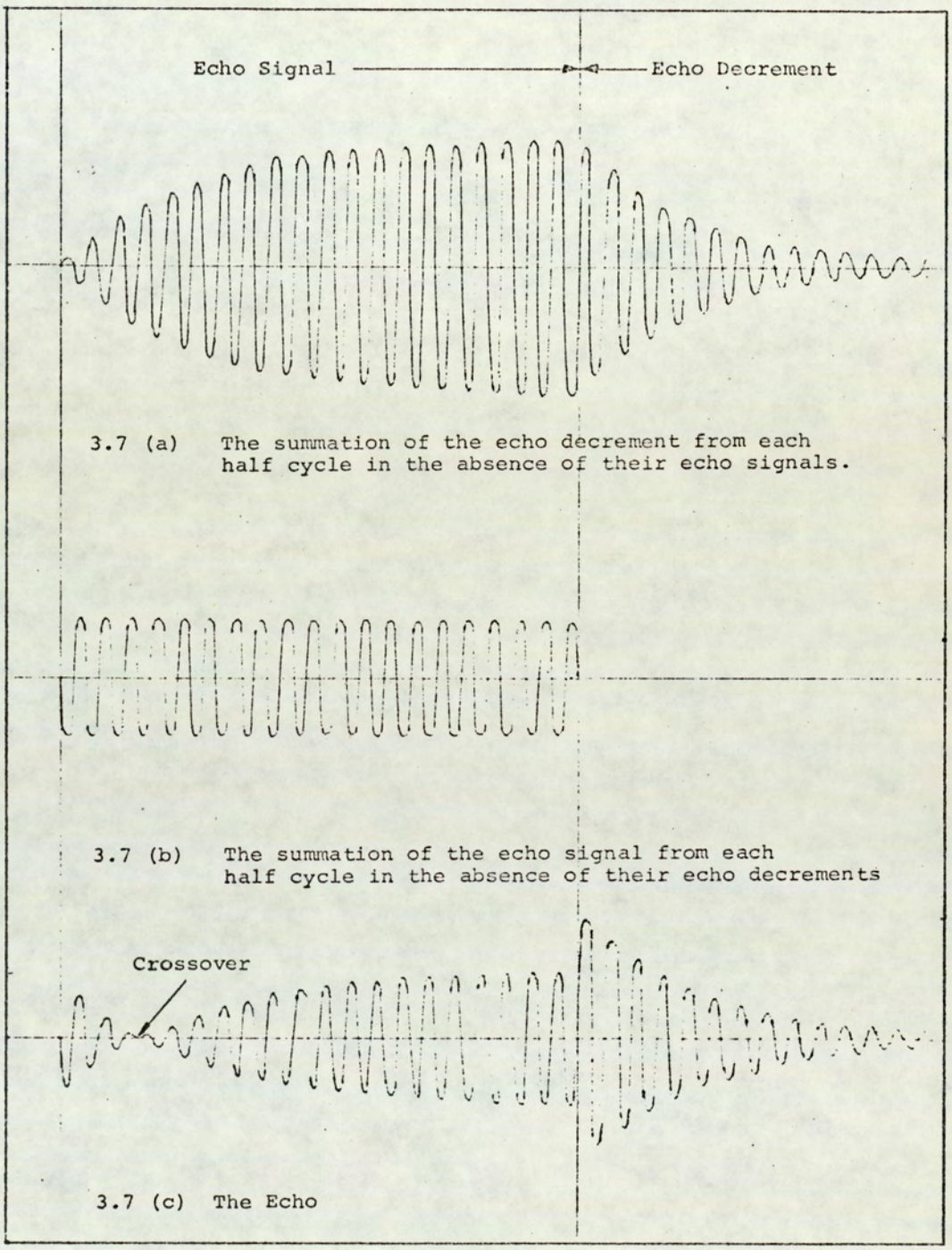

3.7 (a) The summation of the echo decrement from each half cycle in the absence of their echo signals.

3.7 (b) The summation of the echo signal from each half cycle in the absence of their echo decrements

3.7 (c) The Echo

Fig. 3.7

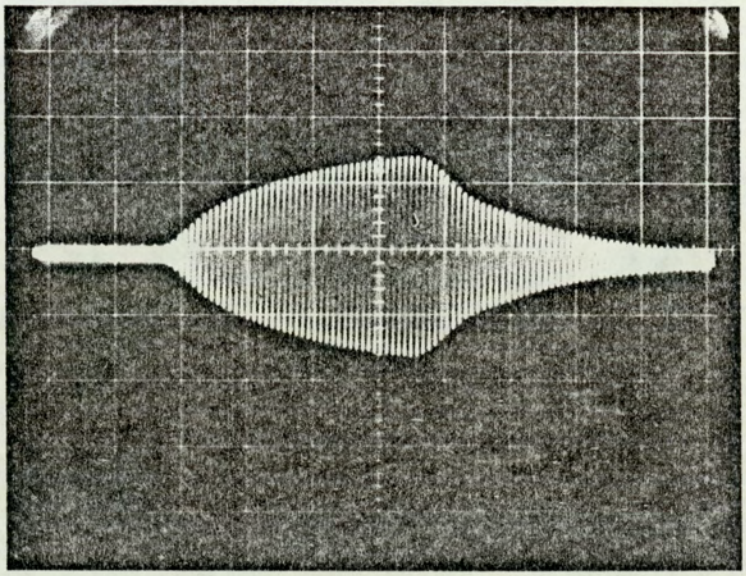

Fig. 3.8 Oscilloscope trace showing actual motion of the resonator of figure 3.3.

at the steady state point, Z_L will at some time have been equal to the line impedance Z_o. At that instant the reflection at the junction will be zero and therefore so will the echo. The term crossover is used to describe this effect.

When the steady state condition has been reached the displacement of Z_L adjacent to the junction must be twice the amplitude of the incident wave. Therefore when the burst comes to an end the resonator (Z_L) will start to launch a wave with this amplitude, this portion of the echo is called the echo decrement.

Since it is being suggested that the echo is made up of reflected waves from the junction and transmitted waves from the resonator (Z_L) it should be possible, by summing all the reflected waves and summing all the transmitted waves, as in figure (3.6a), to obtain two components which when superimposed produce the echo. The effect of doing this is shown in figure (3.7). Transmitted waves, on summation, are seen to rise exponentially toward a steady state value then,at the instant in time when the last reflected cycle has left the junction, decay in the same manner. This curve figure (3.7a) represents the actual displacement of the resonator, as it goes through its transient and steady states, due to the disturbing influence of the incident wave. Therefore if a second transmission line, used to receive only, is joined to the resonator, a wave of this shape will be transmitted. Figure (3.8) shows the oscilloscope trace of the received wave from this set up. The only part of curve (a) representing a transmitted wave from the

resonator is that which occurs when the disturbing force has ceased. i.e. the portion termed the echo decrement. Curve (b) is produced as a result of summing all the half cycles reflected from the junction. This is the echo one would get if the displacement of the resonator, as shown in curve (a), did not take place, which is tantamount to saying that the line is terminated with an infinite impedance Hence it is an inverted replica of the incident wave. Superposition of these curves, shown in figure (3.7c), does in fact give the required picture.

Terminating Impedance With Losses

The echo technique so far described has been used to measure material losses. Pelmore (34). The method being to construct a resonator from the specimen material and use it as the terminating impedance for the line. Introducing losses to the end of the line can produce quite dramatic changes in the shape of the echo; therefore a brief explanation, in terms of what has already been said, will be given.

It has been shown that the exponential shape of the echo results from the transient response of the terminating impedance Z_L to the input burst, and therefore at a time greater than five times the time constant a steady state condition will be reached. Beyond that point the junction, because the impedance was assumed lossless, was equivalent to a free boundary and hence total

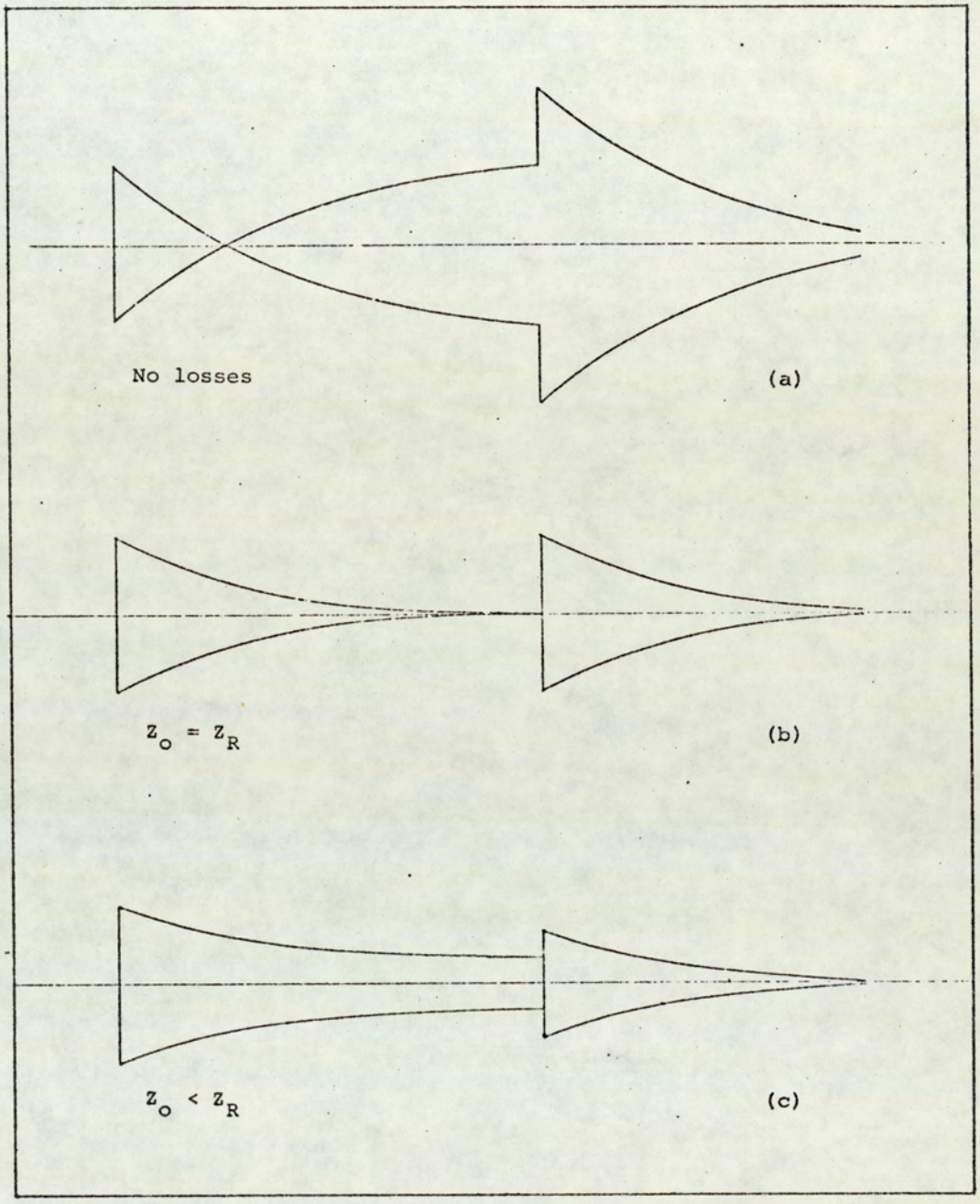

Fig. 3.9 The presence of losses in the resonator can produce quite drastic changes in the shape of the echo.

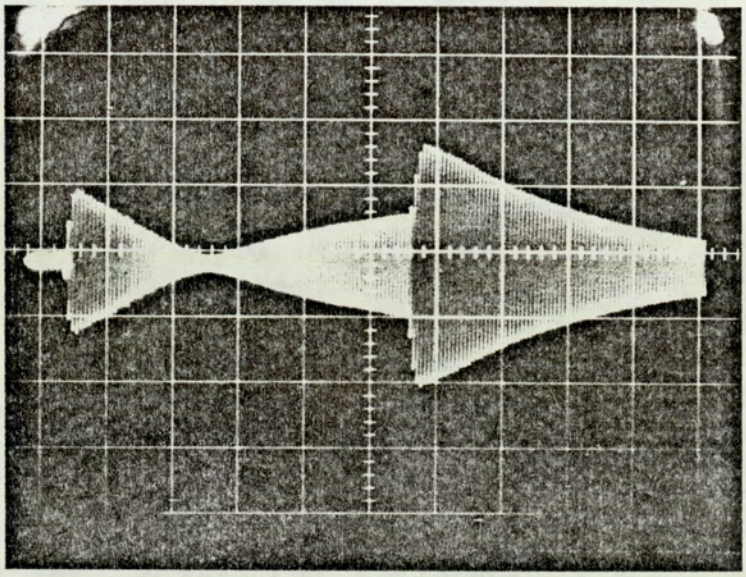

Fig. 3.10 Oscilloscope trace showing echo from the resonator of figure 3.3 at its third harmonic. The decrement is stepped and has three oscillations per step.frequency = 74.73.KHz

noninverted reflection occurred.

Including losses in Z_L insures that its value will not be zero at resonance but will have a magnitude equal to the loss term. This being the situation the amplitude of the steady state part of the echo, termed E_∞, will be dependent upon the losses. Figure (3.9) shows how the shape of the echo varies with increased losses. Denoting the value of Z_L at resonance by Z_R, figure (3.9b) shows that if $Z_o = Z_R$ no reflection occurs in the steady state. Sketch (c) shows that crossover is lost completely when $Z_o < Z_R$, this is to be expected since these values will result in a negative reflection coefficient.

Stepped Decrement

If the impedance Z_L has a harmonic spectrum of resonances, a stepping effect occurs on the echo for modes above the fundamental. An example of the type of impedance possessing such a spectrum would be the line resonator, where the frequency of resonance f_n is n times the fundamental i.e. $f_n = nf_1$. A typical echo obtained from this form of impedance is shown in figure (3.10). The number of oscillations per step will depend on the resonance. If the transmitter frequency is such that it excites the n^{th} harmonic each step will contain n cycles; therefore observation of the echo shown in figure (3.10) will indicate that the resonance is the third harmonic. The magnitude of distortion to the

decrement resulting from this phenomenon is mainly dependent upon the bandwidth of the receiver; since this is tuned to have a resonant peak at the transmitter frequency the effect is not very great, as can be seen from the figure.

To obtain a mathematical expression for this type of echo would require that Z_L, used in equation 3.10, contained a spectrum of resonances of the type described. The solution of 3.10 would consequently be of a considerably more complex form than that already obtained and would demand a great deal more effort in its attainment. However two comments about its character can be made. Firstly, the modulation only occurs during the transient state, which implies that the phenomenon itself has a transient behaviour that decays at approximately the same rate. Secondly it is an effect produced predominantly by the fundamental mode; this is supported by the fact that the step period for any mode is equal to the period of the fundamental.

CHAPTER 4

RESONATOR IMPEDANCES

CHAPTER 4

RESONATOR IMPEDANCES

4.1 Introduction

The concept of mechanical impedance of a system has been borrowed from electrical circuit theory. In the electrical circuit theory the impedance is defined as voltage divided by the current flow, using the analogy of the previous chapter, mechanical impedance is therefore force divided by velocity. Extending this analogue a complete family of relationships resembling those of the electrical theory can be obtained. This kind of approach allows mechanical systems to be described by more meaningful and more measurable parameters. For example it is far easier to measure the resonant frequency, Q or impedance of a system than it is to measure the displacement or force fields. Similarly to obtain the values of the components in an L, C and R electrical circuit measurement of the above three parameters would be made, allowing the required information to be obtained. No one would try to obtain these values by measuring the magnetic and electro-static fields.

The following discussion, on the impedance of mechanical resonators, presents a general method of obtaining an impedance expression in terms of the physical parameters of the resonator. This together with equation 3.10 for the reflection coefficient will

ultimately allow more information to be obtained from the echo about the terminating impedance.

An advantage to be gained by classifying mechanical systems in a similar way to those of electrical is in the application of standard techniques, used in electrical circuit theory, to complex mechanical systems. Such is the case of the Laplace Transforms technique which until quite recently was considered to be a tool more suitable for electrical engineers than mechanical engineers.

Of particular interest in the case of the echo technique is the driving point impedance. This is defined as the applied force at a point divided by the resulting velocity of that point. The driving point impedance is therefore the impedance presented to the end of the acoustic line by the resonator.

If the driving force applied at a point is divided by the velocity at some other point the impedance is then referred to as the transfer impedance.

Expressions for the driving point impedance of various structures can be found in references (35) to (45). There appears to be no general method of obtaining these expressions except to say that the starting point is always the same, in that inevitably, the impedance is given as force divided by velocity. The problem then arises in obtaining an expression for the force. This is quite simple in one dimensional systems, such as beams or rods where the stresses at boundaries are directly related to the driving force

and therefore can be used to obtain the required expression. In the case of two dimensional systems the problem becomes more complex and solutions are restricted to specific cases. An example of this is a disc driven in flexure. Because shear takes place along two axes an expression relating force to stress becomes a function of two variables. To overcome this the force is considered to be of point application at the centre of the disc. This gives the system symmetry by (a) eliminating the possibility of exciting anti-symmetric modes, and (b) reducing the number of variables of position for the point force to one. However this solution does only cover the specific case of centre drive. Of the more general case of a point force at an arbitrary position within the area of the disc the author has found no literature.

4.2 General Expression for Resonator Impedance

The two types of vibration to be considered are transverse and inplane. Transverse vibrations are the type of motions which takes place when the body is in flexure. Normally to obtain this kind of motion the driving force is applied somewhere within the boundary. The governing wave equation will therefore be inhomogeneous. Since the application of this force will in no way effect the boundary conditions, they will be of an homogeneous nature.

This system of equations are in contrast to those

describing inplane vibrations. A body performing this type of motion would be a rod in longitudinal mode. To excite a resonator of this type, using the echo technique previously described, the point of application of the force will be at one of the boundaries. It will be the boundary conditions therefore and not the equation of motion that are inhomogeneous.

The impedance expression to be formulated does not depend on the type of motion or the point of application of the force and as such can be considered to be quite general in its application. However, when a particular case is considered a decision has to be made as to whether the wave equation or the boundary conditions are modified if a final expression is to be obtained.

Assuming that the displacement W of the body under consideration may be represented by a normal-mode expansion, the following expression can be used,

$$W(x,t) = \sum_{n=1}^{\infty} \phi_n Y_n \qquad 4.1$$

in which ϕ_n is a time dependent function associated with the nth mode, and Y_n is the normal-mode solution of a homogeneous wave equation for the body and its associated boundary conditions. Y_n is a function of space only and may be dependent upon one, two or three variables. In obtaining an expression for the driving point impedance for the body two principles will be adopted, the principle of virtual work and D'Alembert's principle.

Also advantage is taken of the orthogonality property which exists between the normal modes Y_n. Therefore the virtual displacement produced by an externally applied force is

$$\delta W(x,t) = \delta\phi_m Y_m \qquad 4.2$$

δ being the Lagrangean symbol indicating the virtual nature of the variation.

For a system with the above displacement the strain energy V will be proportional to $|f(W)|^2$ or

$$V = k\int_o^\nu |f(W)|^2 \, d\nu \qquad 4.3$$

where f(W) is some spatial differential of W(x,t) such that it may be written as

$$\sum_{n=1}^{\infty} \phi_n^2 |f(Y_n)|^2 \qquad 4.4$$

The virtual work of the elasticity forces will be related to the variation in strain energy due to a virtual displacement given by equation 4.2; hence

$$\delta V = - \frac{\partial V}{\partial \phi_m} \delta\phi_m \qquad 4.5$$

Making the necessary insertions from equations 4.3 and 4.4 and performing the differentiation 4.5 becomes

$$\delta V = - 2k\phi_m \delta\phi_m \int_o^\nu |f(Y_m)|^2 \, d\nu \qquad 4.6$$

The inertia forces associated with the displacement W(x,t) will be

$$dT = - \rho \sum_{n=1}^{\infty} \ddot{\phi}_n Y_n d\nu \qquad 4.7$$

Assuming a virtual displacement $\delta W(x,t)$ the virtual work of the inertia forces over the whole body is

$$\delta T = - \rho \sum_{n=1}^{\infty} \ddot{\phi}_n \delta\phi_m \int_o^{\nu} Y_n Y_m d\nu \qquad 4.8$$

The orthogonality property of the normal modes is part of the Sturm-Lioville theorem reference (46) and can be written as

$$\int_o^{\nu} Y_n Y_m d\nu = 0 \quad (m \neq n) \qquad 4.9$$

Therefore equation 4.8 becomes

$$\delta T = - \rho \ddot{\phi}_m \delta\phi_m \int_o^{\nu} Y_m^2 \, d\nu \qquad 4.10$$

The expressions given by 4.6 and 4.10 represents the total work done by the resonator. If the vibration is produced by a force F, the virtual work done by this force will be

$$F \, \delta W(x,t)$$

or

$$F \delta\phi_m Y_{mf} \qquad 4.11$$

The subscript f indicates the need to evaluate Y_m at

the point of application of the force. If the motion were produced by a distributed force Y_{mf} would be the value of Y_m integrated over the area of application of the force. The equilibrium condition of D'Alembert allows the following equation to be obtained

$$2k\phi_m \int_o^\nu |f(Y_m)|^2 d\nu + \rho\ddot{\phi}_m \int_o^\nu Y_m^2 d\nu = F\, Y_{mf} \qquad 4.12$$

The velocity of any point on the body will be

$$u = \dot{W}(x,t) \qquad 4.13$$

or

$$u = \dot{\phi}_m Y_{mu}$$

where the subscript u implies the point of evaluation of Y_m. To obtain an expression for impedance the ratio F/u must be found; in it's Laplacean Transformation this becomes

$$\bar{z} = \int_o^\nu (2k|f(Y_m)|^2 + \rho s^2 Y_m^2) d\nu / s Y_{mf} Y_{mu} \qquad 4.14$$

Therefore providing the strain energy function is known and the normal mode solutions can be obtained the above expression can be used to find the driving point or transfer impedances. For the driving point impedance $\bar{z}_L$, $Y_{mf} = Y_{mu}$ and the product therefore may be replaced by Y_{md}^2. If comparison is made between equation 4.14 and the expression for the impedance of a series L - C electrical circuit, the following analogues may be made:

$$L \rightarrow \rho \int_o^{\nu} Y_m^2 \, d\nu \; / \; Y_{md}^2 \qquad 4.15$$

and

$$1/c \rightarrow 2k \int_o^{\nu} |f(Y_m)|^2 \, d\nu \; / \; Y_{md}^2 \qquad 4.16$$

It should be appreciated that k represents; in part, the relationship between stress and strain, and as such, if losses are considered, may be complex. This follows from expression 2.18 in chapter two. Therefore equation 4.16 will become the sum of two terms, one being analogous to the resistive term in an expression for the impedance of a series L, C and R electrical circuit.

4.3 Line Resonator

The commonest and probably the simplest system to find an impedance expression for is the Line or Rod resonator. Two factors are responsible for the relative ease in which this problem is solved. Firstly the spectrum of resonances is harmonic allowing the infinity of solutions to be described in terms of harmonic functions. Secondly the line resonator can be considered in terms of a one dimensional system, providing the limits given in section 3.2 are observed.

The wave equation for a one dimensional system is given by equation 3.7; using Laplace Transforms and including a term for the driving force, this may be

written as

$$(E + \eta s)\frac{\partial^2 \bar{W}}{\partial x^2} - \rho s^2 \bar{W} = \bar{G} \qquad 4.17$$

G will be a function of space and time. If the force is applied at one of the boundaries G will be zero and the system becomes a boundary value problem. It is not necessary to know its value, as it's presence in equation 4.17 is only to emphasize the condition of inhomogenity produced when the driving force lies between the boundaries. Assuming that one of the end boundaries is free (i.e. at x = 0) the normal mode solution to this equation is

$$\bar{W} = \sum_{n=1}^{\infty} \bar{\phi}_n \cos \bar{\gamma}_n x \qquad 4.18$$

where

$$\gamma_n^2 = - s^2 / (c_o^2 + s\eta/\rho) \qquad 4.18a$$

The strain energy function and the inertia forces are

$$\bar{V} = \tfrac{1}{2}(E + \eta s) \int_o^{\nu} (\frac{\partial \bar{W}}{\partial x})^2 \, d\nu \qquad 4.19$$

$$d\bar{T} = - \rho s^2 \sum_{n=1}^{\infty} \bar{W}_n \, d\nu \qquad 4.20$$

Using the procedure in section 4.2 the impedance can now be obtained. Therefore

$$\bar{Z} = - B \int_o^{\ell} \bar{Y}_n \bar{G}' \, dx + B(E + \eta s) \bar{Y}_n \frac{\partial \bar{Y}_n}{\partial x} \Bigg|_o^{\ell} \qquad 4.21$$

is the impedance of the line, B the cross-sectional area A of the line divided by s Y_{nf} Y_{nu} and ℓ its length. The expression is made up of two parts, one a function of the wave equation and the other a function of the boundary conditions. If the driving point impedance at the boundary $x = \ell$ is required ($x = 0$ being a free boundary), $\bar{G}'$ will be zero and $Y_{nf} = Y_{nu}$. Giving

$$\bar{Z}_L = A\rho s \tan \gamma_n \ell/\gamma_n \qquad 4.22$$

for the transfer impedance between the two end boundaries. $\bar{G} = 0$, $Y_{nf} = Y_n$ and $Y_{nu} = 1$; therefore

$$\bar{Z}_T = A\rho s \operatorname{Sin}\gamma_n \ell/\gamma_n \qquad 4.23$$

Results 4.22 and 4.23 are identical to those obtained by reference (29) and (35).

The driving point impedance for a point d somewhere within the boundaries will be given when $\bar{G}' \neq 0$, $Y_{nf} = Y_{nu}$ and the second term of equation 4.21 is equal to zero. As a result

$$\bar{Z}_L = \left(\frac{C^2\gamma^2_n}{s} + \frac{\eta\gamma^2_n}{\rho} + s\right)M/2 \operatorname{Cos}^2\gamma_n d \qquad 4.24$$

where M is the total mass of the line resonator, and $\gamma_n = n\pi/\ell$. Equation 4.24 has been obtained by reference (29) using the technique given by reference (39).

The accompanying Q for solutions 4.22 and 4.24 is the same and can be obtained from either equation 4.18a or 4.24 and is given as

$$Q_{mn} = \rho\omega_n/\gamma_n^2\eta \qquad 4.25$$

To obtain an expression for the echo, as described in Section 3.3, for a line terminated by a line resonator equation 4.22 will be applicable. Insertion into equation 3.10 for the reflection coefficient results in

$$R(s) = (\bar{Z}_o\gamma_n - A\rho\text{stan}\gamma_n\ell)/(\bar{Z}_o\gamma_n + A\rho\text{stan}\gamma_n\ell) \qquad 4.26$$

Using the Laplace transform of expression 3.13 as the forcing function and inverting the sum

$$g(s)\ R(s) \qquad 4.27$$

into the time domain a relationship for the echo results. A standard technique for inversion of 4.27 is by sumation of residues about each pole, reference (46). Because of the infinity of poles contained in equation 4.26 an exact solution is not possible; therefore approximations have to be made by considering only dominant poles. The poles of the reflection coefficient are found by solving for s between equation 4.18a and the denominator of equation 4.26. i.e.

$$s = \mp\ \omega_n/2Q_{mn} \pm (\omega_n^2/4Q_{mn}^2 - \gamma_n^2C^2)^{\frac{1}{2}} \qquad 4.28$$

where γ_n is complex and a solution of

$$\gamma_n C\alpha\text{Cot}\gamma_n\ell = \omega_n/2Q_{mn} \pm(\omega_n^2/4Q_{mn}^2 - \gamma_n^2C^2)^{\frac{1}{2}} \qquad 4.29$$

Solving these equations will give the exact position of the

poles in the s plane; however this can only be achieved by numerical computation unless approximations are made. The problem is greatly simplified if the resonator material is considered lossless. This transforms equations 4.28 and 4.29 to

$$s = \pm j\gamma_n C \qquad 4.30$$

and

$$\tan\gamma_n \ell = \pm j\alpha \qquad 4.31$$

where α is the ratio $Z_o/A\rho C$. Putting the solutions of 4.31 into 4.30 gives

$$s = -\frac{C}{2\ell} \ln \left|(1 + \alpha)/(1 - \alpha)\right| \pm j\omega_n \qquad 4.32$$

The zeros are obtained in a similar way and are given as

$$s = -\frac{C}{2\ell} \ln\left|(1 - \alpha)/(1 + \alpha)\right| \pm j\omega_n \qquad 4.33$$

Using the theorem

$$L^{-1}F(s) = \Sigma \text{ residues of } F(s)\exp(st) \qquad 4.34$$

a dominant pole approximation can now be obtained. The solution to this problem is given by references (30) and for the case of a lossless resonator the expression for the echo signal is

$$f(t) = A \sin(\omega_s t + \theta) + 4A\frac{\omega_s A_1 A_2}{\omega_n A_3 A_4} \exp(-A_1 t)\sin(\omega_n t + \alpha') \qquad 4.35$$

where

$$A_1 = \frac{C}{2\ell} \ln\left|(1+\alpha)/(1-\alpha)\right| \qquad \tan\theta = \frac{4\omega_s A_1 (A_1^2 + (\omega_n^2 - \omega_s^2))}{(A_1^2 + (\omega_n^2 - \omega_s^2))^2 - 4\omega_s^2 A_1^2}$$

$$A_2 = \left|A_1^2 + \omega_n^2\right|^{\frac{1}{2}}$$

$$\tan\alpha' = \frac{\omega_n (A_1^2 - (\omega_n^2 - \omega_s^2)) - 2A_1^2\omega_n}{A_1 (A_1^2 - (\omega_n^2 - \omega_s^2)) + 2A_1\omega_n^2}$$

$$A_3 = \left|A_1^2 + (\omega_n - \omega_s)^2\right|^{\frac{1}{2}}$$

$$A_4 = \left|A_1^2 + (\omega_n + \omega_s)^2\right|^{\frac{1}{2}} \qquad \omega_n = n\pi C/\ell$$

As with expression 3.14 section 3.3 the first term of equation 4.35 represents the reflection of the incident signal at the line-resonator boundary, and therefore has a frequency identical to the launched frequency. This is the echo that would result if the resonator were not set in motion (i.e. of infinite impedance). The second term is the actual displacement of the resonator and unlike equation 3.14 is seen to be at the natural frequency of the resonator. Therefore it would seem that at crossover the launched frequency and the natural frequency of the resonator are the same. Consider that $\omega_s = \omega_n$ in equation 4.35 then

$$f(t) = A \sin(\omega_n t + \theta) + 4A \frac{A_2}{A_4} \exp(-A_1 t) \sin(\omega_n t + \alpha') \qquad 4.36$$

and

$$A_2 = \left|A_1^2 + \omega_n^2\right|^{\frac{1}{2}} \qquad \tan\theta = \frac{4\omega_n A_1}{A_1^2 - 4\omega_n^2}$$

$$A_4 = \left|A_1^2 + 4\omega_n^2\right|^{\frac{1}{2}} \qquad \tan\alpha' = \frac{-\omega_n A_1}{A_1^2 + 2\omega_n^2}$$

A condition that should follow from $\omega_s = \omega_n$ for crossover to occur is $\tan(\theta - \alpha') = 0$. Evaluation of this leads to

$$\tan(\theta - \alpha') = -\frac{A_1 \omega_n}{2\omega_n^2 - A_n^2} \qquad 4.37$$

from which it can be seen that the two components of 4.36 will only be in anti-phase when $A_1 = 0$, which is tantamount to saying that the line impedance be zero. Therefore in the case of the line resonator the presence of the line does not effect the resonant frequency, but does produce a phase difference between reflected and resonator transmitted signals.

From the experimental point of view this phase shift will be compensated for, in order to obtain crossover, by adjusting the launched frequency. Inevitably this will lead to the situation that $\omega_s \simeq \omega_n$ at crossover and that for a line resonator the resonant frequency is best obtained from the echo decrement.

A system is very often described in terms of its coupling Q and oscillations to crossover. Q is related to the log decrement by $Q = \pi/\Delta$ where Δ is the log decrement and, from equation 4.36, can be shown to be

$$A_1 2\pi/\omega_n$$

Therefore the coupling Q is

$$Q_{cn} = \omega_n/2A_1 \qquad 4.38$$

Crossover is defined as the point where $f(t) = 0$. If

this occurs at a time $2n_x \pi/\omega_n$, the oscillations in that period will be

$$n_x = \frac{\omega_n}{4\pi A_1} \ln \left| 16(A_1^2 + \omega_n^2)/(A_1^2 + 4\omega_n^2) \right| \qquad 4.39$$

or since $\omega_n^2 >> A_1^2$

$$n_x = \frac{Q_{cn}}{\pi} \ln 2 \qquad 4.40$$

The velocity of sound in the resonator can be obtained from the relationship

$$C = \omega_n \ell / n \pi \qquad 4.41$$

From equations 4.38, 4.40 and 4.41 an expression for Young's modulus of the resonator can be found i.e.

$$E_R = \frac{Z_o}{\pi} \frac{\ell}{A} \frac{\omega_n}{n} \operatorname{Coth} \left| \frac{n}{n_x} \frac{\ln 2}{2} \right| \qquad 4.42$$

Table 4.1 shows the data used and the results obtained for the Brass resonator of Figure (3.10).

ρ_o	8.1×10^3 kg/m^3	Known Data
C_o	4.216×10^3 m/s	Known Data
A_o	$\pi 10^{-6}/4$ m^2	Measured
ℓ_R	7×10^{-2} m	Measured
A_R	$\pi 10^{-5}$ m^2	Measured
n	3	Experimental
ω_n	$2\pi 74.731 \times 10^3$ Hz	Experimental
n_x	35	Experimental
E_R	10.03×10^{10} N/m^2	Equation 4.42
C_R	3.49×10^3 m/s	Equation 4.41

Table 4.1

4.4 Bar In Flexure

If the force (the line) is applied to the bar so that it's direction is normal to the axis of the bar, and it's point of application lies between the end boundaries, the motion produced is said to be transverse of flexural. Motion of this type is performed by the tynes of a tuning fork.

Consider a bar of length ℓ, cross-sectional area A and radius of gyration about it's neutral axis k_1. Then according to the Bernoulli-Euler theory the equation of motion has the form

$$Ek_1^2 \frac{\partial^4 \bar{W}}{\partial x^4} + s^2 \rho \bar{W} = \bar{G} \qquad 4.43$$

where E, ρ and G have the same meaning as before. Also the strain energy function can be written as

$$V = \tfrac{1}{2} Ek_1^2 \int_0^{\nu} \left| \frac{\partial^2 \bar{W}}{\partial x^2} \right|^2 d\nu \qquad 4.44$$

and the inertia force as

$$dT = - \rho s^2 \sum_{n=1}^{\infty} \bar{W}_n d\nu \qquad 4.44$$

Assuming the normal mode expression of 4.1 the impedance expression can be obtained directly from equation 4.14. By suitable manipulation of the terms the impedance can be written as

$$\bar{Z}_L = B \int_0^{\ell} \bar{Y}_n \bar{G}' dx + Ek_1^2 B \left| \frac{\partial Y_n}{\partial x} \frac{\partial^2 Y_n}{\partial x^2} - Y_n \frac{\partial^3 Y_n}{\partial x^3} \right|_0^{\ell} \qquad 4.45$$

Again it can be seen that this expression is made up of two terms, the second term being totally a function of the boundary conditions. The simple boundary conditions that can exist are

1) Simply supported $\quad Y_n = \frac{\partial^2 Y_n}{\partial x^2} = 0$

2) Clamped $\quad Y_n = \frac{\partial Y_n}{\partial x} = 0$ $\qquad$ 4.46

3) Free $\quad \frac{\partial^2 Y_n}{\partial x^2} = \frac{\partial^3 Y_n}{\partial x^3} = 0$

Therefore when the limits are inserted the second term of equation 4.45 is zero for any combination of the above boundary conditions. Considering a bar of which boundary condition 1) applies at both ends the normal function will be

$$Y_n = \mathrm{Sin}\beta_n x \qquad 4.47$$

where $\beta_n = n\pi/\ell$. Insertion into equation 4.45 leads to a driving point impedance of

$$\bar{Z}_L = \left(\frac{C^2 k_1^2 \beta_n^4}{S} + S\right) M/2 \sin^2 \beta_n d \qquad 4.48$$

'd' being the point of drive measured from one of the ends. Losses can be accounted for by replacing C^2 by $C^2 + s\eta/\rho$, this will then give a material Q of

$$Q_n = \rho\omega_n / k_1^2 \beta_n^4 \eta \qquad 4.49$$

Letting

$$C_n = C^2 k_1^2 \beta_n^4 N_n$$

$$R_n = \eta k_1^2 \beta_n^4 N_n/\rho \qquad 4.50$$

$$N_n = M/2\sin^2\beta_n d$$

Equation 4.48 becomes

$$\bar{Z}_L = \frac{C_n}{S} + R_n + N_n s \qquad 4.51$$

This allows the reflection coefficient to be written as

$$R(s) = -1 + 2(Z_o + R_n)s/(N_n s^2 + (Z_o + R_n)s + C_n) \qquad 4.52$$

Because of the similarities between this expression and that of 3.13 a relationship for the echo can be obtained in the same way. At resonance the echo signal is

$$f(t) = A\left|\sin\omega_n t - 2\frac{\omega_n}{\omega_D}\exp\left(-\frac{Z_o+R_n}{2N_n}\right)t\sin\omega_D t\right| \qquad 4.53$$

This of course, assumes that the drive frequency is $\omega_n = (C_n/N_n)^{\frac{1}{2}}$. The frequency of the decrement ω_D is

$$\omega_D = (\omega_n^2 - (Z_o + R_n)^2/4N_n^2)^{\frac{1}{2}} \qquad 4.54$$

meaning that the actual resonant frequency of the resonator is lowered by both the line and internal friction. It can be seen that the term $Z_o/2N_n$ is a function of the line and it's position along the bar i.e.

$$Z_o/2N_n = Z_o\sin^2\beta_n d/M \qquad 4.55$$

Therefore best results are obtained by minimizing the

ratio Z_o/M and driving at a point close to a node. Assuming that $\omega_D \simeq \omega_n$ the total Q of the system is given by

$$1/Q_T = 1/Q_{cn} + 1/Q_{mn}$$

$$= \Delta'/\pi = Z_o/N_n\omega_n + R_n/N_n\omega_n$$

$$= \frac{Z_o 2\sin^2\beta_n d}{\omega_n M} + \frac{nk_1^2\beta_n^4}{\rho\omega_n} \qquad 4.56$$

and the oscillations to crossover by

$$n_x = \frac{Q_T}{\pi} \ln 2 \qquad 4.57$$

4.5 Disc in Flexure

The comments made in the previous section apply equally as well to the problem considered here. Although the problem here is in two dimensions, as opposed to the uni-dimensional systems of 4.3 and 4.4, the procedure is identical and there are no additional problems. The work however does become more involved when carrying out the integration of the normal mode functions. This is obviously because the normal mode shapes are described by non-harmonic functions. The property of orthogonality for the normal modes still applies and therefore equation 4.14 for the impedance can be used directly.

According to the classical theory, the equation of motion for the transverse displacement W of a plate

of thickness h and Poisson's ratio σ is given by

$$D\nabla^4\bar{W} + \rho s^2\bar{W} = \bar{G} \qquad 4.57$$

where

$$D = Eh^2/12(1 - \sigma^2) \qquad 4.58$$

The strain energy function given by reference (47) for a circular plate with the origin at its centre is

$$V = \frac{D}{2}\int_0^{\nu} \Big| (\nabla^2\bar{W})^2 - 2(1 - \sigma)\frac{\partial^2\bar{W}}{\partial r^2}(\nabla^2\bar{W} - \frac{\partial^2\bar{W}}{\partial r^2}) + 2(1 - \sigma)\Big(\frac{\partial^2\bar{W}/r}{\partial r\partial\theta}\Big)^2\Big| \, d\nu \qquad 4.59$$

the inertia force as before is

$$dT = -\rho s^2 \sum_{n=0}^{\infty} \bar{W}_n d\nu \qquad 4.60$$

The normal mode function can be found by solving the equation

$$\nabla^4 Y - k^4 Y = 0 \qquad 4.61$$

where $k^4 = \omega^2\rho/D$ and Y is the normal mode expansion. Equation 4.61 is the same as that of 4.57 with $\bar{G} = 0$ and the displacement W, which is a function of time and space, replaced by Y, which is a function of space only. Assuming that the boundary conditions possess symmetry with respect to one or more diameters and that the disc contains no holes, the solution of 4.61 is

$$Y = \sum_{n=0}^{\infty} Y_n \cos n\,\theta \qquad 4.62$$

Y_n being the normal mode shape in terms of r and having the form

$$A_n J_n(kr) + C_n I_n(kr) \qquad 4.63$$

J_n is a Bessel function of the first kind and I_n it's modified form. A_n and B_n are coefficients to be determined by the appropriate boundary conditions.

Utilizing the impedance expression 4.14 together with 4.59, 4.60 and 4.62 the following relationship for the driving point impedance can be obtained.

$$\bar{Z}_L = H\int_0^{2\pi}\int_0^a \bar{G}' Y_n \cos n\theta \; r\,d\theta\,dr + \frac{H}{2}\int_0^{2\pi} r\left|\frac{\partial Y_n}{\partial r} M_{rr} + Y_n V_r\right|_0^a d\theta \qquad 4.64$$

M_{rr} is the bending moment about the θ vector and V_r is the Kelvin-Kirchoff edge reaction. H is the plate thickness h divided by s Y_{nd}^2, and 'a' is the radius. The three basic boundary conditions for a circular plate are

1)	Simply Supported	$Y_n = M_{rr} = 0 \Big\vert_{r=a}$	
2)	Clamped	$Y_n = \frac{\partial Y_n}{\partial r} = 0 \Big\vert_{r=a}$	4.65
3)	Free	$M_r = V_r = 0 \Big\vert_{r=a}$	

It can be seen that for a plate possessing any one of these conditions the second term of equation 4.64 will be zero when the limits are inserted. Therefore the impedance becomes, after integrating with respect to θ

Mode	0,0	1,0	2,0	3,0	4,0	5,0	6,0	7,0	8,0	9,0
K^2_m	10.216	39.771	89.104	158.183	247.005	355.568	483.872	631.914	799.702	987.216

Table 4.2 Values of $K_m^2 = \omega_m a^2 (\rho/D)^{\frac{1}{2}}$ for a clamped disc.

(First ten symmetric modes)

Mode	0	1	2	3	4	5	6	7	8	9
0	10.216	21.26	34.88	51.04	69.666	90.739	114.213	140.056	168.245	198.756
1	39.771	60.82	84.58	111.01	140.108	171.803				
2	89.104	120.08	153.81	190.30						
3	158.183	199.06								

Table 4.3 Values of K_m^2 for the first 22 modes of a clamped disc.

$$\bar{Z}_L = H(Dk^4 + \rho s^2)\pi \int_o^a Y_n^2 \, r \, dr \qquad 4.66$$

Y_n^2 wil contain products of Bessel functions, when multiplied by r these form standard integrals, solutions of which can be found in reference (48).

Consider the case of a circular plate with a fixed (Clamped) boundary. In satisfying boundary condition 2) the normal mode shapes (eigen functions) are

$$Y_n = A_n(J_n(kr) - J_n(ka)\ I_n(kr)/I_n(ka)) \qquad 4.67$$

and the resulting frequency equation, obtained by satisfying both conditions and putting K = ka is

$$J_n(K)I_{n+1}(K) + I_n(K)J_{n+1}(K) = 0 \qquad 4.68$$

The eigenvalue K is a dimensionless frequency parameter, related to ω_m by

$$\omega_m = K_m^2 D^{\frac{1}{2}}/a^2\rho^{\frac{1}{2}} \qquad 4.69$$

The values of K_m^2 for the first 10 symmetric modes (i.e. n = 0) are given in table 4.2 and for the first 22 modes in Table 4.3. These were obtained from a more comprehensive set of results given in reference (49).

Substituting expression 4.67 in equation 4.66 and performing the integration, the driving point impedance for a thin disc with a fixed boundary is

$$\bar{Z}_L = (\frac{D'k^4}{s} + s)MA_n^2J_n^2(K_m)/Y_{nd}^2 \qquad 4.70$$

where $D' = D/\rho$ and Y_{nd}^2 is obtained by squaring equation

4.67 and evaluating at the point of drive i.e.

$$Y_{nd}^2 = A_n^2 J_n^2(K_m)(J_n(K_m\alpha)/J_n(K_m) - I_n(K_m\alpha)/I_n(K_m))^2$$

4.71

α is the ratio d/a where d is the radius of the point at which the impedance is to be measured.

The expression for the normal mode shape of a simply supported disc is identical to 4.67, and so integration of Y_n^2 will be the same as for the fixed boundary. However, because of the difference in the second terms of boundary conditions 1) and 2) the factoring of terms after integration does not take the same form. The resulting impedance expression therefore becomes

$$\bar{Z}_L = (\frac{D'k^4}{s} + s)MA_n^2 J_n^2(K_m)P/Y_{nd}^2 \qquad 4.72$$

where K_m now satisfies the frequency equation for a simply supported disc (reference 49) i.e.

$$J_n(K)I_{n+1}(K) + I_n(K)J_{n+1}(k) = 2KJ_n(K)I_n(K)/(1-\sigma)$$

4.73

and P has the value

$$(1+2K_m^2/(1-\sigma)^2 - 2(1+n)/(1-\sigma) - 2K_m I_{n+1}(K_m)/(1-\sigma)I_n(K_m))$$

4.74

Comparing equations 4.70 and 4.48 it can be seen that they are identical in form and therefore will result in a similar expression for the echo produced in an acoustic transmission line, when the terminating impedance

is a fixed disc. Therefore from equation 4.51

$$C_n \equiv D'k^4 N_n \qquad 4.75$$

$$N_n \equiv MA_n^2 J_n^2(K_m)/Y_{nd}^2 = M/U_n \qquad 4.76$$

Equations 4.54 to 4.57 can now be used without modification to give

$$\omega_D = (\omega_m^2 - Z_o^2/4N_n^2)^{\frac{1}{2}} \qquad 4.77$$

where $Z_o/2N_n$ is now $Z_o U_n/2M$.

The line to disc coupling Q will then be

$$Q_c = \pi\rho h^2 C_p K_m^2/\sqrt{12}\ Z_o U_n \qquad 4.78$$

Cp is the plate velocity given by equation 2.16 chapter two, U_n is the ratio $Y_{nd}^2/A_n^2 J_n^2(K_m)$, and ρ the density of the plate. Equation 4.57 will then give the number of oscillations to crossover as

$$n_x = \rho h^2 C_p K_m^2 \ell n 2/\sqrt{12}\ Z_o U_n \qquad 4.79$$

For the above expressions to have any physical meaning the value of U_n must be known. This of course will vary according to the drive position on the plate. In the case of the rod inflexure the amplitude of $\bar{Z}_L$, Q_{cn} or n_x as a function of drive position can be obtained from standard Sine Tables.

The full expression for U_n can be written as

$$U_n = (J_n(K_m\alpha)/J_n(K_m) - I_n(K_m\alpha)/I_n(K_m))^2 \qquad 4.80$$

U_n FOR CLAMPED DISC

MODE	α = 0.0	0.1	0.2	0.3	0.4	0.5	0.6	0.7	0.8	0.9
0.0	10.939	10.449	9.083	7.130	4.978	3.011	1.504	0.566	0.130	0.009
0.1	0.000	0.775	2.647	4.540	5.411	4.855	3.281	1.564	0.433	0.036
0.2	0.000	0.036	0.488	1.827	3.714	4.935	4.502	2.708	0.899	0.086
1.0	19.629	15.988	7.993	1.560	0.091	2.039	3.581	2.854	1.085	0.110
0.3	0.000	0.001	0.073	0.593	2.054	4.039	4.964	3.759	1.493	0.164
1.1	0.000	3.218	7.891	6.976	2.088	0.026	2.018	3.312	1.803	0.226
0.4	0.000	0.000	0.010	0.170	1.001	2.912	4.819	4.590	2.176	0.274
1.2	0.000	0.288	2.958	6.688	5.528	0.996	0.485	2.963	2.450	0.382
2.0	29.611	18.451	2.474	1.154	4.763	2.023	0.085	2.456	2.494	0.417
0.5	0.000	0.000	0.001	0.045	0.448	1.925	4.284	5.123	2.894	0.417
1.3	0.000	0.018	0.747	3.944	6.561	3.368	0.008	2.132	2.944	0.578
0.6	0.000	0.000	0.000	0.011	0.188	1.196	3.581	5.371	3.607	0.594
2.1	0.000	7.623	10.727	1.764	1.347	4.031	0.581	1.151	2.852	0.652
0.7	0.000	0.000	0.000	0.003	0.076	0.710	2.856	5.369	4.283	0.803
1.4	0.000	0.001	0.150	1.797	5.531	5.368	0.675	1.186	3.226	0.806
2.2	0.000	1.126	7.771	7.131	0.144	3.026	2.282	0.217	2.856	0.921
3.0	39.478	16.269	0.124	6.383	1.109	1.928	2.637	0.079	2.722	0.956
0.8	0.000	0.000	0.000	0.001	0.029	0.406	2.197	5.174	4.895	1.045
1.5	0.000	0.000	0.026	0.696	3.834	6.253	2.072	0.427	3.295	1.063
2.3	0.000	0.105	3.130	8.389	2.818	0.911	3.544	0.025	2.560	1.211
0.9	0.000	0.000	0.000	0.000	0.011	0.227	1.649	4.869	5.469	1.332
3.1	0.000	13.133	7.190	0.996	4.886	0.006	3.283	0.228	2.207	1.276

TABLE 4.4

U_n FOR CLAMPED DISC

α

MODE	0.0	0.1	0.2	0.3	0.4	0.5	0.6	0.7	0.8	0.9
0.0	10.939	10.449	9.083	7.130	4.978	3.011	1.504	0.566	0.130	0.009
1.0	19.629	15.988	7.993	1.560	0.091	2.039	3.581	2.854	1.085	0.110
2.0	29.611	18.451	2.474	1.154	4.763	2.023	0.085	2.456	2.494	0.417
3.0	39.478	16.269	0.124	6.383	1.109	1.928	2.637	0.079	2.722	0.956
4.0	49.350	10.972	4.582	3.469	2.411	2.043	1.630	1.416	1.351	1.623
5.0	59.222	4.986	9.571	0.125	4.014	1.958	0.706	2.766	0.072	2.216
6.0	69.086	0.844	8.098	5.184	0.105	2.031	3.243	0.577	0.500	2.525
7.0	78.959	0.241	2.242	5.360	4.854	1.969	0.076	0.598	1.967	2.425
8.0	88.811	3.424	0.184	0.191	1.066	2.024	2.656	2.789	2.424	1.931
9.0	98.702	9.143	4.797	3.249	2.456	1.975	1.652	1.420	1.241	1.207

Table 4.5

U_n FOR CLAMPED DISC

MODE	α 0.0	0.1	0.2	0.3	0.4	0.5	0.6	0.7	0.8	0.9
0.0	10.939	10.449	9.083	7.130	4.978	3.011	1.504	0.566	0.130	0.009
0.1	0.000	0.775	2.647	4.540	5.411	4.855	3.281	1.564	0.433	0.036
0.2	0.000	0.036	0.488	1.827	3.714	4.935	4.502	2.708	0.899	0.086
0.3	0.000	0.001	0.073	0.593	2.054	4.039	4.964	3.759	1.493	0.164
0.4	0.000	0.000	0.010	0.170	1.001	2.912	4.819	4.590	2.176	0.274
0.5	0.000	0.000	0.001	0.045	0.448	1.925	4.284	5.123	2.894	0.417
0.6	0.000	0.000	0.000	0.011	0.188	1.196	3.581	5.371	3.607	0.594
0.7	0.000	0.000	0.000	0.003	0.076	0.710	2.856	5.369	4.283	0.803
0.8	0.000	0.000	0.000	0.001	0.029	0.406	2.197	5.174	4.895	1.045
0.9	0.000	0.000	0.000	0.000	0.011	0.227	1.649	4.869	5.469	1.332

Table 4.6

This equation in fact shows how the admittance varies as a function of d for any given mode. The condition that U_n is zero implies that the impedance Z_L is infinite, which will be the situation at any one of the nodes. Putting $U_n = 0$ in 4.80 results in an equation identical to the one given by reference (49) for determining the position of the nodes for a calmped disc. The values of U_n for the first 22 modes for values of α between 0 and 1 in steps of 0.1 are given in Table 4.4. Table 4.5 gives the first 10 symmetric modes and Table 4.6 the first 10 modes containing no nodal circles.

4.6 General Discussion

The major purpose of this chapter is to demonstrate a method of obtaining impedance expressions for mechanical resonators. It is presented as support for the discussion of the echo in the previous chapter, by illustrating how that discussion applies to all types of resonators. An example of this would be the oscillations to crossover, where from the three systems considered it is seen that n_x is proportional to the density of the resonator and inversly proportional to the characteristic impedance of the line.

The most useful aspect of the foregoing equations is that they highlight the inaccuracies that may occur, due to the presence of the line, when measuring resonant

frequencies. This is most obvious in the case of flexure, where for the rod and disc (equations 4.54 and 4.77) the decrement frequency is seen to be lower than the natural frequency of the resonator. In both cases the magnitude of this damping is proportional to the characteristic impedance of the line and it's position on the resonator. Considering the clamped disc for example, the frequency of the decrement goes down as U_n increases. This would appear to conflict with experiment however since as shown in the following table the inverse happens.

α	U_n	f_n (measured)
0.00	19.629	16.591×10^3 Hz
0.38	0.000	16.146×10^3 Hz
0.64	3.547	16.357×10^3 Hz

Table showing how the measured frequency varies with U_n for the 1, 0 mode using a 1 mm diameter line.

The reason for this contradictory behaviour stems from the crossover method used to obtain these results. From the analogies made earlier of force/voltage and velocity/current it may be assumed that for frequencies above resonance the velocity lags the force, and for frequencies below resonance the force lags the velocity. In other words at $\omega > \omega_n$ the velocity of the resonator will lag the force producing it. In view of this, the apparent frequency anomaly in the above table can be

explained. Consider the echo shown in Figure 3.7. As previously stated plot 'b' is the echo that would be recieved if the line were terminated by an infinite impedance. It is at the same frequency ω_n as the incident wave but 180° out of phase. Plot 'a' is the actual displacement of the resonator and is drawn in phase with the incident wave and at the natural frequency ω_n of the resonator. In the case under consideration this is not the situation since the displacement of the resonator is at ω_D. Therefore at the point where the amplitudes of plot 'a' and plot 'b' are the same, the cancellation will not occur, because around this area the sine waves will not have a phase difference of 180°. To obtain a crossover it is necessary to adjust the phase of plot 'a' so that at the point of equal amplitude an anti phase condition occurs. This can only be done by producing a phase lag and to do this ω must be increased. As U_n increases therefore the phase lag has to increase, hence the drive frequency must be increased for crossover to occur.

The error produced by this frequency damping can be minimised by keeping U_n or Z_o small. Unless an absolute value of ω_n is required, as in the case of measuring resonator parameters, this error will not be of significant magnitude to create problems. The natural frequency of the resonator may be obtained from

$$\omega_n = 2\pi\omega_D/(4\pi^2 - \Delta^2)^{\frac{1}{2}}$$

where ω_D and Δ can be measured from the echo decrement.

Mode	n_x exp.	n_x calc.	f exp. KHz	f calc. KHz
0,1	5	4	8.93	8.76
0,2	6	5	14.25	14.37
1,0	9	6	16.36	16.38
0,3	6	6	20.07	21.03
1,1	15	11	23.97	25.05
0,4	8	7	27.13	28.7
1,2	no c/over	28	32.48	34.84
2,0	-	52	-	36.71
0,5	11	9	34.57	37.38
1,3	-	137	-	45.73
0,6	16	13	43.04	47.05
2,1	no c/over	∞	46.14	49.47
0,7	20	18	52.06	57.7

Table 4.7 Experimental and Calculated values of n_x and frequency for Mild Steel clamped disc α=0.64

Mode	n_x exp.	n_x calc.	f exp. KHz	f calc. KHz
0,1	0	2	8.76	8.76
0,2	7	6	14.05	14.37
1,0	no c/over	∞	16.15	16.38
0,3	15	15	20.23	21.03
1,1	13	10	24.09	25.05
0,4	43	46	26.93	28.7
1,2	11	7	32.63	34.84
2,0	15	10	34.7	36.71
0,5	no c/over	147	41.31	37.38
1,3	13	9	42.29	45.73
0,6	no c/over	481	44.97	47.05
2,1	81	108	46.1	49.47
0,7	-	1604	-	57.7
1,4	13	15	52.37	57.7
2,2	no c/over	90	59.066	63.37
3,0	33	33	63.15	65.17

Table 4.8 Experimental and Calculated values of n_x and frequency for Mild Steel clamped disc α=0.38

U_n For Clamped Disc

α

MODE	0.30	0.31	0.32	0.33	0.34	0.35	0.36	0.37	0.38	0.39
0.0	7.130	6.917	6.702	6.487	6.270	6.053	5.837	5.621	5.405	5.191
0.1	4.540	4.686	4.821	4.943	5.052	5.148	5.230	5.297	5.350	5.388
0.2	1.827	2.007	2.191	2.380	2.572	2.766	2.961	3.154	3.345	3.532
1.0	1.560	1.178	0.851	0.579	0.361	0.196	0.082	0.018	0.000	0.026
0.3	0.593	0.693	0.803	0.924	1.056	1.198	1.351	1.154	1.685	1.866
1.1	6.976	6.556	6.099	5.162	5.104	4.584	4.059	3.539	3.033	2.547
0.4	0.170	0.211	0.259	0.316	0.382	0.458	0.543	0.640	0.749	0.869
1.2	6.688	6.862	6.975	7.021	7.000	6.911	6.755	6.533	6.251	5.914
2.0	1.154	1.615	2.101	2.593	3.069	3.512	3.906	4.236	4.494	4.671
0.5	0.045	0.059	0.077	0.099	0.127	0.160	0.200	0.248	0.305	0.371
1.3	3.944	4.350	4.747	5.125	5.476	5.792	6.063	6.281	6.441	6.535
0.6	0.011	0.015	0.021	0.029	0.040	0.053	0.070	0.091	0.117	0.149
2.1	1.764	1.127	0.628	0.273	0.065	0.000	0.069	0.257	0.548	0.918
0.7	0.003	0.004	0.006	0.008	0.012	0.017	0.023	0.032	0.043	0.057
1.4	1.797	2.120	2.470	2.843	3.236	3.637	4.043	4.446	4.834	5.199
2.2	7.131	6.329	5.468	4.580	3.698	2.855	2.081	1.405	0.846	0.423
3.0	6.383	6.377	6.174	5.793	5.262	4.616	3.895	3.143	2.402	1.712
0.8	0.001	0.001	0.001	0.002	0.003	0.005	0.007	0.011	0.015	0.021
1.5	0.696	0.877	1.088	1.332	1.609	1.918	2.257	2.624	3.013	3.149
2.3	8.389	8.382	8.217	7.895	7.426	6.825	6.117	5.328	4.492	3.643
0.9	0.000	0.000	0.000	0.001	0.001	0.001	0.002	0.003	0.005	0.008
3.1	0.996	1.687	2.453	3.226	3.942	4.547	4.995	5.256	5.315	5.173

Table 4.9

U_n For Clamped Disc

MODE	α = 0.6	0.61	0.62	0.63	0.64	0.65	0.66	0.67	0.68	0.69
0,0	1.504	1.385	1.271	1.163	1.061	0.965	0.874	0.789	0.710	0.635
0,1	3.281	3.101	2.920	2.740	2.561	2.385	2.211	2.042	1.877	1.718
0.2	4.502	4.366	4.217	4.055	3.883	3.702	3.512	3.316	3.116	2.912
1.0	3.581	3.610	3.614	3.593	3.547	3.479	3.389	3.279	3.152	3.010
0.3	4.964	4.940	4.893	4.822	4.729	4.614	4.478	4.323	4.150	3.962
1.1	2.018	2.261	2.489	2.697	2.879	3.034	3.157	3.248	3.304	3.325
0.4	4.819	4.921	4.997	5.046	5.068	5.060	5.023	4.957	4.862	4.739
1.2	0.485	0.712	0.966	1.239	1.522	1.806	2.083	2.344	2.582	2.790
2.0	0.085	0.212	0.387	0.604	0.852	1.125	1.405	1.689	1.965	2.223
0.5	4.284	4.488	4.672	4.834	4.971	5.079	5.156	5.200	5.210	5.185
1.3	0.008	0.010	0.079	0.212	0.400	0.635	0.906	1.204	1.515	1.828
0.6	3.581	3.847	4.106	4.352	4.581	4.790	4.972	5.125	5.244	5.327
2.1	0.581	0.325	0.140	0.031	0.000	0.046	0.162	0.342	0.576	0.850
0.7	2.856	3.148	3.443	3.739	4.029	4.310	4.574	4.818	5.036	5.221
1.4	0.675	0.386	0.175	0.046	0.000	0.036	0.150	0.332	0.575	0.864
2.2	2.282	1.838	1.402	0.996	0.640	0.352	0.145	0.028	0.002	0.068
3.0	2.637	2.237	1.180	1.384	0.982	0.628	0.342	0.137	0.023	0.004
0.8	2.197	2.483	2.784	3.097	3.417	3.739	4.057	4.367	4.660	4.932
1.5	2.072	1.561	1.102	0.709	0.394	0.168	0.037	0.001	0.059	0.204
2.3	3.544	3.269	2.906	2.480	2.017	1.549	1.103	0.707	0.384	0.153
0.9	1.649	1.912	2.198	2.505	2.829	3.167	3.514	3.865	4.212	4.550
3.1	3.283	3.282	2.153	2.908	2.569	1.162	1.719	1.273	0.856	0.500

Table 4.10

Tables 4.7 and 4.8 show results obtained from experiments carried out on a clamped mild steel disc. The disc, 5.5 cm diameter and 1.25 mm thick, was machined in and concentric with a larger disc 19.2 cm diameter and 3.3 cm thick. Acoustic line parameters are as shown in Table 4.1. Two experiments were carried out, one at $\alpha = 0.38$ and one at $\alpha = 0.64$, to measure the frequency at crossover and the number of oscillations to crossover. Comparisons were then made with calculated values obtained from equations 4.69 and 4.79. To compute n_x for the values of α chosen it is necessary to know U_n in these regions. Tables 4.9 and 4.10 show these values.

The accuracy of the frequency measurements varies with mode, it is only the first three modes however that can be considered as satisfactory results. With the exception of only one all the experimental values are low compared with theory. This effect is due to the influence of rotary inertia and shear, allowance for which is omitted from the classical theory of plate vibrations. A reduction in the ratio of thickness to diameter for the disc would minimize the effect but would lower the frequency range at which the modes occur and create problems in measurement.

The values of n_x are very good in view of the dominant pole approximation that has been made and the distribution of the modes. A useful point to observe about these values of n_x is their use in mode identification.

This is extremely obvious in the case of 0, 7 and 1, 4 modes in table 4.8 where the resonant frequencies are the same.

CHAPTER 5

END RESONANCES OF CYLINDERS (SOLID AND HOLLOW)

5.1 Introduction

5.2 Discussion of Experiments

5.3 Discussion of Results

CHAPTER 5

END RESONANCES OF CYLINDERS (SOLID AND HOLLOW)

5.1 Introduction

Resonant modes of vibration occur in many structures, in general the whole volume of the body plays a part in determining the natural frequency and the displacement field. In the case of an end resonance this is not so. The motion associated with end resonance in cylinders is confined to the first few diameters of length, the remainder being virtually unaffected. Hence the situation arises that the resonant frequency is a function of the cylinder diameter only.

The phenomenon was first observed by Oliver ref. (50). Oliver carried out experiments to measure the dispersion of the lower modes of propogating waves in a cylindrical rod, and observed a resonance associated with it's ends. His results showed that the end resonance was coupled to a propogating mode, which resulted in the gradual leakage of stored energy down the rod. The results of this thesis show this to be the case for the axi-symmetric mode only. Of the anti-symmetric modes very little energy it lost to a propogating wave which explains why Oliver could only detect such modes with transmitter and reciever at the same end.

No exact mathematical solution is known for the study of finite or semi-infinite rods, of which end resonance

is part. Publications ref. (51), (52) and (9) do exist however which offer approximate solutions, the above three giving special attention to the computation of the end resonant frequency. Of the literature found on the topic of end resonance only one made any reference to the anti-symmetric end modes. There are three possible reasons for this.

a) They were only briefly mentioned by Oliver and it is probable that their existance is not well known.

b) The problems created by the consideration of a third displacement component would make the mathematics extremely difficult to handle, and

c) The problems involved in exciting such modes experimentally. The later of these has been overcome by the use of the echo technique described earlier.

Non existance of exact solutions for a rod with a free boundary normal to it's axis arise from the inability to satisfy the accompanying boundary conditions, that is that stresses σ_{zz} and σ_{zr} vanish. It is generally accepted that both stresses will only disappear simultaneously if higher branches of the propogating mode are generated at the boundary to cancel the excess stress. The position of end resonance, for the axisymmetric mode, on the frequency spectrum is approximately $\Omega = 3$. Examination of the dispersion curves of Figure 2.1, Chapter two will show that there is one mode with a real propogation constant and an infinite number which have complex propogation at this frequency. Therefore an accurate

solution is impossible. The approximate solutions of ref. (51), (52) and (9) are all based on this theory, each one considering various numbers of modes. The results of experimental work carried out by McMahon ref. (53) on the vibration of cylinders of various lengths, show that as the length to radius ratio h/a increased the inplane and corresponding flexural modes of discs approach a common mode, where the partical displacement is predominantly at the ends of the cylinder. His results show that this is true for both the symmetric and anti-symmetric modes.

Booker and Sagar, ref. (54), for similar experiments have presented results of the resonant frequencies for a finite aluminium rod with a h/a ratio of 30. The results show a number of unidentified resonances. Points on the frequency spectrum where these modes occur, do infact coincide with those of the anti-symmetric end resonances.

The anti-symmetric modes all have the common feature that their frequency is of the order of 10% below the cut off frequency of the lowest propogating mode of their family. For example the family of F(2,n) modes of figure 2.3 Chapter Two have an end resonance 10% below the cut off frequency at the F(2,1) mode, and for the F(3,n) family 10% below the F(3,1) mode. The modes are easily identified by the number of nodal diameters they possess, the general rule being that the F(m,1) mode will have a displacement pattern, on the end boundary, containing m nodal diameters. These diameters are continued as

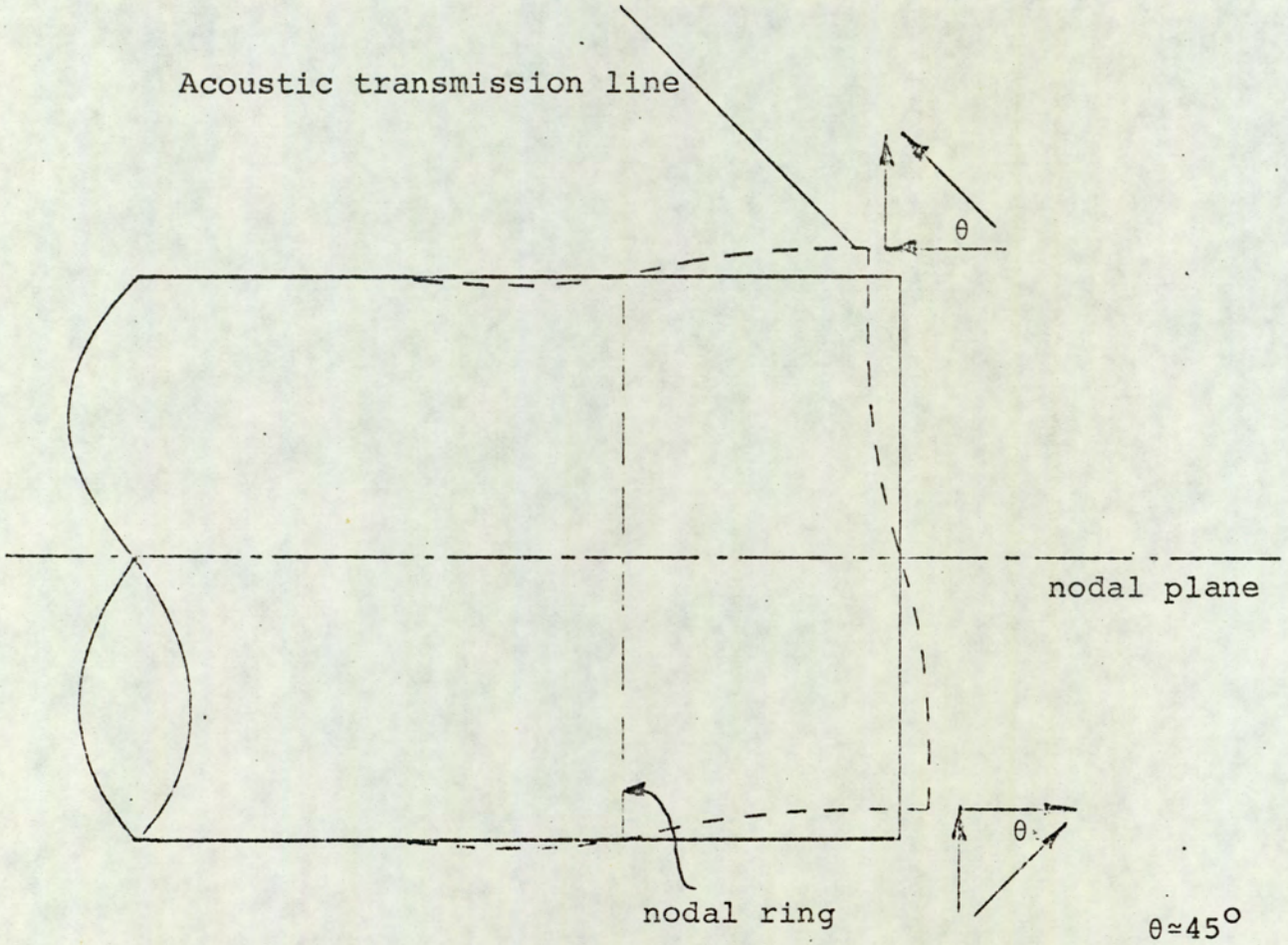

Fig. 5.1 Orientation of transmission line with respect to cylindrical axis. Displacement components have approximately the same magnitude at the periphery giving a resultant displacement at 45° to the axis.

Cut-off and Disc Frequencies

Mode	σ	0	0.1	0.2	0.3	0.4
F(2,1)	rod	2.33618	2.34056	2.34446	2.3794	2.35107
	disc	2.33620	2.34020	2.34323	2.34559	2.34749
	$\frac{\text{rod}}{\text{disc}}$	0.99999	1.00015	1.00052	1.00100	1.00152
F(3,1)	rod	3.54520	3.57165	3.59461	3.61455	3.63199
	disc	3.54522	3.56942	3.58734	3.60107	3.61189
	$\frac{\text{rod}}{\text{disc}}$	0.99999	1.00062	1.00203	1.00374	1.00556
F(8,1)	rod	8.27184	8.43074	8.57730	8.71031	8.82962
	disc	8.27186	8.41679	8.52994	8.61972	8.69218
	$\frac{\text{rod}}{\text{disc}}$	1.00000	1.00166	1.00555	1.01051	1.01581

Table 5.1 Comparison of cut-off values of Ω for a solid cylinder with corresponding inplane disc values. $\Omega = \omega a/C_s$.

nodal planes down the axis of the rod and declare themselves as nodal lines parallel to the axis, at the periphery. In addition there exist a nodal ring at a distance from the end face which varies according to frequency.

Another characteristic which is common to these modes is the amplitude of the radial and axial displacements at the edge where the cylindrical and plane surfaces meet. Experiments have shown that the magnitude of these displacements are equal, and therefore best coupling to these modes is obtained when the acoustic line makes an angle of 45° to the axis of the cylinder. Figure 5.1 shows how the line is orientated with respect to the maximum displacement.

For hollow cylinders the angle of the resultant displacement varies according to wall thickness. Thin wall cylinders couple best with the line joined to the rod normal to the axis.

Since the end resonant frequencies of the anti-symmetric modes bear a relationship to their cut off frequencies the values of the latter were calculated. This was achieved by using equation 2.46, Chapter Two. Computation of the natural frequencies for contour vibrations of thin discs using the equations given by Love (p 498) show, somewhat surprisingly, that the cut-off and disc frequencies are almost identical. Table 5.1 gives a comparison between the two frequencies for the modes F(2,1), F(3,1) and F(8,1), and various values of Poisson's Ratio. A complete set

of results for cut-off frequencies and disc frequencies for the first nine anti-symmetric modes are given in Appendix 5.1.1 Poisson's Ratio from zero to 0.4 in steps of 0.01.

5.2 Discussion of Experiments

From the equations of the preceeding chapter it can be shown that

$$n_x = \omega n M_n \ell n 2/\pi Z_o \qquad 5.1$$

where Z_o is the characteristic impedance of the line, ω_n the natural frequency of the resonator and M_n its equivalent mass. The values of M_n for the three cases considered in Chapter 4, are as follows. For the line resonator

$$M_n \propto M$$

where M is the total mass of the resonator. Experiment shows in fact that this is true since for the line resonator $n_x \propto \omega_n$. In the case of the Bar and Disc in flexture M_n is proportional to $M/2\sin^2\beta_n d$ and M/U_n respectively. In the latter two systems it can be seen that M_n is dependent upon mode and position of the line and would be infinite if the line coincided with a node. The line resonator however does not have this

Material	Aluminium		Aluminium		M. Steel		M. Steel		Brass		Brass		Nickel		Pyrex Glass	
σ / a cm	0.33 / 1.75		0.33 / 3.5		0.285 / 1.75		0.285 / 1.27		0.37 / 1.6		0.37 / 2.54		0.315 / 1.27		0.195 / .936	
MODE	f KHz / Ω	n_x	f KHz / Ω	n_x	f KHz / Ω	n_x	f KHz / Ω	n_x	f KHz / Ω	n_x	f KHz / Ω	n_x	KHz / Ω	n_x	KHz / Ω	n_x
2,1	60.663	80	30.601	120	62.846	200	86.363	104	44.324		27.633	n°c/o	81.355	95	124.806	n°c/o
	2.107		2.112		2.14		2.133		2.113		2.118		2.118		2.111	
0,1	86.608	n°c/o	43.48	n°c/o	86.217	n°c/o	118.07	n°c/o	64.517		40.199	n°c/o	114.36	n°c/o	160.534	"
	3.009		3.002		2.936		2.917		3.075		3.081		2.977		2.715	
3,1	92.533	110	46.692	100	96.006	210	131.817	126	66.585		41.720	113	123.992	"	190.710	"
	3.215		3.223		3.269		3.256		3.174		3.198		3.228		3.225	
4,1	121.873	n°c/o	61.326	140	126.368	280	173.621	n°c/o	86.744		54.439	103	162.786	"		
	4.234		4.233		4.303		4.288		4.135		4.173		4.238			
5,1	149.769	"	75.536	120	155.623	340			106.027		66.741	120	200.393	"		
	5.203		5.214		5.229				5.054		5.116		5.217			
6,1	177.428	"	89.394	130	184.313	n°c/o			124.865		78.678	95				
	6.164		6.171		6.276				5.952		6.031					
7,1	204.839	"	103.116	170	212.655	"			143.547		90.498	114				
	7.116		7.118		7.241				6.842		6.937					
8,1			116.637	180					161.994		102.191	106				
			8.052						7.721		7.833					
9,1			130.045						180.144		113.821	186				
			8.977						8.586		8.725					
10,1									198.521		125.36	126				
									9.462		9.61					

Table 5.2
Experimental results for end resonant frequencies of solid cylinders $\Omega = \omega a/c_s$

characteristic since the line can not be coupled to a node. In general therefore if Z_o is constant throughout the experiments

$$M_n = n_x/f_n k \qquad 5.2$$

If the end mode becomes coupled to a propagating wave, as in the case of the axi-symmetric mode, the value of M_n will become large and correspondingly so will n_x. This feature of the echo technique can be used to determine when end modes are coupled to propagating waves, and to obtain the equivalent lumped masses of each mode. The value of k for the 1 mm line use, data of which is given in table 4.1, Chapter 4, is 0.193.

Due to the shortage of information relating to end resonances it is necessary first of all to establish their frequency spectrum. Rods of a variety of materials, chosen to give a wide spread of Poisson's Ratio, were therefore prepared and, in each case, thin discs were also cut from the rod. These were used to obtain the cut-off frequencies and, using the method described by Onoe ref. (55) and extended by Bell and Sharp, ref. (56), to evaluate Poisson's Ratio. Table 5.2 gives these results. The equivalent lumped masses can be found using equation 5.2.

Experiments were then conducted on hollow cylinders. Identification of modes was difficult becuase of the availability of thin walled cylinders only. Therefore a solid brass bar 0.4 meters long was bored out to

MODE \ b/a	0	1/4	3/8	1/2	3/4	13/16	7/8	.92
2,1	27.633	22.451						
3,1	41.720	40.798	37.168					
4,1	54.439	54.415	52.992	48.596				
5,1	66.741	66.824	66.258	64.128	39.01		20.949	
6,1	78.678	78.849	78.521	77.695	52.899	42.46	29.8	21.45
7,1	90.498	90.702	90.409	90.238	67.29	55.22	39.774	21.085
8,1	102.191	102.383	102.068	102.205	82.057	68.595	50.602	36.145
9,1	113.821	113.989	113.861	113.941	96.959	82.438	62.124	41.946
10,1	125.36	125.520	125.374	125.481	111.849	96.587	74.321	54.136
11,1				136.933	126.543	110.907	86.876	67.475
12,1				148.422	140.174	125.396	99.929	81.891
13,1					154.206	139.782	113.253	97.265
14,1						154.28	126.855	113.34

b = inner diameter. a = outer diameter

Table 5.3

Measured end resonant frequencies for brass hollow cylinders of various wall thicknesses

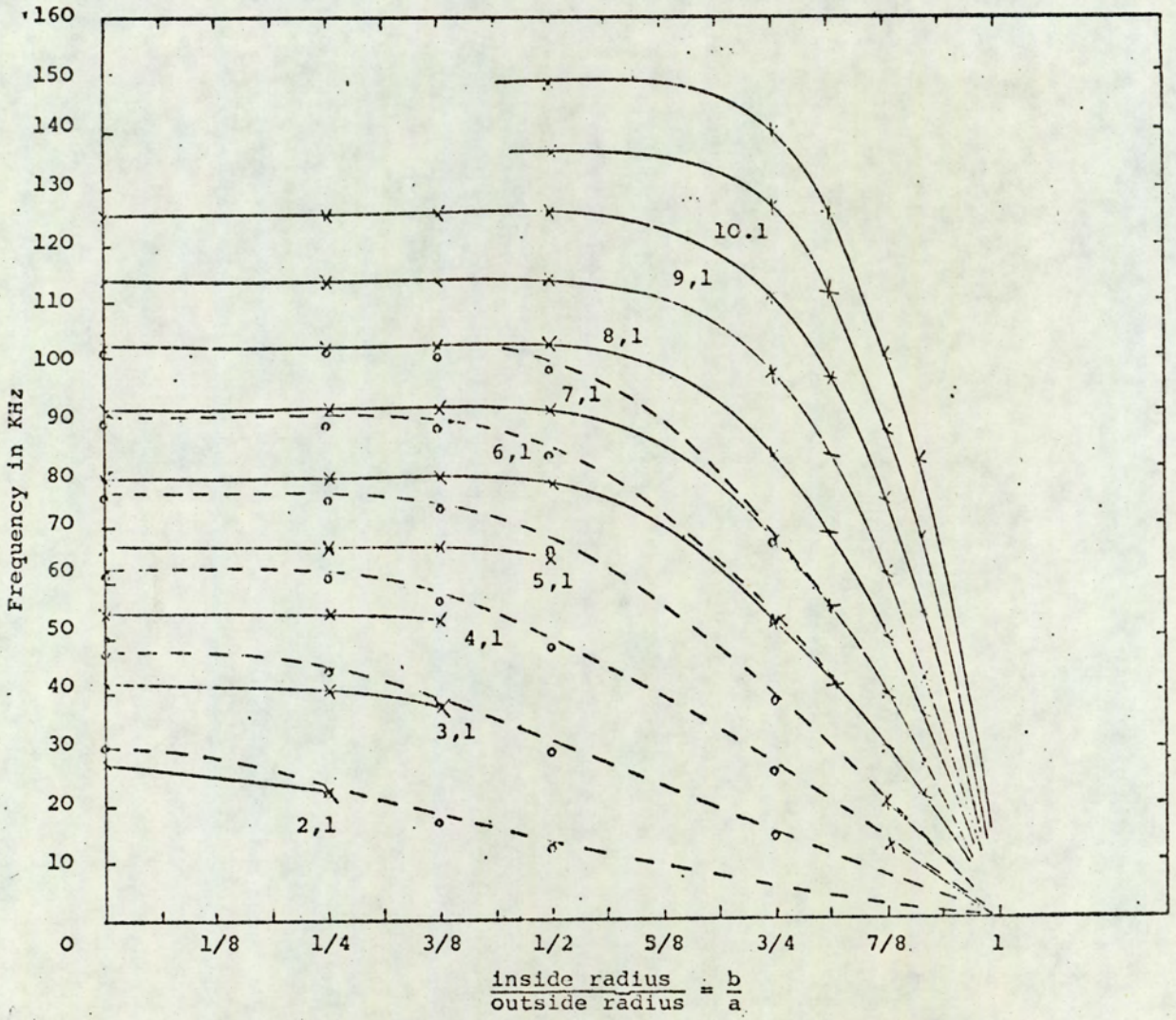

Fig. 5.2 Resonant frequencies of end modes in a brass hollow cylinder and in plane modes of a brass ring. (x): cylinder experiment; (o): ring experiment; (----): cut-off frequencies for hollow cylinder.

various inside diameter, and a set of results taken at each stage. This procedure enabled the modes, initially identified for the solid cylinder, to be followed through to the thinwall condition. In parallel with this, a thin disc was cut from the bar and corresponding diameter holes machined in it. Details of these results are given in table 5.3 and plotted in Figure 5.2.

The major characteristic of the axi-symmetric mode that sets it apart from the anti-symmetric is the extremely high Q that it displays. This is evident from the inability to obtain a crossover for this mode. The Q for the system is defined as 2π times the ratio of stored energy to dissipated energy, if the material losses are considered to be zero the material Q becomes infinite and the system is described by Q_c, the coupling Q, only. In other words, the only form of energy dissipation is via the propagating wave in the line. Since the line parameters are unchanged throughout the experiment the large Q of the symmetric mode must be due to the existance of the coupled propagating wave along the bar. This would appear to be an anomalous state of affairs as a propagating wave would lead to an additional dissipation of energy and hence lower the Q value. For a semi-infinite bar this would probably be the situation. However the presence of a second boundary of a finite bar means that the stress wave is reflected back along the bar and in doing so sets up an end resonance. For a finite bar therefore the axi-symmetric end mode occurs at both ends, this effectively doubles the value of the

coupling Q since there will be twice the amount of stored energy. This in itself however, does not explain why the Q of this mode is, not double but, many times greater than those of the surrounding modes. It must be considered therefore that other modes of resonance exist, and in fact whether the coupled L(0,1) mode is propagatory or not.

Zemanek has shown that the reflection coefficient for the L(0,1) mode, below the cut-off frequency of the second axi-symmetric mode, is complex with a magnitude of unity. His theoretical results show that the phase angle between the incident and reflected waves is dependent upon frequency, and that at the end resonant frequency the magnitude of phase shift is π. In other words the wave is reflected in antiphase when the end resonance exist. For a finite bar then, the L(0,1) mode produces a standing wave along its length, since the reflection of this wave at both ends will change phase by 180°. The interesting feature of this is that the bar has a resonant condition along its length at the same frequency irrespective of length. It is therefore proposed that the high coupling Q for the axis-symmetric end mode results from the relatively large amount of energy stored by the end and length resonant modes.

An experiment was devised to test the validity of this proposal. The axi-symmetric end resonance was excited in a 15.24 cm long mild steel bar 3.5 cm diameter. Both ends became resonant and, with the aid of a probe, a

small amplitude standing wave was observed along the length. The resonance was induced by an accoustic line coupled at one end of the bar. Heat was then applied to the remote end to lower its resonant frequency. Thermal conduction was kept to a minimum by cooling the centre of the bar with a stream of cold water. The lowering of the end resonant frequency, by heating, ensured that only one end could be at resonance and that at the non-resonant end the phase angle of the reflection coefficient would cease to be 180^{o}. This would ultimately prevent a standing wave condition occurring along the length of the bar, and hence lower the coupling Q. The experiment showed quite definitely a fall in the Q value, but the condition was hard to maintain because of the propagation of heat to the resonant end.

Another experiment was therefore required to give a more convincing result. Two bars of the same length and diameter but of dissimilar material were joined together end to end. The joint was made using Permabond. This gave a good joint without the need to heat the bars local to the join. The choice of the material of the bars was made so that there was a few percent difference between their end resonant frequencies. This of course would ensure that only one of the ends would become resonant when the symmetric mode was excited. Mild steel and nickel were chosen. The choice of these materials also has the advantage that the cut-off frequency for the L(0,2) mode in each bar is approximately equal. Together with the closeness of their Poisson's ratio this

	Nickel		Steel		Composite bar driven at			
Dia / length	9.53cm / 25.4mm		9.8cm / 25.4mm		Nickel end		Steel end	
Mode	Frequency KHz	n_x	Frequency KHz	n_x	Frequency KHz	n_x	Frequency KHz	n_x
2,1	81.355	95	86.363	104	81.557	130	86.394	100
0,1	114.36	n^o c/o	118.07	n^o c/o	114.210	n^o c/o	118.402	210
3,1	123.992	"	131.817	126	123.9	"	131.903	130
4,1	162.786	"	173.621	200	162.807	"	173.723	200

Table 5.4

Table showing results of composite bar experiment

	Aluminium		Steel		Composite bar driven at			
Dia / Length	3.5 cm / 35 cm		3.5 cm / 112.3 cm		Aluminium end		Steel end	
Mode	Frequency KHz	n_x	Frequency KHz	n_x	Frequency KHz	n_x	Frequency KHz	n_x
2,1	60.663	80	62.846	144	60.73	70	62.743	240
0,1	86.608	$no_{c/o}$	85.922 / 86.217	$no_{c/o}$	86.003 / 86.604	$no_{c/o}$	86.039	$no_{c/o}$
3,1	92.533	110	96.006	180	92.74	70	95.82	170
4,1	121.873	$no_{c/o}$	126.368	$no_{c/o}$	121.83	130	126.116	240

Table 5.5

Table showing results of composite bar experiments

would minimise the influence of the joint boundaries. Measurements were made on both bars before jointing, and then corresponding reading taken on the composite bar. The results for this experiment are shown in table 5.4. A similar experiment was carried out on 3.5 cm mild steel and aluminium bars,table 5.5 gives details of the results.

5.3 Discussion of Results

The end resonant frequencies for the materials considered in table 5.2 are seen, for the anti-symmetric modes, to vary by only a few percent. There are many possible reasons for this spread, most of them experimental and therefore at the present time the dependence of these end modes upon Poisson's ratio must be considered as too small to be measured by the technique used. Support for this comment may be drawn from the results shown for the disc in the previous chapter, where the frequency was seen to be a function of U_n. In the case of the disc U_n is dependent upon the line dimensions and point of coupling, for end resonance however added to this must be the angle of coupling and therefore in the absence of theoretical solution the exact dependence upon Poisson's ratio is not known.

The results obtained for the symmetric mode can be considered more reliable since their coupling Q factor is comparatively large, and therefore the damping produced

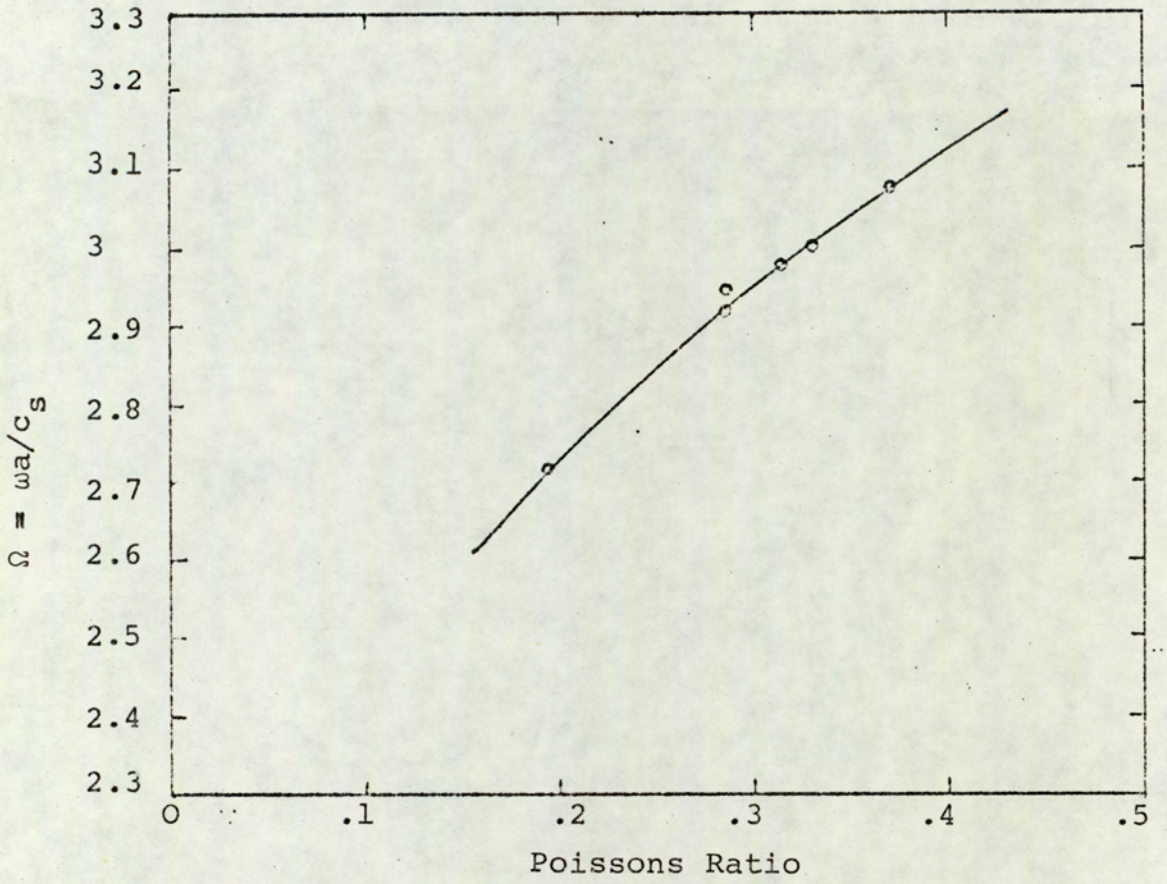

Fig. 5.3 Experimental results showing variation of axi-symmetric end modes with Poissons Ratio.

by the line is small. A plot of the symmetric modes versus Poisson's ratio is shown in Figure 5.3. The curve indicates an almost linear relationship between the symmetric end mode and Poisson's ratio.

It is generally accepted, as indicated by the relevant literature, that the origins of end resonance lie in the complex roots of the frequency equation, forming the basis for the approximate solution mentioned previously. There is no doubt that the results obtained, particularly by Zemanek, lends support to this reasoning but there are other conditions that could be explained by the same results. To maintain a stress free condition at the end of a semi-infinite bar the above author's results show that the amplitude of the first complex mode has a peak at the end resonant frequency. If the end resonance is considered as being produced by a surface wave at the end face of the bar the net stress at the resonant frequency may still be zero. In other words the apparent maximum displacement of the complex modes may in fact result from the omission of the stress produced by the surface wave, when summing the stress at the end boundary. This leads to the possible situation that the propagatory modes, of a real, complex or imaginary propagation constants, do not have a maximum amplitude at the end resonant frequency because of the existance of a surface mode. The possibility of this concept may seem more acceptable in terms of the anti-symmetric modes. Because these modes do not couple to a real propagatory wave they can only be excited at the boundary at which they

occur, this leads to the question of whether a surface mode induces complex waves in the bar, thereby maintaining a zero stress condition.

The results for the hollow cylinders given in table 5.3 are plotted in Figure 5.2. The cut-off frequencies for the first six modes are indicated by the broken curves. Results of the experiments carried out on the rings, shown as circled points, are seen to follow the cut-off frequencies quite closely. Joining the points for the end modes results in the continuous curves of this figure.

As the ratio of inner to outer diameter gets larger (i.e. the wall thickness gets smaller) the modal frequencies fall and converge to produce a denser spectrum. For values of b/a less than 1/32 the frequency spectrum remains virtually unchanged. The degree to which a mode is effected by an increase in this ratio depends upon its order, the higher ones being the less sensitive for values of b/a less than 1/2. Since the broken curves represent the cut-off frequencies for the lowest mode in each family F(m,n),it would appear that cut-off is the highest frequency that an end mode may occur. The results obtained for the first four modes (Figure 5.2) shows that beyond the points at which the broken and continuous curves would appear to cross these modes could not be excited, implying therefore, that above cut-off an end resonance ceases to exist. If, as discussed above, the frequency of the end mode is dictated by the resonance of a surface wave, and

that this wave induces complex modes in the bar, it would follow that at frequencies above cut-off, energy storage in the surface mode is prevented by the existance of a propagatory wave along the bar.

The results for the composite Nickel Steel bar, shown in Table 5.4, are consistent with the proposals made. Given in the table are the results of frequency and crossover measurements made before the bars were joined. These results indicate that in the case of both bars a crossover for the symmetric mode could not be obtained. Joining the bars together, in the manner mentioned, and taking readings from each end in turn the results obtained are seen to be quite different. In the case of steel the value of n_x goes from a number much greater than oscillations in the burst to 210, whereas driving from the nickel end has an apparently unmeasurable effect. In fact from the shape of the echo it was obvious that for the nickel, when joined to the steel, the value n_x was far greater than that of the isolated bar. Figure 5.4 shows results obtained by Zemanek for the phase shift between the incident and reflected L(0,1) mode at the end face of a cylindrical bar. The two features of these curves which are of particular interest in this part of the discussion are:-

a) The 180^{c} phase shift that occurs with end resonance

and b) The difference in the shape of the curves above and below resonance, in particular the plateau region above the end frequency.

It has already been commented that when both ends of a bar

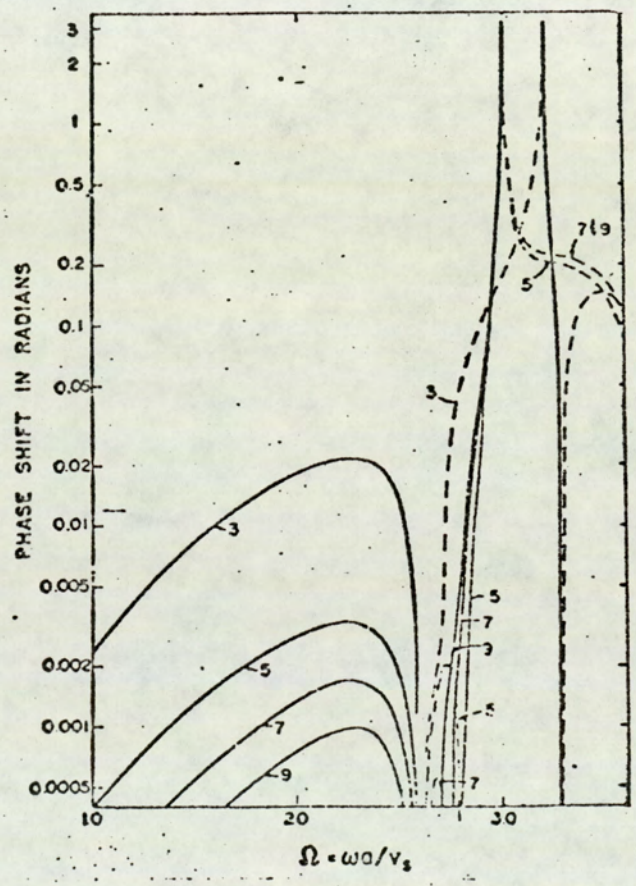

Fig. 5.4 Reflection coefficient of the L(0,1) mode at the end boundary of a semi-infinite bar. The numbers refer to the number of modes considered to satisfy the end boundary conditions (——):Positive phase shift;(---): Negative phase shift: $\sigma = 0.3317$

are at resonance a standing wave is set up along the whole length, resulting in a high Q_c for this mode. Consideration of the results given in Table 5.4 will show that, when the composite bar is driven from the nickel end, the end resonance of the nickel bar is excited. This frequency being below that of the end resonance of the steel bar, the latter is not excited at the remote end. Because of this it would be expected that Q_c fall in value. However Figure 5.4, shows that at frequencies below end resonance the phase shift drops steeply to zero. Therefore a wave arriving at the end face of the steel bar will be reflected in phase, which is the behaviour expected from a clamped boundary. With the 180^{o} phase shift at the drive end a standing wave condition will result along the length of the bar, hence the high Q_c obtained.

When the bar is driven at the steel end the situation is reversed, the drive frequency is now above that of the end resonance at the remote end. At frequencies above end resonance it is seen (Figure 5.4) that the phase shift does not fall directly to zero, therefore for this configuration a standing wave does not occur. This situation is similar to that obtained in the heated bar experiment. Since energy is only stored at one end, as with the anti-symmetric modes, Q_c falls giving the value of n_x shown in Table. 5.4.

The results obtained for the aluminium and steel bars, given in Table 5.5, show that when the end resonant frequencies are close to each other a large amount of energy is stored when driven from either end, implying a standing wave condition along the length.

CHAPTER 6

END RESONANCE OF PLATES AND STRIPS

CHAPTER 6

END RESONANCE OF PLATES AND STRIPS

6.1 Introduction

The study of wave propagation in infinite plates has developed in much the same manner as has the theory for infinite cylinders. This coincidence of histories is not altogether surprising because of the similarities that exist between the two fields. Discoveries made for one geometry would, by applying the same reasoning, automatically lead to similar findings for the other.

Early theories for the propagation of waves in plates were published independantly in 1889 by Rayleigh (57) and Lamb (58). Except for a later study by Lamb (59), in 1917, the topic appears to have remained virtually undisturbed until the 1950's. Since the publication of Holder's (5) work in 1951, involving a study of longitudinal modes in cylinders and slabs, the two topics have become strongly linked. As with cylinders, the frequency spectrum for modes of real, imaginary and complex propagation has been extensively explored, resulting in an almost complete understanding of the behaviour of their dispersion curves.

The introduction of a second pair of surfaces to assimilate the geometry of an infinite bar of rectangular cross-section, greatly increases the complexities involved in the theory of vibrations of plates. In the case of an infinite cylinder the problem of satisfying boundary conditions

on two pairs of surfaces does not arise and therefore solutions can be obtained. A general solution for infinite rectangular sectioned bars however has not yet been obtained. This is not peculiar to infinite bars, for if comparison is made with thin plates, the solutions of flexural and inplane vibrations of discs can be obtained without great difficulty , whereas general solutions for similar motions in plates with rectangular boundaries can not. Exact solutions for specific ratios of width to depth of an infinite rectangular bar have been obtained by Mindlin and Fox (59), the results allow a limited number of points to be found within the frequency spectrum. The slope of the dispersion curves at these points can also be obtained from the equations given. How these curves behave between these points and how curves relating to complex propagation behave is not resolved.

Unlike cylinders, strips and plates have been found, experimentally, to support only one end resonant mode. In the case of cylinders it was found that each family of propagating modes, except for the lowest anti-symmetric family, had its associated end resonance. The modes of propagation in strips or plates form only two families, one symmetric and one anti-symmetric, and therefore it is not surprising that only one end resonant mode should exist, and further more that it should be associated with the symmetric family. Because of the similarities in the displacement fields of the anti-symmetric modes, in that they all have a common node in the middle plane, it is thought that they couple to the lowest mode, which has zero

cut-off frequency, hence preventing a storage of energy in an end resonance. A similar relationship does not exist between the symmetric modes therefore an end resonance associated with these modes occurs.

It was stated in the last chapter that the mechanism of end resonance is generally explained in terms of modes with complex propagation. The spacial decay of such modes does not signify a dissipation of energy, but simply the character of the mode. That the wave decays on propagation into the body does indeed lead to the question of destination of the energy possessed by the mode. It would appear that early investigators rejected the possibility of such modes on the grounds of this apparent anomally. However, since the complex propagation constants have negative conjegate counterparts, at any frequency, within the range that they exist, two waves, propagating in opposite directions but decaying in the same sense, will be generated. The net result is that the complex modes only occur as standing waves, and hence do not represent a transportation of energy. Therefore at the end of a semi-infinite cylinder or the boundary of a semi-infinite plate an infinite number of standing waves of this nature exist.

The presence of these modes is also used to explain the problems involved in obtaining solutions for plates or cylinders of finite volume, in that the stresses at the boundaries will be zero only when all these modes are taken into account.

Edge resonances of plates were first reported by Shaw (60). His observations of these modes were made while

carrying out vibrational experiments on Barium titanate discs. The results show that, for discs with radius to thickness ratio greater than 1, a mode exist for which the frequency is independant of the disc radius and the motion of vibration takes place mainly at the periphery.

Using a second order theory, developed in reference (61), Gazis and Mindlin (62) obtained, numerically, a value for the edge resonant frequency of a circular disc and a semi-infinite plate. The plotted results indicate that, in a similar way to semi-infinite cylinders, the reflection coefficient for an incident wave impinging on the boundary undergoes a phase change of 180° at the edge resonant frequency, and that the amplitude ratio of the first complex mode has a peak value at this frequency.

Onoe (63), using an approximate theory based on an energy principle, arrived at a frequency value for the end resonance of a finite strip. His computed and experimental results show that the technqiues used are in good agreement, however the results obtained relate specifically to the anisotropic case and therefore are not really applicable to the considerations of this chapter.

The theoretical results obtained by Torvik (64) for a semi-infinite plate with a Poisson's Ratio of 0.31 agree very well with the results given in this thesis and those obtained experimentally by McMahon (53) and Shaw (60). Torvik used a similar approach to Onoe in that his method involved minimising the work done at the boundary by suitably choosing coefficients for the modes involved. His results

take into account 22 modes, the incident and reflected lowest symmetric mode and the first ten complex modes and their negative conjugates. The plotted results display identical characteristics to those given in reference (62).

The theoretical work of this chapter is based on that of Rayleigh and Lamb, the values for the end resonances of semi-infinite plates and strips were obtained using the method employed by Zemanek in the case of semi-infinite cylinders. Stress summation has been considered for 12 modes, two real and ten complex. In the case of the semi-infinite plate the end resonant frequencies, have been obtained , for eleven values of Poisson's Ratio between 0.1 and 0.5. For the semi-infinite strip nine values were computed within the same range of Poinsson's Ratio. In both cases the values have been found to lie on almost straight lines, and therefore a plot of the results allow intermediate points to be obtained graphically.

To test the accuracy of using twelve modes results were computed taking account of 22 modes at a value of Poisson's Ratio of 0.35, the results were then compared.

6.2 Basic Theory

The starting point for the treatment of wave propagation in infinite plates is identical to that adopted for cylinders. Equations 2.20 to 2.23 therefore are applicable as they stand to the theory of plates. The solutions for the displacement component, obtained by solving equations 2.22

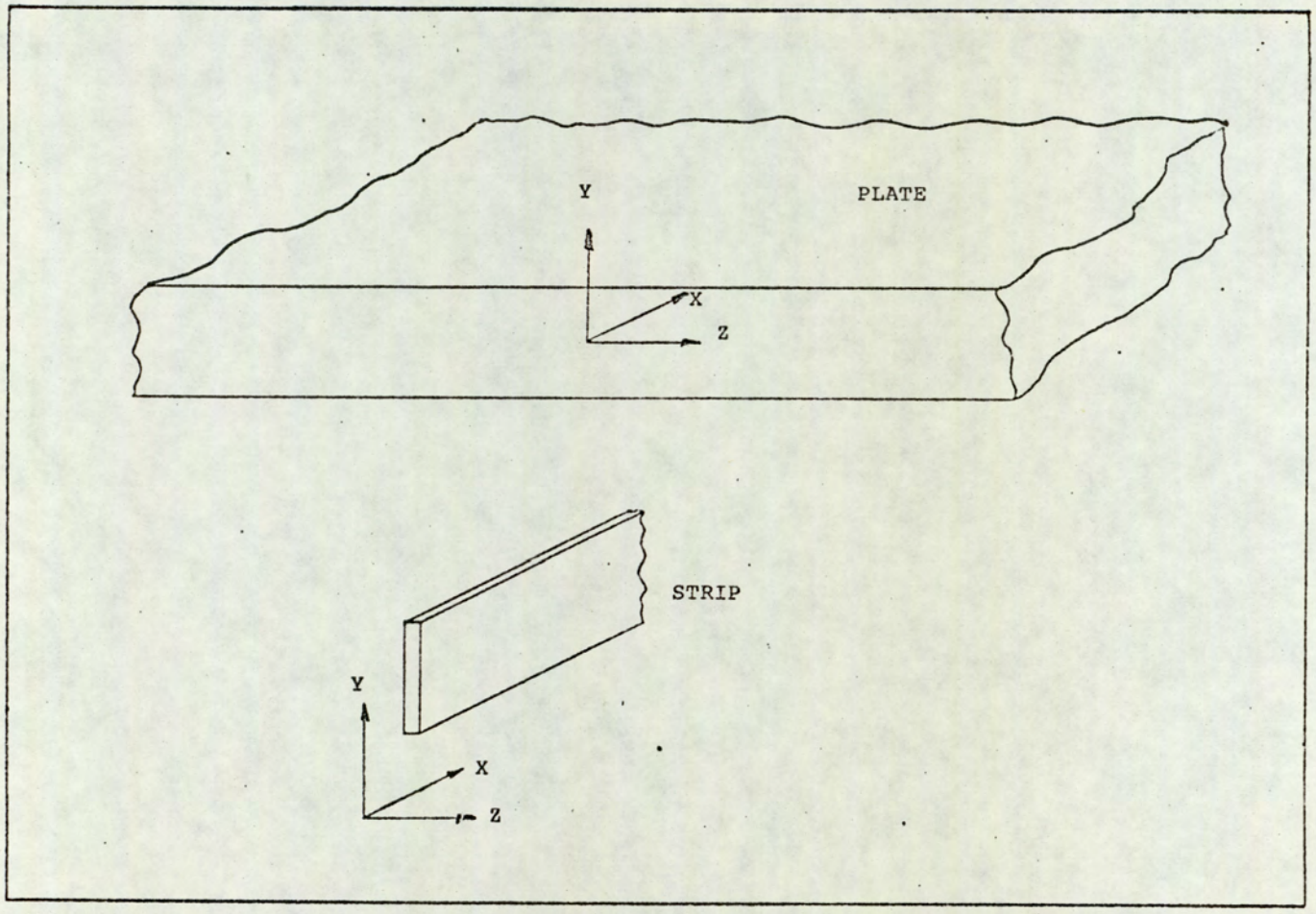

Fig. 6.1(a) The orientation of strip and plate with respect to the co-ordinate axis. Wave propagation takes place in the x direction only.

and 2.23 and inserting the results into equation 2.21, will, because of the geometry, now be described in terms of trigonometrical and hyperbolic functions.

Considering a plate lying in the x - z plane, with plane wave propagation in the x direction, the plane strain solution for the symmetric displacement components are

$$u_x = j|B\gamma Cos\alpha y + C\beta Cos\beta y|\ expj(\gamma x - \omega t)$$

$$u_y = -|B\alpha Sin\alpha y - C\gamma Sin\beta y|\ expj(\gamma x - \omega t) \qquad 6.1$$

$$u_z = O$$

where $\alpha^2 = \delta^2\omega^2/C_s^2 - \gamma^2$, $\beta^2 = \omega^2/C_s^2 - \gamma^2$ 6.2

and B and C are constants with respect to x and y. The symbol δ, the ratio of the shear and dilatational velocities, will depend upon the system considered. That is for an infinite plate this ratio will be C_s/C_d, where C_d is, as given by equation 2.15, the dilatational velocity in an unbounded media, and for an infinite strip C_s/C_p, where C_p is the plate velocit- given by equation 2.16. The arrangements for strip and plate are shown in figure 6.1(a). For a plate or strip, with boundaries y = ±b, the conditions to be satisfied are that both the plane and shear stresses at these boundaries be zero. The expressions for the stresses at the boundaries

$$\sigma_{yy} = \rho C_s^2|(1/\delta^2 - 2)\Delta + 2\varepsilon_{yy}| \qquad 6.3$$

$$\sigma_{xy} = \rho C_s^2\ \varepsilon_{xy} \qquad 6.4$$

are obtained from equations 2.4 by substituting the subscripts

$$\begin{aligned} 1 &\rightarrow xx \\ 2 &\rightarrow yy \\ 3 &\rightarrow zz \\ 4 &\rightarrow yz \\ 5 &\rightarrow zx \\ 6 &\rightarrow xy \end{aligned} \qquad 6.5$$

and expressing Lame's constants in terms of velocities. Δ is the areal dilatation $\varepsilon_{xx} + \varepsilon_{yy}$. The strain components may be written as

$$\varepsilon_{xx} = \frac{\partial u_x}{\partial x}, \qquad \varepsilon_{yy} = \frac{\partial u_y}{\partial y} \qquad 6.6$$

and $$\varepsilon_{xy} = \frac{\partial u_y}{\partial x} + \frac{\partial u_x}{\partial y}$$

Making the substitution of 6.1 and 6.6 into equations 6.3 and 6.4 and evaluating at the boundaries $y = \pm b$, results in the following frequency equation.

$$\tan\beta b/\tan\alpha b = 4\alpha\beta\gamma^2/(\beta^2 - \gamma^2)^2 \qquad 6.7$$

This is the Rayleigh-Lamb frequency equation for the propagation of symmetric waves in an infinite plate. The frequency equation for an infinite strip is identical to 6.7 with the value of δ^2 in equation 6.2 changed i.e. in non dimensional form 6.2 becomes

$$\alpha^2 b^2 = \delta^2\Omega^2 - \gamma^2 b^2, \qquad \beta^2 b^2 = \Omega^2 - \gamma^2 b^2 \qquad 6.8$$

where $\Omega^2 = \omega^2 b^2 / C_s^2$

For a plate the dilatational wave will travel at the bulk velocity and therefore the ratio δ, in terms of Poisson's Ratio, will be

$$\delta^2 = (1 - 2\sigma)/2(1 - \sigma) \qquad 6.9$$

from equations 2.14 and 2.15. In the case of the strip, the wave will travel at the plate velocity giving a ratio of

$$\delta^2 = (1 - \sigma)/2 \qquad 6.10$$

from equations 2.14 and 2.16. If, in either case, the dimension 2b is small compared to the wavelength in the y direction the frequency equation 6.7 reduces to

$$\omega = 2\gamma C_s (1 - \delta^2)^{\frac{1}{2}} \qquad 6.11$$

For a thin plate therefore, δ^2 has the value given by 6.9 and equation 6.11 becomes

$$\begin{aligned} \omega &= \gamma (E/\rho(1 - \sigma^2))^{\frac{1}{2}} \\ &= \gamma C_p \end{aligned} \qquad 6.12$$

using equations 2.14 and 2.16. Substituting 6.10 in 6.11 gives the limiting case for the strip. As the dimension 2b becomes small, the strip becomes a rectangular bar. The resulting frequency equation from equation 6.11 is

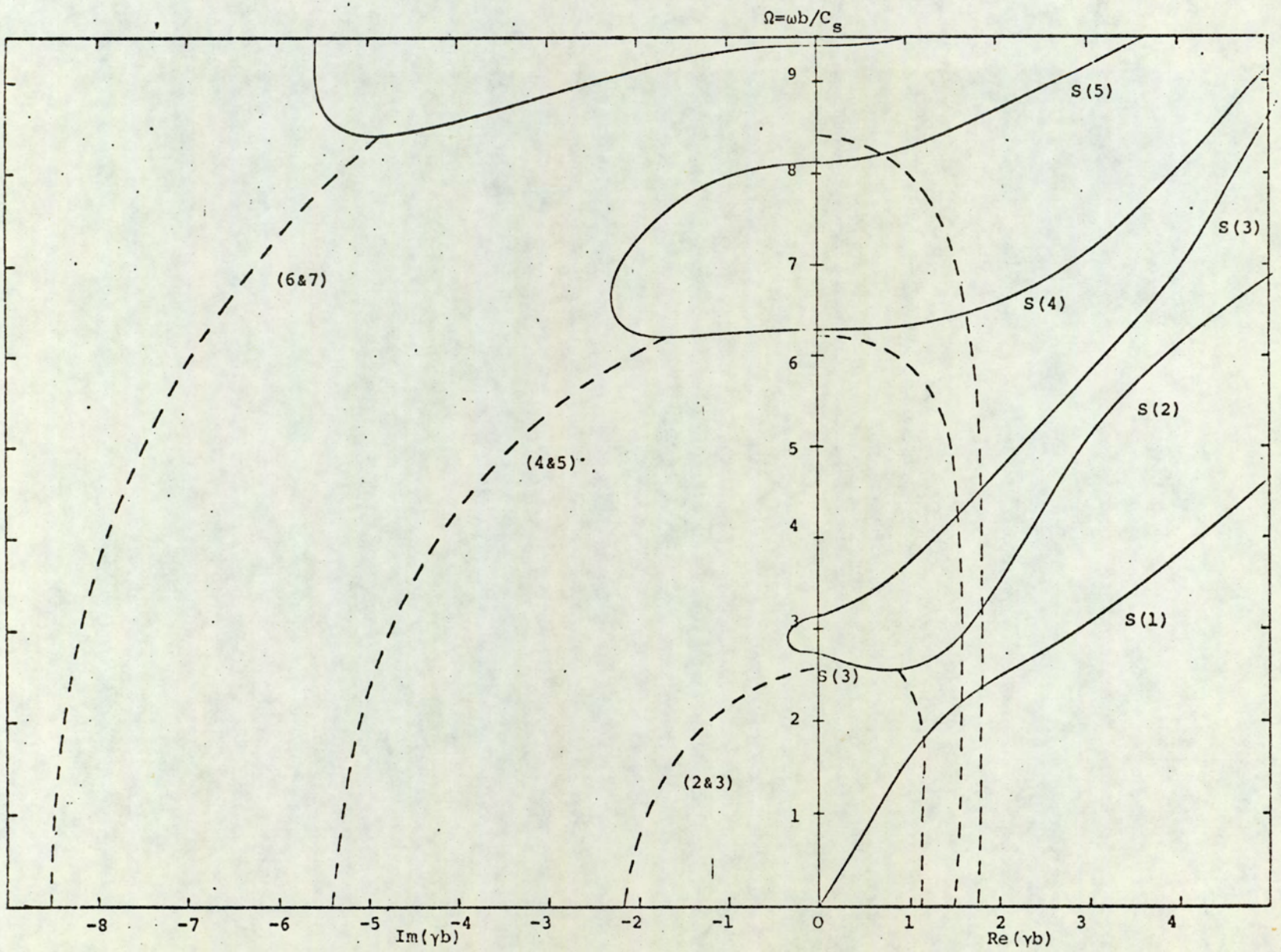

Fig. 6.1 Dispersion curves for symmetric modes of propagation. (——): real or imaginary modes; (---): complex modes; $\delta^2 = 0.335$.

$$\omega = \gamma(E/\rho)^{\frac{1}{2}}$$

$$= \gamma C_o \qquad 6.13$$

where C_o is the longitudinal velocity for waves of infinite wavelength in a bar.

The Rayleigh-Lamb equation has real, imaginary and complex solutions. Figure 6.1 shows part of the frequency spectrum obtained from this equation. Computations were made using a value of $\delta^2 = 0.335$, thus for a strip $\sigma = 0.33$ and for a plate $\sigma = 0.248$.

The cut-off frequencies are obtained by allowing $\gamma b \to 0$ in equation 6.7, this produces

$$\mathrm{Sin}\beta b \mathrm{Cos}\alpha b = 0 \qquad 6.14$$

which has the solutions

$$\Omega = n\pi \qquad 6.15$$

$$\Omega = (2n + 1)\pi/2\delta^2 \qquad 6.16$$

$(n = 0, 1, 2, 3 \ldots \text{etc})$

Modes having solutions 6.15 are 'thickness-shear' modes having only one component of displacement u_x. The solutions 6.16 give 'thickness-stretch' modes with displacement u_y only.

The intersection of the complex dispersion curves with the zero frequency axis can be found by allowing Ω to approach zero with γb remaining finite, in equation 6.7. Following this procedure the resulting frequency equation, given by Jones and Ellis (65), is

$$\text{Sinh}(2\gamma b) = -2\gamma b \qquad 6.17$$

The first 20 roots of this equation are given in Table 6.1

Modes	Re(γb)	Jm(γb)
2 and 3	1.12576	2.10620
4 and 5	1.55157	5.35627
6 and 7	1.77554	8.53668
8 and 9	1.92940	11.69918
10 and 11	2.04685	14.85406
12 and 13	2.14189	18.00493
14 and 15	2.22172	21.15341
16 and 17	2.29055	24.30034
18 and 19	2.35105	27.44620
20 and 21	2.40501	30.59130
22 and 23	2.45372	33.73581
24 and 25	2.49810	36.87909
26 and 27	2.53887	40.02363
28 and 29	2.57656	43.16709
30 and 31	2.61161	46.31032
32 and 33	2.64436	49.45337
34 and 35	2.67510	52.59627
36 and 37	2.70407	55.73903
38 and 39	2.73144	58.88168
40 and 41	2.75740	62.02424

Table 6.1

Special solutions of the Rayleigh-Lamb equation are

those of the Lam'e modes. These are analogous to the Lamb modes discussed in Chapter 2. Consideration of equation 6.7 will show that when $\beta=\gamma$ the solution is

$$\beta b = \gamma b = (2n + 1)\pi/2 \qquad 6.18$$

and the frequency equation using 6.8 becomes

$$\Omega = (2n + 1)\pi/(2)^{\frac{1}{2}} \qquad 6.19$$

Writing the stresses 6.3 and 6.4 in full

$$\sigma_{yy} = \rho C_s^2 \left| (\gamma^2-\beta^2) B\mathrm{Cos}xy + 2\beta\gamma C\mathrm{Cos}\beta y \right| \mathrm{expj}(\gamma x - \omega t) \qquad 6.20$$

$$\sigma_{xy} = j\rho C_s^2 \left| (\gamma^2-\beta^2) C\mathrm{Sin}\beta y - 2\alpha\gamma B\mathrm{Sin}xy \right| \mathrm{expj}(\gamma x - \omega t)$$

and applying the boundary conditions $\sigma_{xy} = \sigma_{yy} = 0$ at $y = \pm b$ the amplitude ratio

$$\frac{B}{C} = \frac{2\gamma\beta\mathrm{Cos}\beta b}{(\gamma^2-\beta^2)\mathrm{Cos}\alpha b} = \frac{(\gamma^2-\beta^2)\mathrm{Sin}\beta b}{2\gamma\alpha\mathrm{Sin}\alpha b} \qquad 6.21$$

is obtained. Therefore when the condition 6.18 is substituted in 6.20 and 6.21 the stresses become

$$\sigma_{yy} = 2\rho C_s^2 \beta\gamma C\mathrm{Cos}\beta y \ \mathrm{expj}(\gamma x - \omega t)$$

$$\sigma_{xy} = 0 \qquad 6.22$$

and the displacements from equation 6.1 for the Lam'e modes become

$$u_x = jC\beta\mathrm{Cos}\beta y \ \mathrm{expj}(\gamma x - \omega t)$$

$$u_y = C\gamma\mathrm{Sin}\beta y \ \mathrm{expj}(\gamma x - \omega t) \qquad 6.23$$

The important features of the foregoing equations are that a) the wave operating is a shear wave, b) the phase velocity is $\sqrt{2}\ C_s$, and c) the shear stress is zero everywhere. Because of the latter of these it follows that for a bounded plate there remains only one boundary condition to be satisfied i.e. $\sigma_{xx} = 0$. This may be written as

$$\sigma_{xx} = -2\rho C_s^2 \beta^2 \mathrm{Cos}\beta y \ \mathrm{expj}(\gamma x - \omega t) \qquad 6.24$$

For the incident and reflected waves the pane stress becomes

$$\sigma_{xx} = -2\rho C_s^2 \beta^2 \mathrm{Cos}\beta y \mathrm{Cos}\beta x \ \mathrm{expj}(-\omega t) \qquad 6.24$$

where $\beta = (2n + 1)\pi/2b$.

The stress σ_{xx} therefore will be zero when $\beta x = (2p + 1)\pi/2$,

or $x = (2p + 1)b/(2n + 1)$ 6.25

$(p = 1, 2, 3, \text{etc})$

For frequencies satisfying equation 6.19 a plate, of infinite extent in the z direction, or a thin strip will have all boundary conditions satisfied if the dimension in the x direction satisfies equation 6.25. In addition to being important solutions, from the point of view that they are the only exact ones known, it will be seen that these modes have interesting effects on the computed values of end resonances, in the following section.

6.3 End Resonances of Semi-infinite Strips and Edge Resonances of Semi-infinite Plates.

The frequency spectrum shown in figure 6.1 has a character very similar to that obtained by Zemanek, shown in Chapter 2, for the axi-symmetric modes in cylinders. As with cylinders the complete frequency spectrum takes up four quadrants resulting from the identical way in which the roots occur. Since the Rayleigh-Lamb frequency equation only contains terms in γ^2 it is obvious that the real and imaginary values of γ can be positive or negative for the same solution. For the complex roots, consideration of the equation used to obtain their zero frequency intercepts (equation 6.17) will show that any combination of positive and negative real or imaginary parts of γb will result in the same solution. This becomes more apparent if $2\gamma b$ is replaced by a + jc and the whole equation expanded. The following symultaneous equations are obtained.

$$\text{Cos}\ (c) = -\ (a)/\text{Sinh}(a)$$

$$\text{Cosh}\ (a) = -\ (c)/\text{Sin}\ (c) \qquad 6.26$$

from which it is seen that, since both right and left hand sides are even functions, the sign of a or c do not affect the solutions. Therefore the complete spectrum is made up of real modes that occur in pairs, imaginary modes that occur in pairs, and complex modes that occur in groups of four. In infinite plates, strips or cylinders the non-real

modes will only be encountered in problems of transient waves or non-uniform loading. For finite or semi-infinite bodies the imaginary and complex modes are also associated with edge vibrations.

In considering edge or end resonance it should be appreciated that imaginary and complex modes are only admissable if they represent a spacial decay on propagation into the body. Therefore the imaginery part of γ must always be positive, this eliminates one of the imaginary modes and one pair of the complex modes.

Consider a semi-infinite body extending to $x = \infty$ with a boundary at $x = 0$. Since the stresses σ_{xx} and σ_{xy} cannot both be made zero by assuming the reflection of one mode, account must be taken of cancellation effects produced by the stresses of other modes. Hence the boundary conditions at $x = 0$ are written as

$$\sum_{m\neq o}^{\infty} \sigma_{xxm} = \sum_{m=o}^{\infty} \sigma_{xym} = 0 \qquad 6.27$$

The end resonances of strips or plates have been found experimentally to occur only below the cut-off frequency of the second symmetric mode, marked s(2) figure 6.1. Below this frequency there are two modes with real propagation constants and an infinity of complex modes. Considering only frequencies in this region of the frequency spectrum these modes alone need be accounted for. It is obvious that the infinite number of complex modes cannot be included in the summation and that some realistic figure must be

chosen. For all the results obtained 12 modes were taken into account. To check whether the accuracy would be improved by considering more modes, a duplicate set of results were obtained for a value of $\delta^2 = 0.325$ using 22 modes. The resonant frequency was found to be only 0.02% in error and was deemed, therefore, not worth the extra cost of obtaining all results with this number of modes.

When considering the problem of end resonances it is usual, references (9), (64) and (66), to assume that a source at $x = \infty$ excites the s(1) mode, which upon reaching the stress free boundary at $x = 0$, is reflected with reflection coefficient A. In doing so complex modes are generated thereby maintaining a zero stress condition. This approach, while being satisfactory for situations in which end resonances couple to propagating modes, as for symmetric modes in cylinders, is inadequate for strips, where the end mode in general has not been found to couple with a propagating wave. Also, since the driving force is applied at the stress free boundary, as for the experiments of this thesis, the remote source idea is unrealistic. The approach to be developed here, will be that all modes emanate from the free boundary. Two modes, with real propagation constants, will be generated, one relating to the positive value of γ and the other to the negative γ value. These two modes would correspond to the incident and reflected waves of the remote source approach, but in this case both modes travel in the +ve x direction but with apposite sign propagation constants. Because the complex values of γ form negative conjugates the same reasoning may

be applied. There is no difference, mathematically, whether the wave travels in +ve x direction with a -ve γ value or a -ve x direction with a +ve γ value, but the point should be made if the physical situation is to be truely represented.

The plane and shear stresses produced by each mode can be, by utilising equations 6.1 to 6.6 and 6.21, written as

$$\sigma_{xx} = C\rho C_s^2 2\gamma\beta \left| \frac{(2\alpha^2-\omega^2/C_s^2)\mathrm{Cos}\beta b}{(\gamma^2-\beta^2)\mathrm{Cos}\alpha b} \mathrm{Cos}\alpha y - \mathrm{Cos}\beta y \right| \mathrm{expj}(\gamma x-\omega t) \qquad 6.28$$

$$\sigma_{xy} = jC\rho C_s^2(\gamma^2-\beta^2) \left| \mathrm{Sin}\beta y - \frac{\mathrm{Sin}\beta b}{\mathrm{Sin}\alpha b}\mathrm{Sin}\alpha y \right| \mathrm{expj}(\gamma x-\omega t) \qquad 6.29$$

where C is the amplitude coefficient, which in general will be complex. If the bracketed Cosine and Sine terms are represented by C(y) and S(y) respectively and the time dimension is dropped equations 6.28 and 6.29 may be abbreviated to

$$\sigma_{xxn}(y,x) = A_n \ \mathrm{expj}\phi_n \rho C_s^2 2\gamma\beta C(y) \mathrm{expj}\gamma x \qquad 6.30$$

$$\sigma_{xyn}(y,x) = jA_n \mathrm{expj}\phi_n \rho C_s^2(\gamma^2-\beta^2) S(y) \mathrm{expj}\gamma x \qquad 6.31$$

where C is represented in complex form as A expjϕ. Using the mode with the real +ve γ value as reference for all other modes by chosing an amplitude modulus of unity and a phase of zero, the summation of (n + 1) stresses will result in n unknowns. To evaluate these, therefore, n equations containing the unknowns are required. This is achieved by summing the stresses σ_{xx} and σ_{xy} at a total of n points along the half

thickness b of the plate (strip). Proceeding in this manner the plane stresses are set equal to zero at $(n + 1)/2$ equally spaced points and the shear stresses at $(n - 1)/2$ equally spaced points. From equation 6.29 it is seen that the shear stress is zero at $y = \pm b$ & 0 and therefore will in fact be zero at $(n + 2)$ points along the thickness of the plate. If n for the reference modes is 0, so that $A_o = 1$ and $\phi_o = 0$, the unknown coefficients will be $A_n \exp j\phi_n$ where $n = 1, 2, 3$ etc. The mode propagating with a -ve γ value will be represented by $n = 1$, and the first complex pair by $n = 2$ and 3 and so on. The simultaneous equations to be solved are, therefore

$$\sigma_{xxo}(b\, r_i, 0) = -\sigma_{xx1}(b\, r_i, 0) - \sum_{p=2}^{n} \sigma_{xxp}(b\, r_i, 0)$$

$$i = 1, 2, 3 \ldots (n + 1)/2 \qquad 6.32$$

where r is the ratio y/b having a value of

$$r_i = 2(i - 1)/(n - 1),$$

and

$$\sigma_{xyo}(b\, r_k, 0) = -\sigma_{xyi}(b\, r_k, 0) - \sum_{p=2}^{n} \sigma_{xyp}(b\, r_k, 0)$$

$$k = 1, 2, 3 \ldots (n - 1)/2 \qquad 6.33$$

where

$$r_k = (2k - 1)/(n - 1).$$

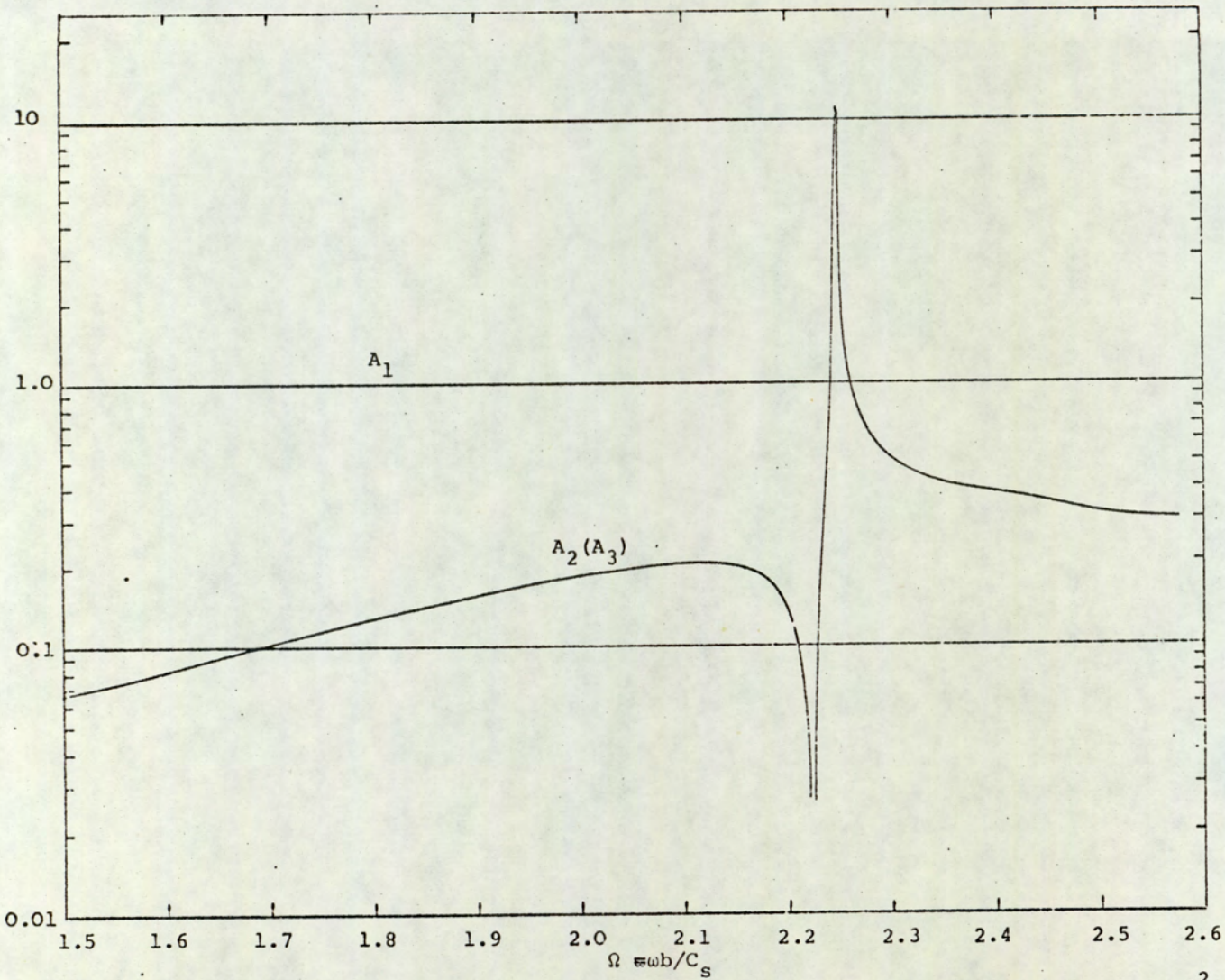

Fig. 6.2 Amplitude coefficients A_1 and $A_2(A_3)$ in the frequency range Ω=1.5 to 2.55. δ^2=0.335. The minimum and maximum amplitudes of $A_2(A_3)$ occur at frequencies of the Lam'e and end resonant modes respectively.

These equations were solved for n = 11 and velocity ratio squared δ^2 = 0.45, 0.4, 0.375, 0.355, 0.325, 0.315, 0.295, 0.275, 0.17 and 0.0.

6.4 Discussion of Results

All calculations were carried out on an I.C.L. 1904S computer. Initially results were obtained for δ^2=0.335 (i.e. for a plate σ = 0.248 and for a strip σ = 0.33) and frequencies Ω = 1.5 (0.01) 2.56. The values of γb were evaluated to six significant figures for these results, but for smaller subdivisions of $\Delta\Omega$ this was increased to eight. The results obtained for the amplitude coefficients A_n for n = 1, 2 and 3 are shown in figure 6.2.

From the two curves it is seen that $A_1 = A_o = 1$ also $A_2 = A_3$, this was not unexpected since this behaviour was reported by Gazis-Mindlin and Zemanek. In fact for all cases considered it was found that $A_{2m} = A_{(2m+1)}$ where m = 1, 2, 3 etc. Because of the interpretation of how the modes are formed, ie. that all modes emminate from the boundary at which the energy source is applied, it might be expected that the energy distribution should be equal between like modes and hence have equal modulus. In the frequency interval Ω=2.222 to 2.225 there occurs a minimum for the amplitude of the first pair of complex modes. The significance of this is that it is the frequency of the Lam'e mode, that is $\Omega=\pi/(2)^{\frac{1}{2}} \simeq 2.2214$ and since all boundary conditions can be satisfied by the existance of the two real modes alone, it is in order that

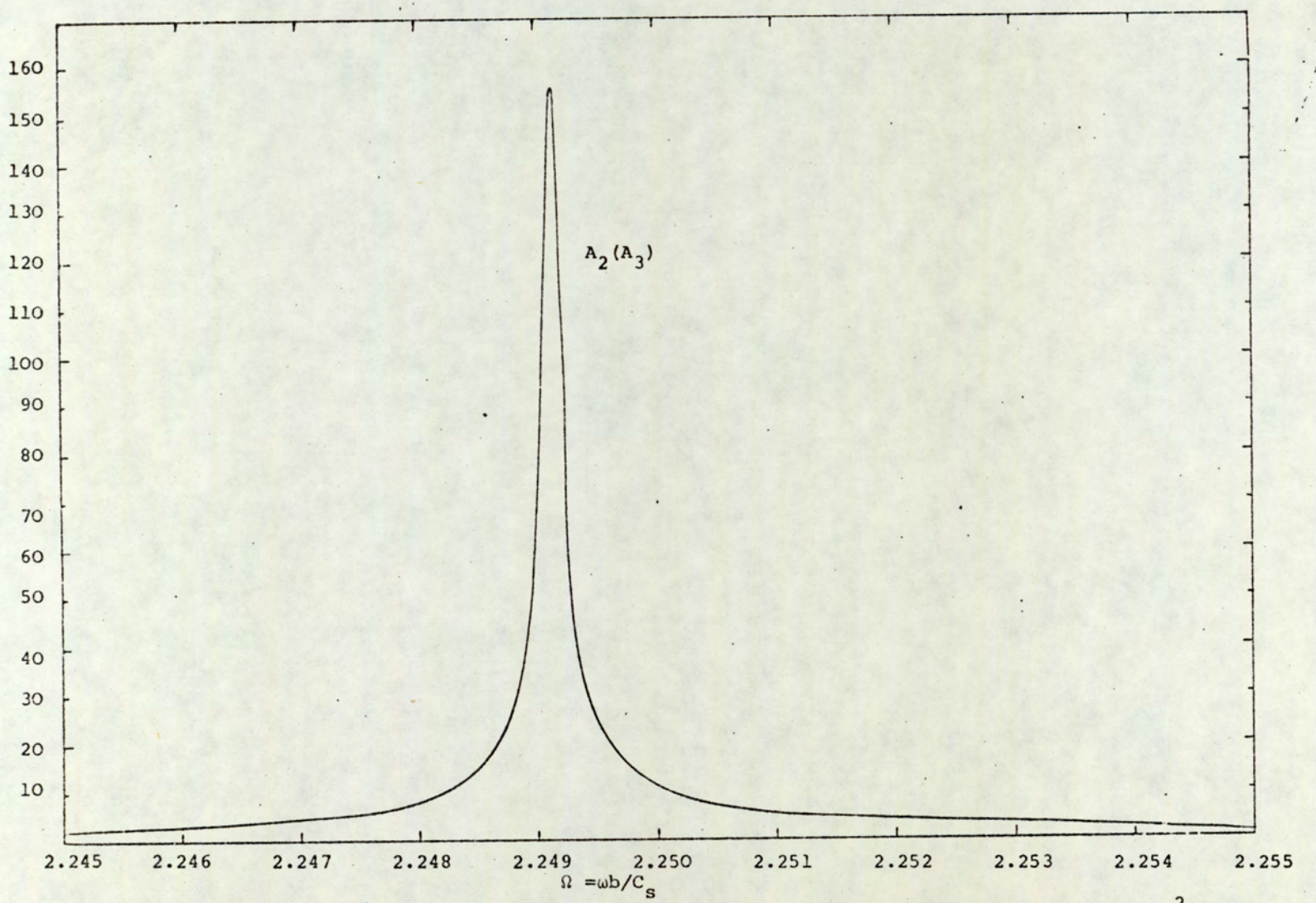

Fig. 6.3 Amplitude coefficients A_1 and $A_2(A_3)$ in the frequency range Ω=2.245 to 2.255. δ^2=0.355. The finite Q of the end resonant mode is due to the existance of a propagating mode.

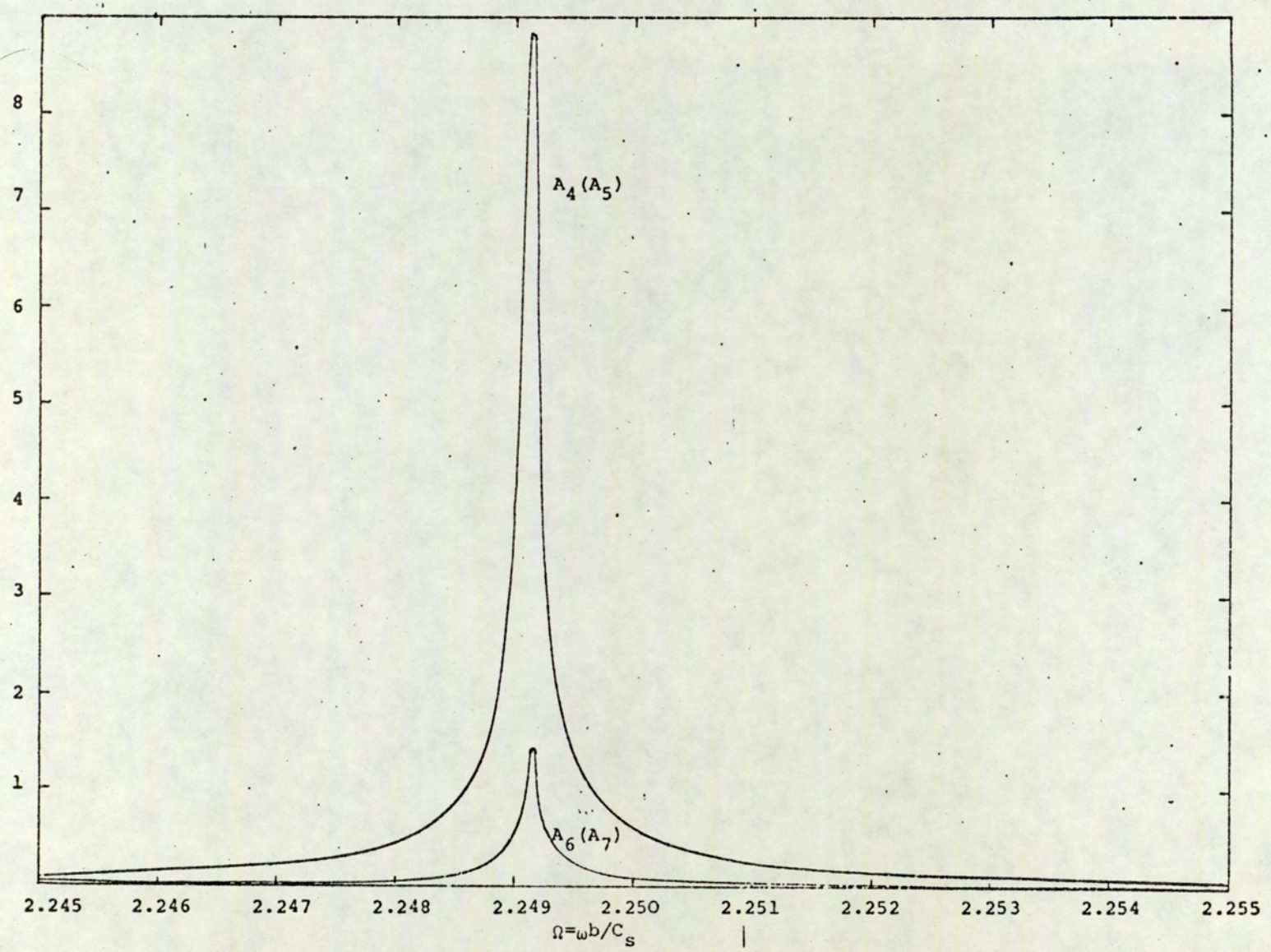

Fig. 6.4 Amplitude coefficients $A_4(A_5)$ and $A_6(A_7)$ in the frequency range $\Omega=2.245$ to 2.55. $\delta^2=0.355$. The Q factor for each of the complex modes is the same.

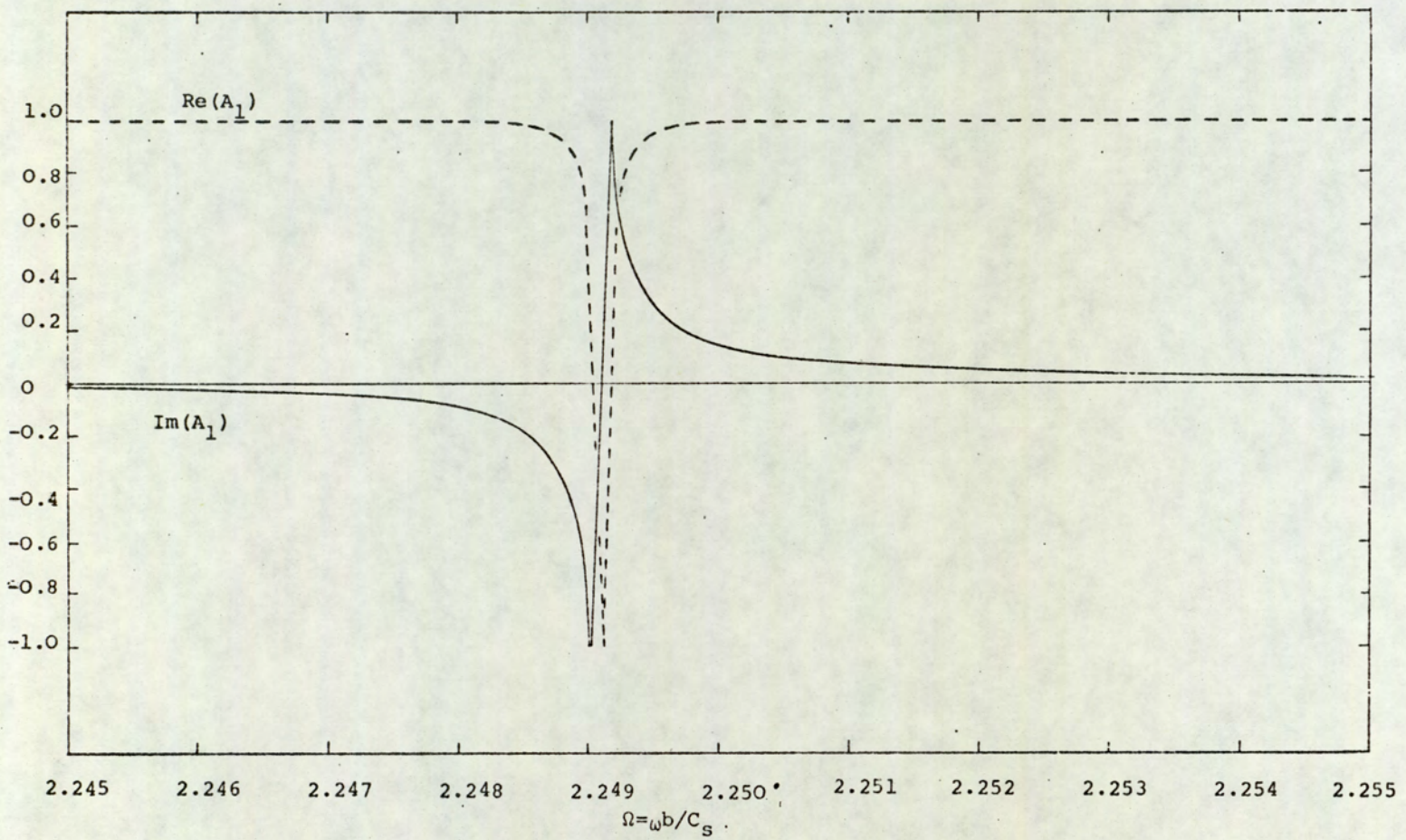

Fig. 6.5 Real and imaginary parts of the coefficient $A_1 \exp j\phi_1$ in the frequency range Ω=2.245 to 2.255. (——): imaginary; (---): real. δ^2=0.335. At resonance the reflection coefficient of the lowest real mode undergoes a change in phase of π radians.

the contribution of modes of a complex nature should be a minimal. Finally, the amplitude coefficient of the first pair of complex modes is seen to have a maximum peak at $\Omega \simeq 2.25$, at which $A_2(A_3)/A_1 >> 1$. Although figure 6.2 shows the value of this maximum at approximately 10, a more detailed exploration, in the vicinity of this frequency, shows that the peak has a maximum of 156.6 and occurs at a frequency of $\Omega = 2.24911$. Figure 6.3 displays the behaviour of the curve in the frequency interval $\Omega = 2.245$ to 2.255. The curves shown in figure 6.4 are the amplitude values for the second and third complex mode pairs, $A_4(A_5)$ and $A_6(A_7)$. It is seen that at this frequency all the complex modes have peak amplitudes and hence produce an end or edge resonance. The real and imaginary parts of $\exp j\phi_1$ are shown in figure 6.5. For frequencies $\Omega << \Omega_e$ the two modes propagating with real values of γ are almost in phase. As end resonance is approached the phase shift becomes 180^o and, when $\Omega >> \Omega_e$, becomes small again. All ten complex modes were found to have the same Q value of approximately 18.75×10^3.

A computed set of results obtained for $\delta^2 = 0.275$ (strip $\sigma = 0.45$, plate $\sigma = 0.31$) allowed direct comparison to be made with those given by Torvik. His results were computed for a plate with a Poisson's Ratio of 0.31 and show a resonance to occur at $\Omega = 2.3295$, with an amplitude ratio of approximately 35. The values obtained by the author were $\Omega = 2.3279$ and $A_2(A_3)/A_o(A_1) = 26$. This amounts to a frequency difference of less than 0.07% and a difference in amplitude of around 27%. The real and imaginary parts

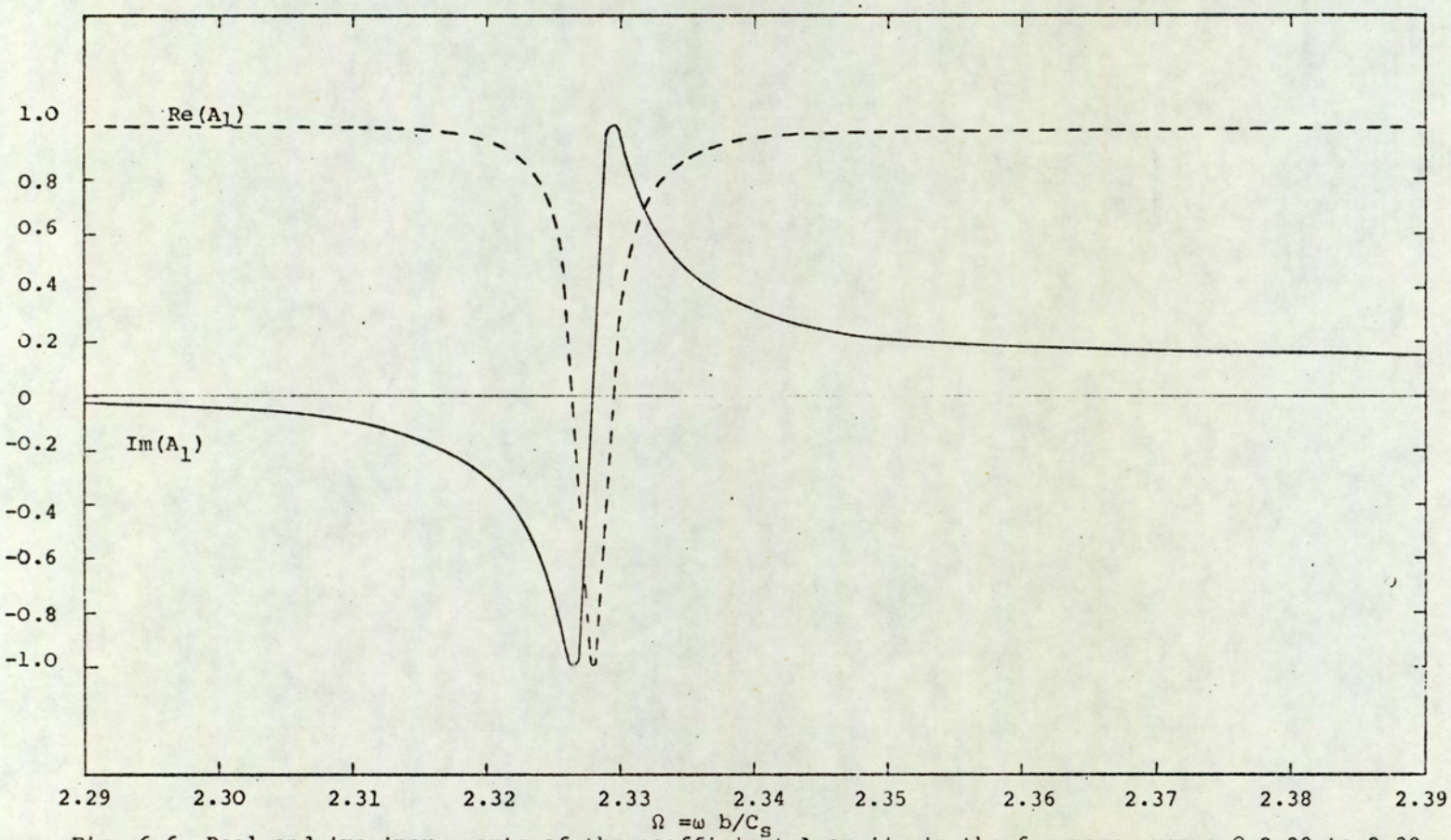

Fig. 6.6 Real and imaginary parts of the coefficient $A_1 \exp j\phi_1$ in the frequency range Ω=2.29 to 2.39. (——): imaginary; (---): real. δ^2=0.275.

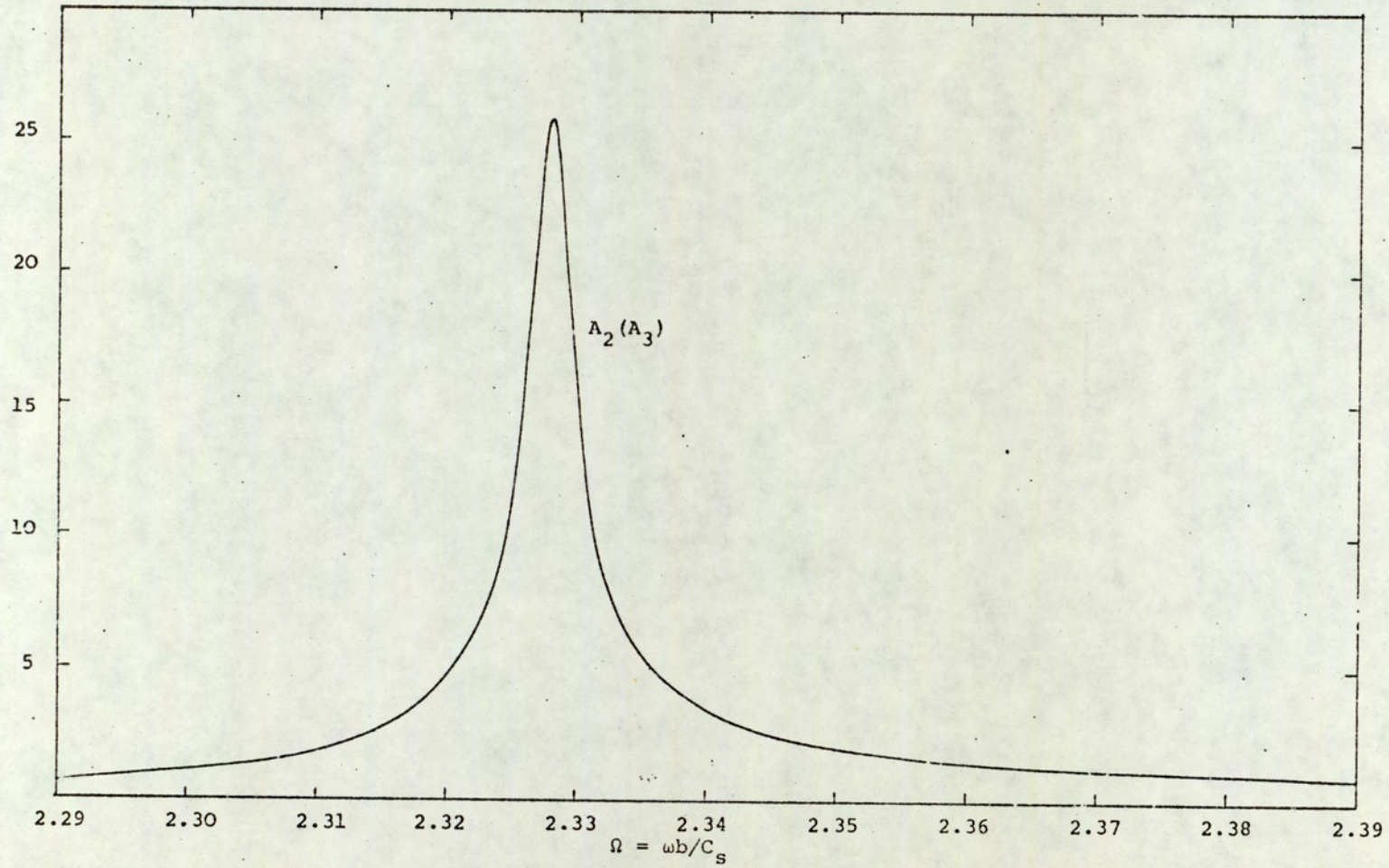

Fig. 6.7 Amplitude coefficient $A_2(A_3)$ in the frequency range Ω=2.29 to 2.39. δ^2=0.275. Note the decrease in Q with decrease in δ^2 by comparison with figure 6.3.

δ^2	σ(strip)	σ(plate)	Ω_e	$A_2(A_3)$	Q
0.45	0.1	0.091	2.07276	763.0	26.574×10^3
0.4	0.2	0.167	2.15304	205.8	9.787×10^3
0.375	0.25	0.2	2.19125	262.0	33.20×10^3
0.355	0.29	0.225	2.22071	316.3	
0.335	0.33	0.248	2.24911	156.6	18.75×10^3
0.325	0.35	0.259	2.2629	94.18	7.8×10^3
0.315	0.37	0.27	2.2764	64.7	4.139×10^3
0.295	0.41	0.291	2.3027	37.8	1.59×10^3
0.275	0.45	0.31	2.3279	25.8	0.776×10^3
0.17		0.398	2.4464	9.6	0.107×10^3
0.0		0.5	2.5995	6.3	0.052×10^3

Table 6.2

Theoretical values of Ω_e (end resonant frequency), $A_2(A_3)$ (amplitude ratio for first complex mode pair) and Q (quality factor calculated from $\Omega_e/(\Omega_2 - \Omega_1)$).

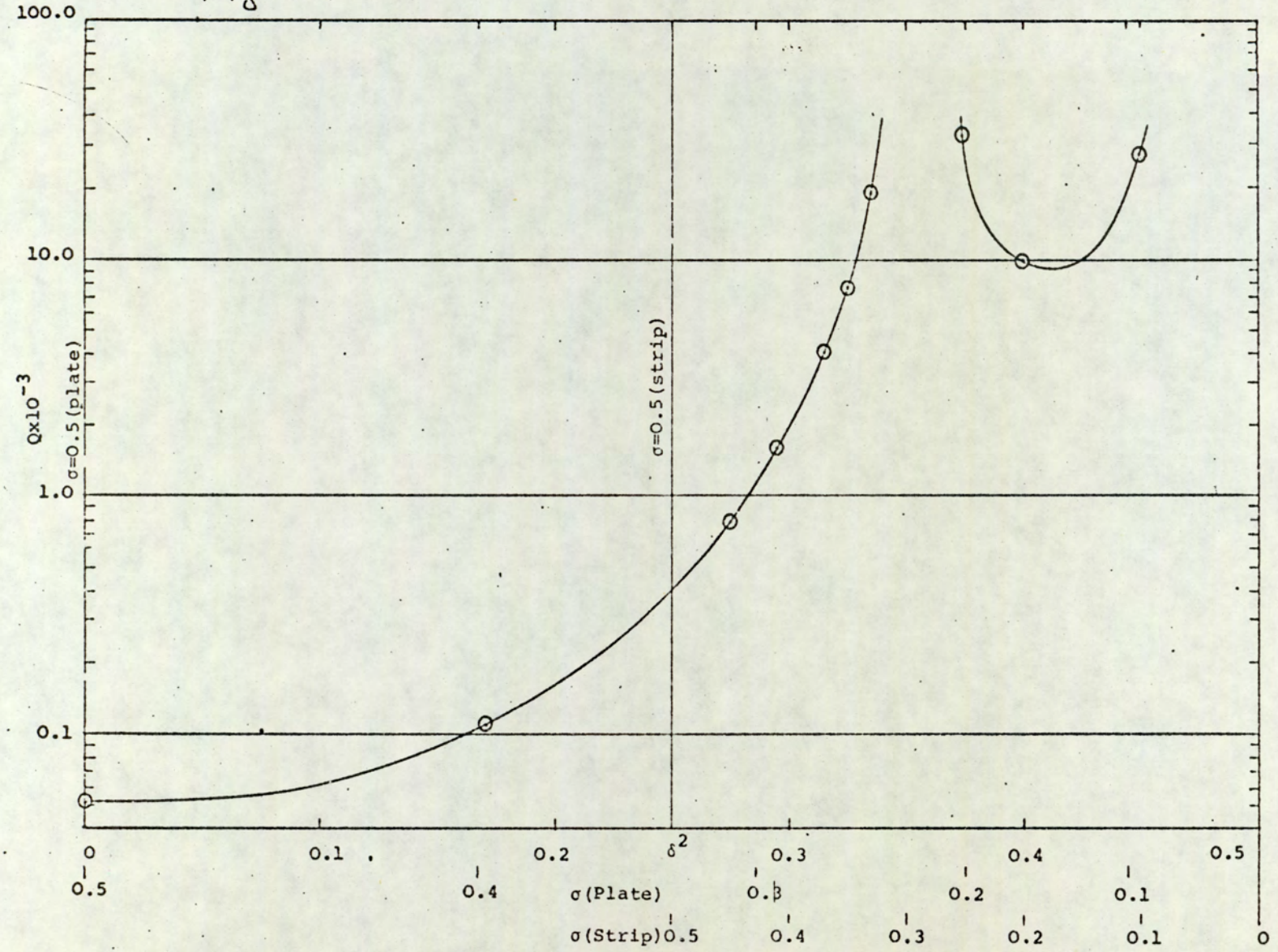

Fig. 6.8 The dependance of Q upon Poisson's Ratio. For a strip read δ^2 between 0.26 and 0.5. Unlike plates, strips made of the more common metals have extremely high Q's.

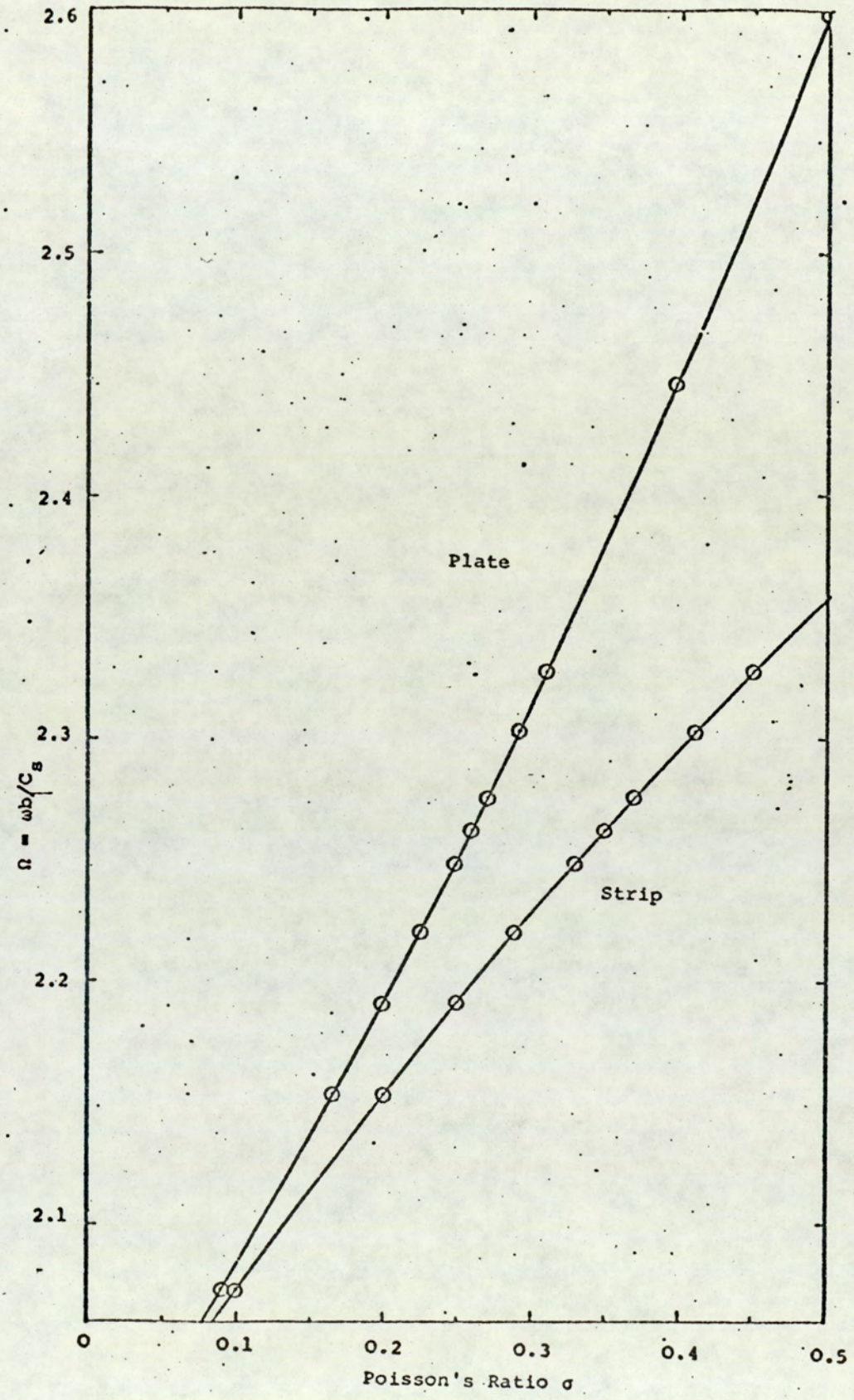

Fig. 6.9 Dependance of end resonant frequency upon Poisson's Ratio. Read upper curve for plate, lower curve for strip.

of $\exp j\phi_1$ and the amplitude coefficients $A_2(A_3)$, for this value of δ^2, are plotted in figures 6.6 and 6.7 respectively. Q has a value of 0.776×10^3.

Except for $\delta^2 = 0.355$ all other values of δ^2 resulted in curves of identical character and therefore no benefit will be gained by presenting them. Table 6.2 gives the relevant information relating to these solutions. The values of Q, calculated by means of the equation $Q = \Omega_e/(\Omega_2-\Omega_1)$ where Ω_2 and Ω_1 are the frequency values at $A_2/(2)^{\frac{1}{2}}$, are also shown graphically in figure 6.8. For δ^2 around 0.355 Q becomes extremely large. This region of the curve has greater relevance to the strip than the plate, since it occurs at the more useful values of Poisson's Ration. If, as Gazis and Mindlin suggest, these resonant modes have a finite amplitude because they are coupled to a propagating mode,it appears that for strips made of the more common metals this coupling becomes very small. This was found to be the case experimentally. In fact if the propagating mode existed at all it contained insufficient energy to excite an end mode at the remote end of the strip.

The dependance of resonant frequency on Poisson's Ratio is shown in figure 6.9. Using this figure in conjunction with that of 6.8 it is seen that the high Q values occur at frequencies of the Lam'e mode. When considering figure 6.2 it was seen that the amplitude of the complex modes became very small, if not zero, at this frequency since all the boundary conditions could be satisfied by the modes with real propagation constants. Therefore since the minimum

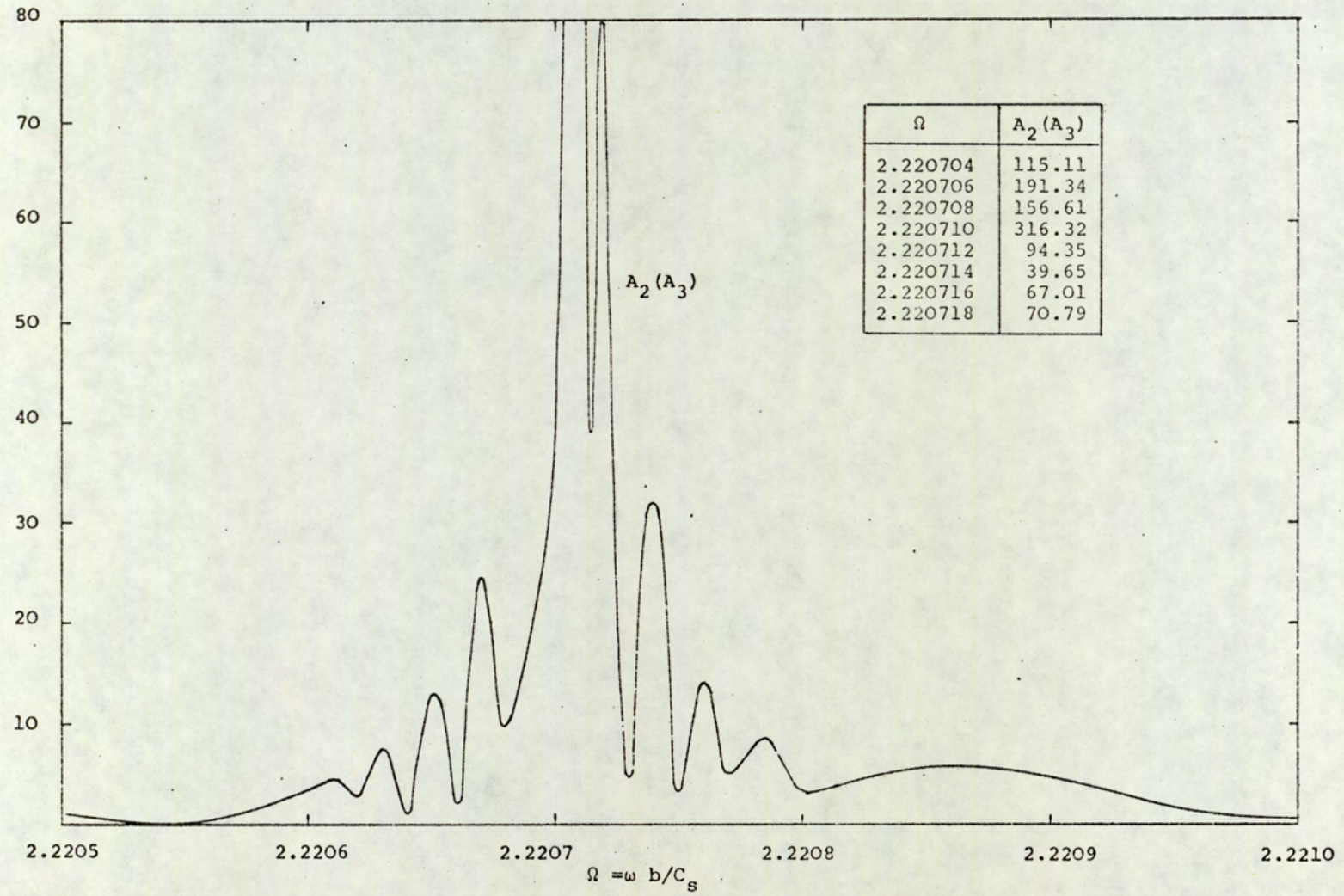

Ω	$A_2(A_3)$
2.220704	115.11
2.220706	191.34
2.220708	156.61
2.220710	316.32
2.220712	94.35
2.220714	39.65
2.220716	67.01
2.220718	70.79

Fig. 6.10 Amplitude coefficient $A_2(A_3)$ in the frequency range Ω=2.2205 to 2.221. δ^2=0.355. Theoretical results obtained when the end resonant frequency is close to Lam'e frequency ($\Omega=\pi/\sqrt{2}$)

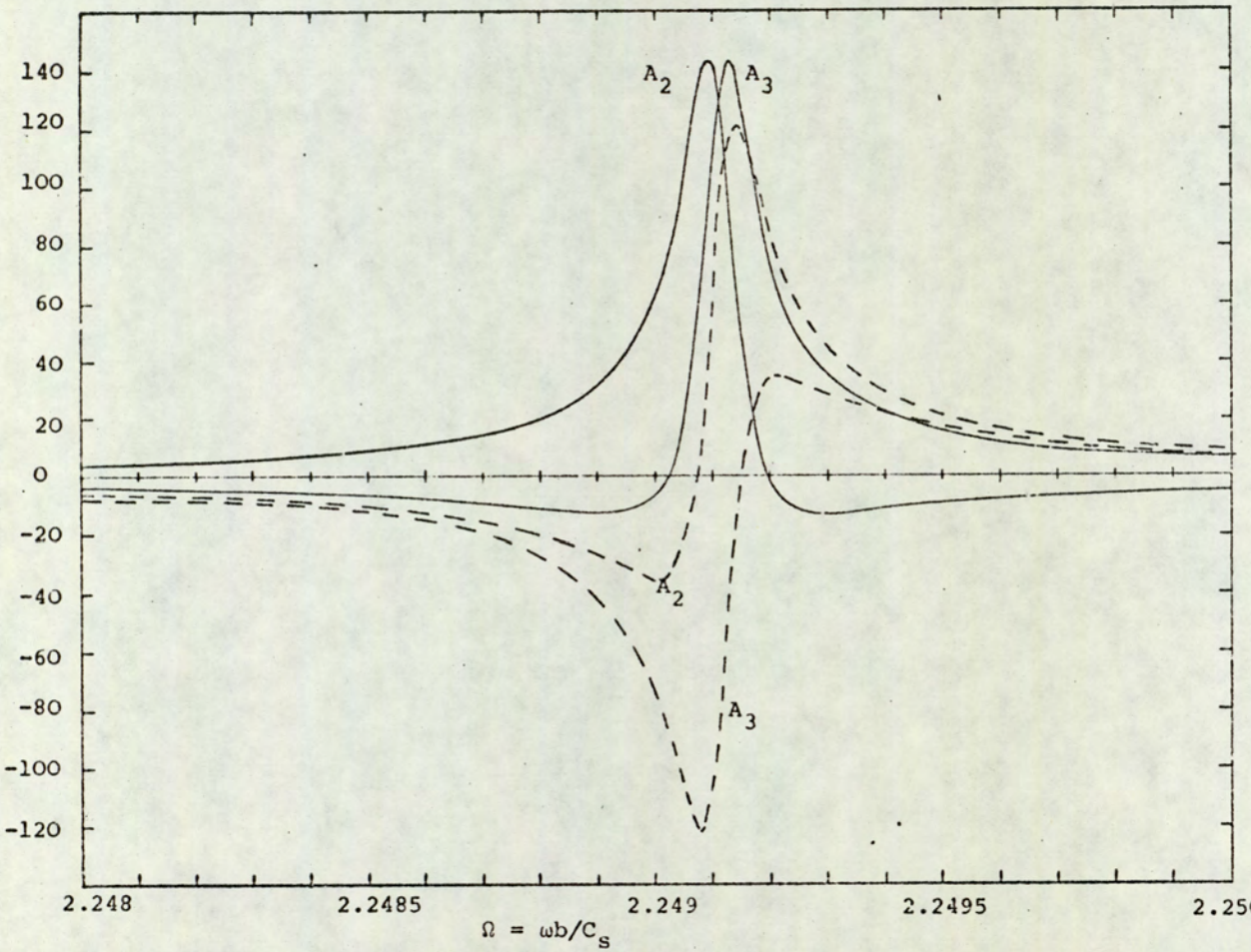

Fig. 6.11 Real and imaginary parts of the coefficients $A_2 \exp j\phi_2$ and $A_3 \exp j\phi_3$ in the frequency range Ω = 2.248 to 2.25. (——): imaginary; (---): real. δ^2 = 0.335.

of figure 6.2, independant of Poisson's Ratio, will always occur at $\Omega=\pi/(2)^{\frac{1}{2}}$, the prospect is now faced that maximum and minimum may be coincident at the relevant value of σ. Results obtained for $\delta^2= 0.355$ are shown in figure 6.10 Unlike solutions for other values of δ^2 the results do not form a smooth curve, but do show a major resonance at $\Omega\simeq 2.22071$. In practice internal friction would prevent this structure from being resolved.

It has been suggested (Zemanek) that the complex modes are generated at an interface in sufficient amplitudes as to cancel the residual stress left by the propagating mode. In context of the above results this would not appear to be wholly the situation since at values of Ω = Lam'e frequency an end resonance would not exist. Also in the vicinity of the Lam'e mode it would be expected that the amplitudes be smaller than elsewhere in the frequency spectrum and not the reverse since residual stresses are a minimum. It is therefore suggested that at the interface the complex modes are generated, to satisfy the boundary conditions, whether it be from within , by the S(1) mode or by an external source, but that the amplitude peak is pertaining to their resonant mode and not as a result of stress in balance. Figure 6.11 shows the way in which the real and imaginary parts of $\exp j\phi_2$ and $\exp j\phi_3$ behave around resonance. For frequencies lower than Ω_e

$$-\exp j\phi_3 = -\exp(-j\phi_2) \qquad 6.32$$

and for frequencies above Ω_e

$$\exp j\phi_3 = \exp(-j\phi_2) \qquad 6.33$$

writing equations 6.30 and 6.31 as

$$\sigma_{xxn}(y,x) = A_n \exp j\phi_n T_n(y) \exp j\gamma x \qquad 6.34$$

and

$$\sigma_{xyn}(y,x) = A_n \exp j\phi_n S_n(y) \exp j\gamma x \qquad 6.35$$

where it can be shown that

$$T_{2n}(y) = - T^*_{2n+1}(y) \qquad 6.36$$

and

$$S_{2n}(y) = -S^*_{2n+1}(y) \qquad 6.37$$

Therefore the sum of the stresses for the two complex modes is totally imaginary below and above resonance but with 180^o difference in phase. As resonance is approached the amplitude coefficients cease to be conjugate pairs and hence the sum of the modes becomes complex, which is tantamount to a propagating wave in both the x and y directions. From figure 6.11 it is seen that at resonance

$$\exp j\phi_3 = -\exp(-j\phi_2) \qquad 6.38$$

which results in the sum of the stresses, produced by these two modes, being totally real.

In short then, for frequencies above and below resonance

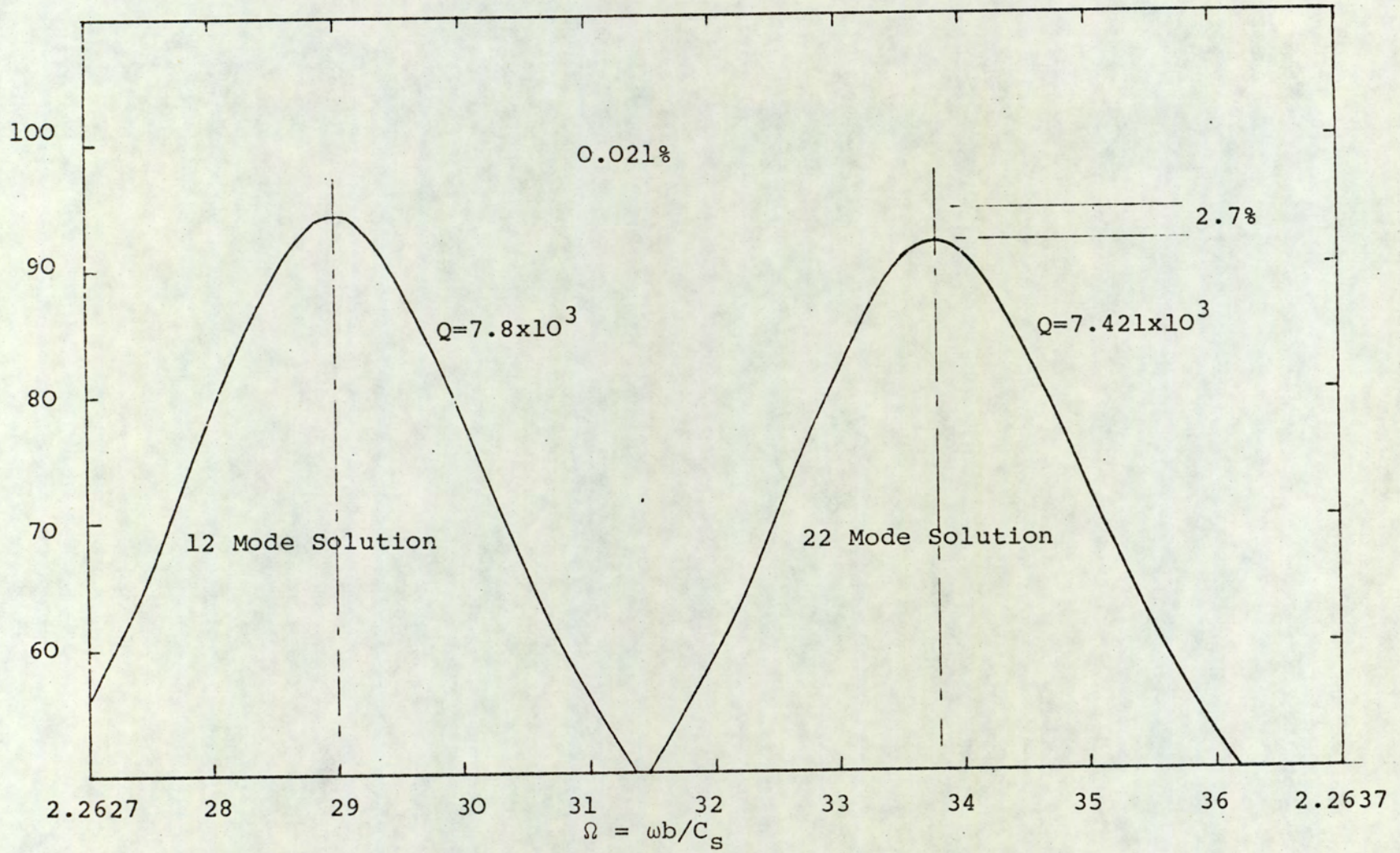

Fig. 6.12 Comparison of 12 and 22 mode solutions. Amplitude coefficient $A_2(A_3)$. $\delta^2 = 0.325$.

the complex modes form standing waves in quadrature to the driving source and therefore do not store energy. This mode of vibration could be termed an anti-resonance. At the end resonant frequency these modes form a standing wave, in phase with the exciting force, and therefore are at resonance.

22 Mode Solution

The summation of 22 modes was considered for $\delta^2 = 0.325$. This value δ^2 was chosen because of its reasonably high Q. Too higher value of Q would of course make pinpointing the resonance costly, and too lower Q would reduce the resolution between the peak obtained for 22 modes and that obtained for 12 modes. Figure 6.12 shows the details of the two peaks in the vicinity of resonance. The curves show an increase in frequency of 0.02%, a drop in amplitude of 2.7% and a drop in Q of 5%. Results obtained by Zemanek for 5, 7 and 9 mode considerations, for the axi-symmetric end resonance of a cylinder, display identical type of behaviour.

6.5 Experimental Results

Frequency measurements were made on eight strips. In all cases the dimensions were such that the length was at least six times the width. The materials used were chosen to give as wider spread of Poisson's Ratio as possible. Discs were cut from six of the strips to enable values of shear

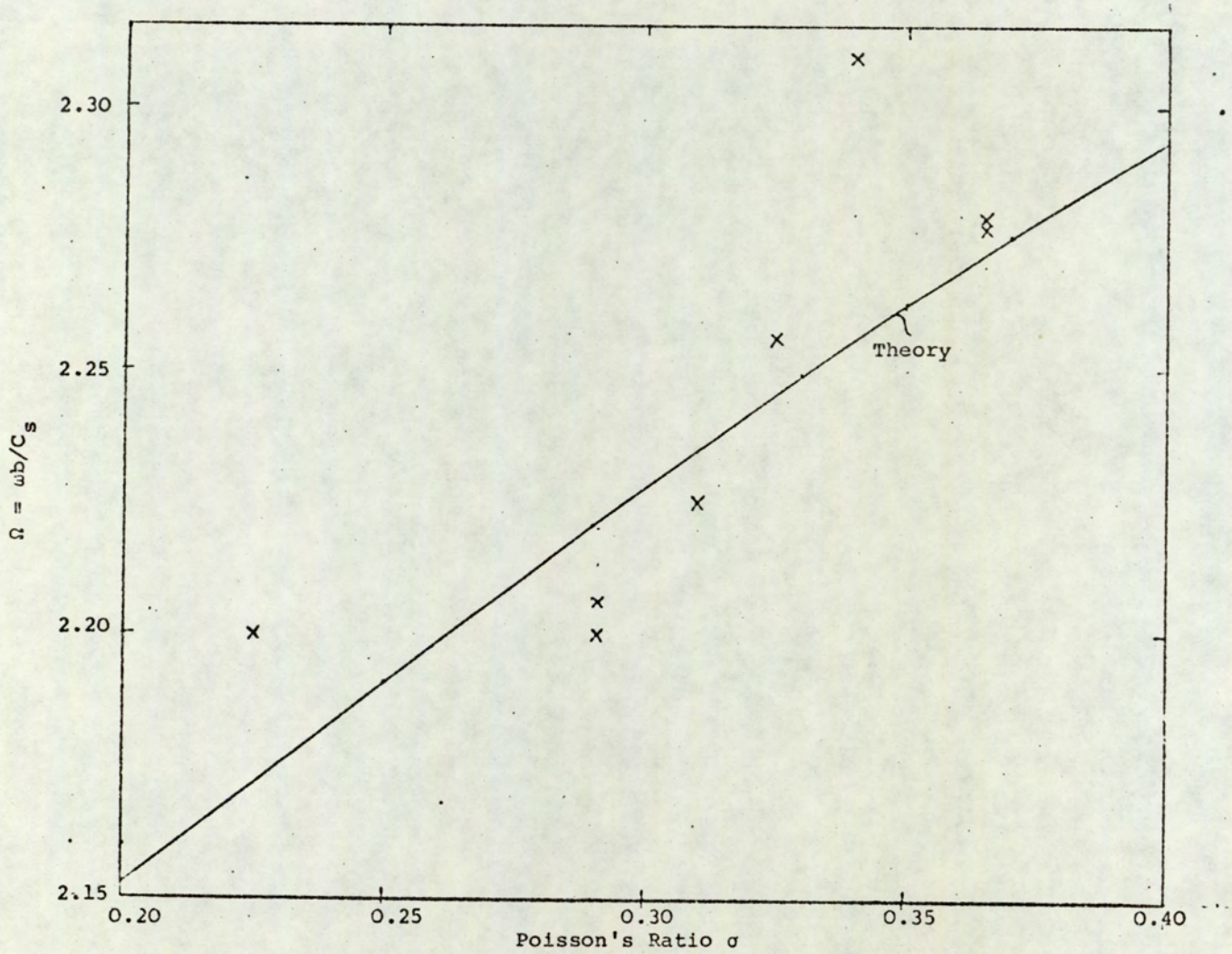

Fig. 6.13 Comparison of experimental and theoretical results of end resonant frequencies, for strips having various values of Poisson's Ratio. A difference in results of 1% would be represented by approximately half a division on the frequency scale.

velocity and σ to be calculated. The dimensions and results obtained are shown in table 6.3 and plotted in figure 6.13.

Material	σ	C_s m/s	Frequency	Width(2b)	Ω_{exp}	Ω theory	%
Brass	0.365	2162	27.502 KHz	5.7 cm	2.277	2.272	-0.3
Brass	0.365	2162	27.383 KHz	5.728cm	2.279	2.272	-0.31
Aluminium	0.34	3133	40.042 KHz	5.75 cm	2.309	2.256	-2.3
Copper	0.325	2280	28.222 KHz	5.801cm	2.256	2.245	-0.5
Mild Steel	0.31	3258	41.968 KHz	5.497cm	2.225	2.235	+0.5
Mild Steel	0.291	3235	17.892 KHz	12.7 cm	2.2067	2.221	+0.6
Mild Steel	0.291	3235	29.812 KHz	7.6 cm	2.2003	2.221	+0.9
Glass	0.225	3450	31.677 KHz	7.625cm	2.1995	2.169	+1.4

Table 6.3

The percentage difference in frequency is seen to lie between -2.3 and +1.4. It is thought that the cause of the error comes mainly from the experimental results, for two reasons. a) The problems associated with obtaining absolute values of frequency, by the echo technique used, was outlined in Section 4.6, Chapter 4. It is obvious, from the table showing the change in frequency with position of coupling, that the measured frequency may be as much as 3% in error when coupling at an anti-node (α=0). The more accurate value being at α=0.38 (since this is almost on the node i.e. U_n=0.0). Therefore since the end resonant frequencies were measured by coupling at the end of the strip, which is the point of maximum amplitude, it is to be expected that errors

occur. It was also pointed out in section 4.6 that not only does the point of drive have an effect but so also does the ratio of characteristic impedance to resonator density. This would appear to be the situation, for as table 6.3 shows the largest error occurs for the materials with the lowest densities (i.e. Aluminium and Glass).

b) All the strips used were cut from rolled stock, hence introducing a certain amount of orthotropy. This would effect the value of velocity and σ depending upon the orientation of the strip.

In conclusion the theoretical results are compared with those obtained experimentally by McMahon (53) for edge resonances of discs. Table 6.4. where the theoretical values

Material	σ	C_s	Ω(McMahon exp.)	Ω(theory)	% Difference
Aluminium	0.344	5150 m/s	2.369	2.373	0.2
Mild Steel	0.293	5170 m/s	2.300	2.304	0.2

Table 6.4

of Ω are obtained from figure 6.9 or by linear extrapolation of the results in table 6.2.

CHAPTER 7

DYNAMIC CLAMPING

CHAPTER 7

DYNAMIC CLAMPING

7.1 Introduction

The recent use of tuning fork resonators in the field of ultrasonic thermometry, Seth (67), Bell (31, 32), Fathimani (68), has created a demand for information relating resonator parameters to their natural frequencies, for this geometry. Because of their complex shape, theoretical solutions are not readily obtainable, and design is based solely upon empirical results. Though not specifically aimed at solving the problem it is thought that the contents of this chapter offers, in part, information relevant to this topic.

Dynamic clamping is a condition that is created by the opposing motion of two bodies vibrating in anti-phase. A typical example of a structure possessing this phenomenon is the tuning fork where, at the base of the tines, because of the constraining effect one tine sets on the other, the angular momentum of one tine exactly balances that of the other. The static equivalent is the clamped reed where it is postulated that the clamp is sufficiently massive to react to momentum changes without energy absorption. Consider the geometry shown in Figure 7.1. When the two tines perform the kind of motion indicated the displacement at point p will be in the x direction only, since the resultant of that in the y direction will be zero. In addition the differential of the displacement in the y direction will be zero. Therefore since

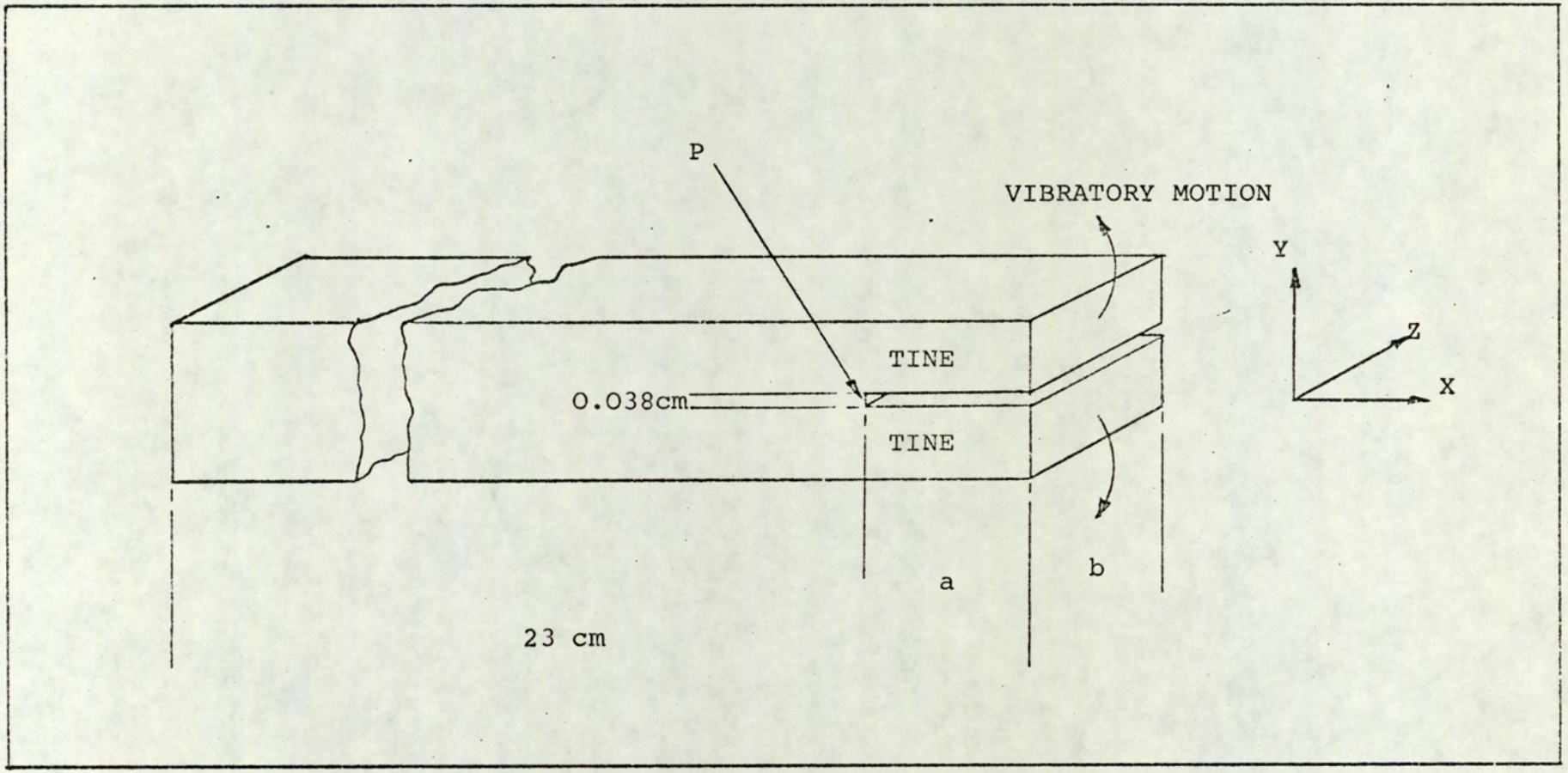

Fig. 7.1 Tuning fork type resonator. The resultant displacement in the y direction at point p is zero due to the opposing motion of the tines.

$$u_y = \frac{\partial u_y}{\partial x} = 0 \qquad 7.1$$

at y = 0 it seems reasonable to assume that the kind of boundary condition that exists should be related to that of clamped. Where the (unrealisable) static clamp gives a boundary condition that

$$u_y = \frac{\partial u_y}{\partial x} = 0$$

at the line origin, for the dynamic case where the origin cannot be precisely define, the positions where these conditions are realised is uncertain. The results are interpreted by developing a dimensionless frequency factor of the form

$$\frac{\text{frequency x (a dimension)}}{\text{(a velocity)}}$$

where h and b are used directly but where "a" can have a correction which is a function of h and b. Of necessity any formula must obey Rayleigh's "Scaling Law" (similitude) and approximate to the classical reed formula when a>>b>>h. The results are expected to extend data to dimension ratios where h is comparable to a and b. In practice the only condition not covered is the case where h>>b and a. The first two reed modes (having transverse nodal lines) have been explored. For the two configurations considered the experimental results have been compared with theoretical solutions obtained for plates of the same dimensions but with statically clamped boundaries. In the case of the resonator

shown in Figure 7.1, for example, each tine is compared with a rectangular plate having a thickness h, length a, and width b, with C.F.F.F. (Clamped, Free, Free, Free,) boundary conditions.

For the case of rectangular plates with boundary condition other than simply-supported, exact solutions are not known, therefore numerical results have to be found using approximate techniques. The values that have been used here, presented by Leissa (69), were evaluated using the Ritz method. This is a variational technique which is based on minimizing the ratio

$$\omega^2 U/T \qquad 7.2$$

where U and T are the maximum values of potential and kinetic energies respectively. The expressions for U and T are obtained by assuming that the deflection of the plate ω can be expressed as a linear series of beam functions. Coefficients relating to these functions are then chosen so as to minimize equation 7.2. A comprehensive discussion on the method is given by Young (70).

7.2 Tuning Fork (as clamped plates)

The tuning fork, as shown in Figure 7.1, is particularly well suited to a discussion on dynamic clamping, since it allows the effect to be presented, not only in terms of

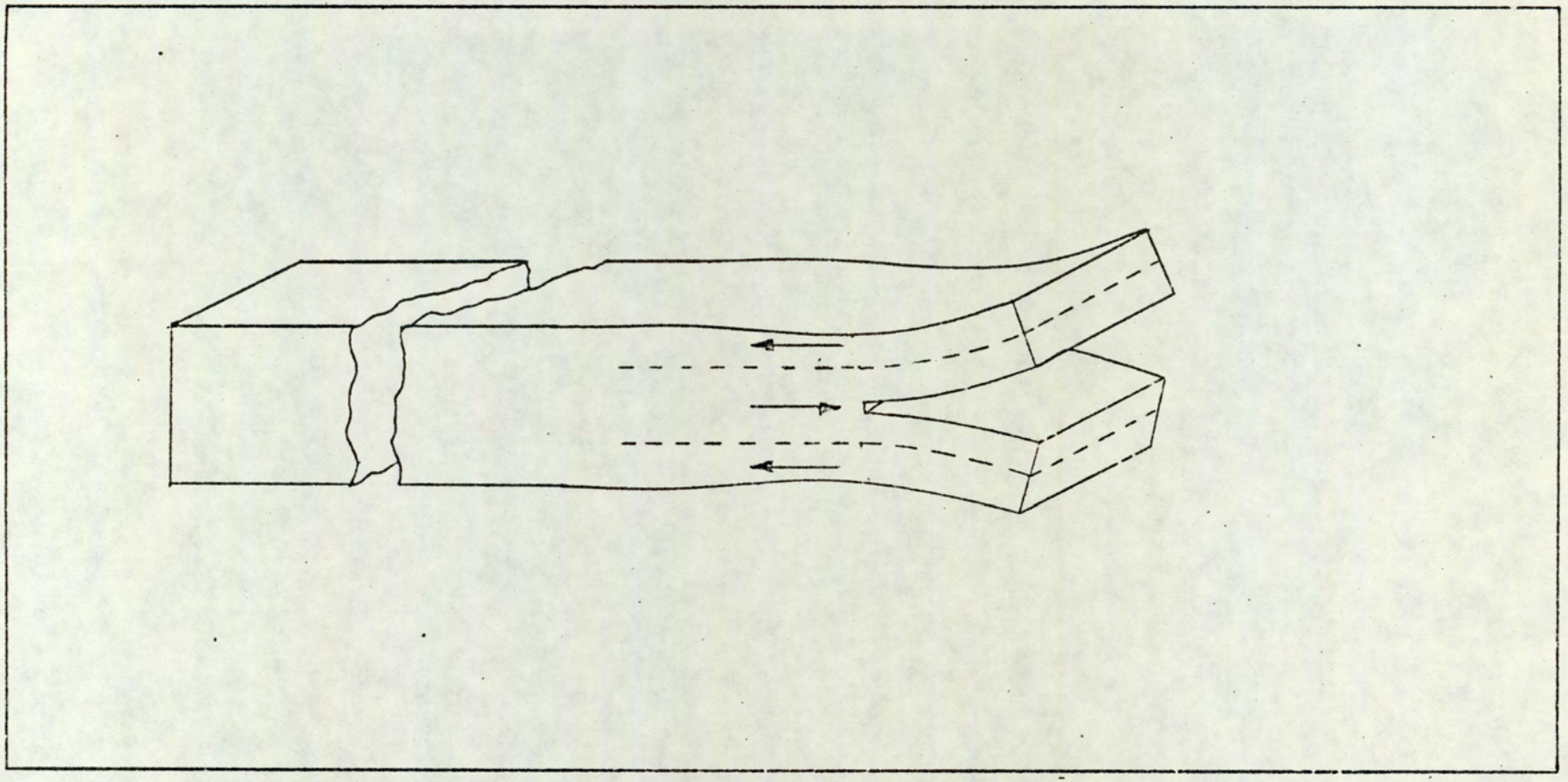

Fig. 7.2 The vibrations of the tines tend to generate a propagating mode with the displacement field shown.

flexural vibrations of plates, but also in terms of propagating waves in rectangular strips. For example, from the classical theory of plates, the assumption is made that for low amplitude vibrations there exists an underformed middle surface "neutral plane" for which the inplane strain is zero. Therefore when the two tines are vibrating in anti-phase the displacement field that they produce, at the end of the strip to which they are joined, will be of the form shown in Figure 7.2. Hence there is a tendancy for a propagating wave of this character to be generated in the strip. However, if the frequency of vibration is well below the cut-off frequnency of the s(2) mode (see Figure 6.1) this type of motion will only couple to the complex modes. This situation then ensures that the energy stored by the vibrating plates is not leaked away to the rest of the structure via a propagating mode.

Experimentally this was supported, for it was found that resonant modes for the tines, which should have occurred at frequencies above cut-off for the s(2) mode, could not infact be excited, and when this frequency range was explored the whole system was set in motion.

The tuning fork type resonators were manufactured from 1.27 cm square bar, by machining a narrow longitudinal slot in one end. Tine length and thicknesses were adjusted by increasing the depth of the slot or reducing the thickness of the bar respectively. In all cases the overall length was 23 cm.

From the classical plate theory the angular frequency

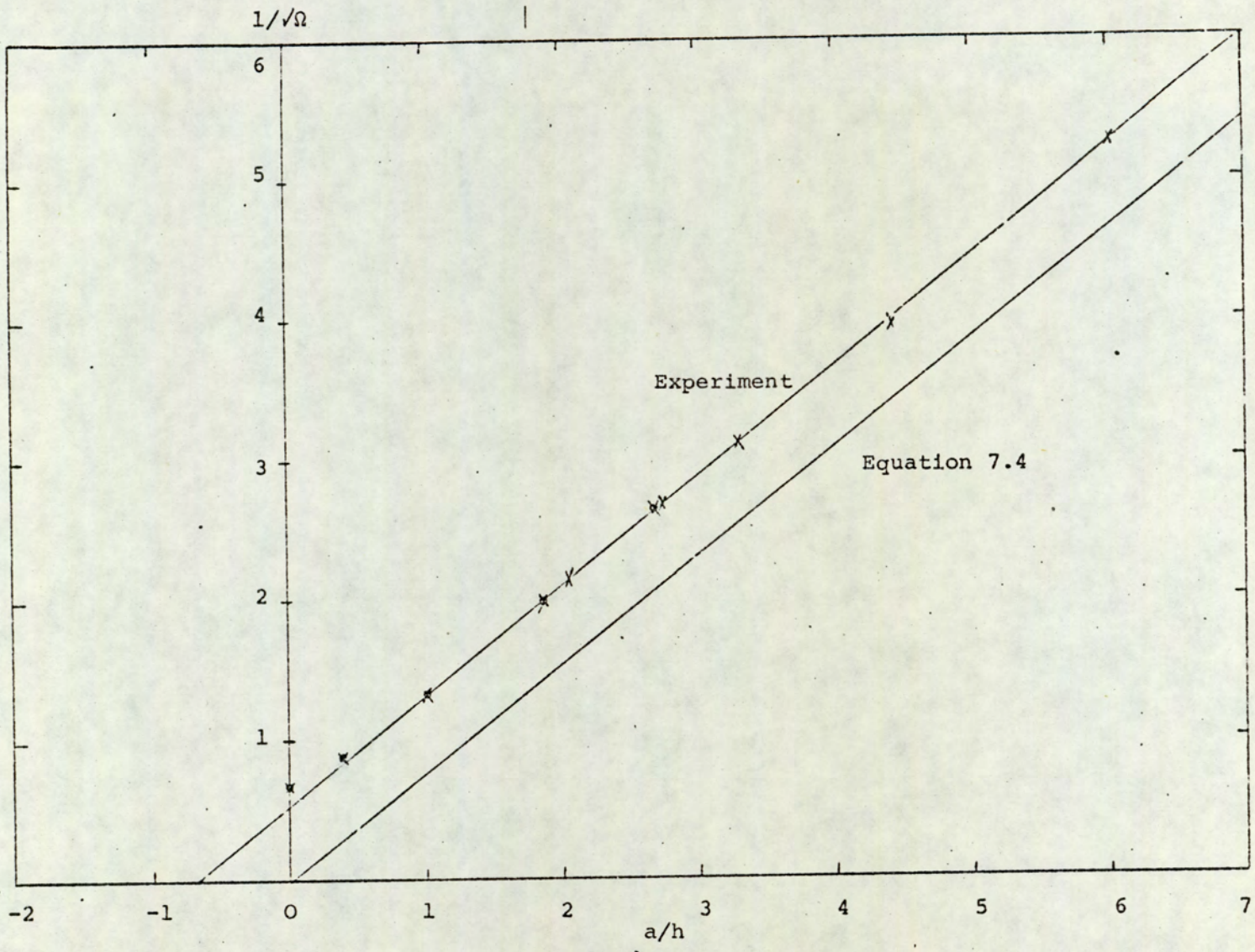

Fig. 7.3 Experimental results for dynamically clamped plates (crossed points), and theoretical curve for statically clamped plates.

for a plate of length a and thickness h is given by

$$\omega = \lambda h C_p / a^2 \sqrt{12} \qquad 7.3$$

where λ is the frequency factor obtained by satisfying the equation of motion and boundary conditions, or as in this instance by the Ritz method. Values of λ are given in reference (69) for all the 21 possible combinations of boundary conditions that exist for a rectangular plate. Using the substitution $\Omega = \omega h / C_s$, and rearranging the terms, equation 7.3 can be written as

$$\frac{1}{\sqrt{\Omega}} = \frac{1}{\sqrt{\lambda}} \left| 6(1 - \sigma) \right|^{\frac{1}{4}} \frac{a}{h} \qquad 7.4$$

This form of equation is arranged to allow the "a" end correction to be investigated. For a change in aspect ratio a/b from 0.125 to 2.0 the value of λ, for the fundamental mode of a C.F.F.F. plate, varies almost linearly from 3.5134 to 3.4575 (Leissa). Therefore chosing a value of 3.49 gives an error, over the above range of a/b, of less than 1%. A plot of $1/\sqrt{\Omega}$ versus a/h for λ = 3.49 and Poisson's ratio σ=0.29,using equation 7.4 is shown in Figure 7.3. Initial experiments were carried out on mild steel specimens with various tine lengths a. The measured frequencies for the fundamental mode together with their corresponding a values are shown in Table 7.1. Ω was calculated using a shear velocity for mild steel of 3235 meters/second.

Frequency KHz	a cm	b cm	h cm	a/h	$1/\sqrt{\Omega}$
8.604	2.032	1.27	0.616	3.299	3.117
12.015	1.651	1.27	0.616	2.680	2.638
21.276	1.143	1.27	0.616	1.856	1.982
47.826	0.635	1.27	0.616	1.031	1.322
108.142	0.254	1.27	0.616	0.412	0.879
180.355	0.000	1.27	0.616	0.000	0.681

Table 7.1 Experimental results for mild steel tuning forks, of various a values. 1.1 mode.

The last frequency value in Table 7.1 is an average value of measured end resonances. Unlike thin strips, which have been found to support only one end resonant mode, a bar of square cross-section has three. The lowest of these has two nodal lines parallel to the sides of the bar and at right angles to each other. This is identical to the nodal pattern displayed by the lowest flexural mode of a completely free square plate. For a rectangular plate with length greater than the width the lowest flexural mode has a displacement pattern similar to the end resonant mode of a strip, that is two parallel nodal lines across the shortest dimension. When the plate becomes square this mode splits to form the second and third modes, the lowest has two nodal lines at right angles to each other passing from corner to corner and the higher has a nodal circle.

An identical behaviour has been found to exist for the end mode of a strip as it approaches the dimensions of a square section bar, therefore the average of these two modes has been taken to obtain the last value in Table 7.1. The values of a/h and $1/\sqrt{\Omega}$ in this table are plotted as circled points in Figure 7.3. For values of Ω less than one the two curves have approximately the same target. The crossed points on the same curve represent results obtained for measurement made on similar specimens with varying values of the parameter h. These results are shown in Table. 7.2.

Frequency KHz	h cm	b cm	a cm	a/h	$1/\sqrt{\Omega}$
18.222	0.616	1.27	1.27	2.062	2.142
15.453	0.465	1.27	1.27	2.062	2.677
11.508	0.287	1.27	1.27	4.425	3.948
8.906	0.211	1.27	1.27	6.020	5.234

Table 7.2 Experimental results for mild steel tuning forks of various h values. 1.1 mode.

Since both sets of results lie on the same straight line and the tangent of both curves is the same it may be assumed that the frequency expression for the dynamically clamped plates is of the form

$$\frac{1}{\sqrt{\Omega}} = \frac{1}{\sqrt{\lambda}} \left|6(1 - \sigma)\right|^{\frac{1}{4}} \left(\frac{a}{h} + k\right) \qquad 7.5$$

where k from figure 7.3 has a value of approximately 0.68. Rearranging 7.5 to give an expression similar to equation 7.3 results in

$$\omega = \lambda h C_p / \sqrt{12}\ (a + kh)^2 \qquad 7.6$$

From which it is seen that, by comparison to statically clamped plates, the length a is apparently increased by a factor proportional to the thickness h of the plate.

An identical set of experiments were carried out on the same specimens to observe the second reed type mode of a C.F.F.F. plate. This mode has a nodal line parallel to the clamped edge. Its λ value has been taken as 21.76, giving the same degree of error over the same range as for the lower mode. Table 7.3 gives the experimental results.

Frequency KHz	h cm	b cm	a cm	a/h	$1/\sqrt{\Omega}$
46.172	0.616	1.27	2.032	3.299	1.345
51.342	0.211	1.27	1.27	6.024	2.18
61.249	0.616	1.27	1.651	2.680	1.168
63.357	0.287	1.27	1.27	4.425	1.683
96.05	0.616	1.27	1.143	1.856	0.933

Table 7.3 Experimental results for mild steel tuning forks. 2.1 mode.

Plotting results in the same way, and comparing curves with that of the 2.1 mode for a C.F.F.F. plate, shows that equation 7.6 may also be applied to this mode. In this case however k has a value of around 1.14. It is obvious therefore that the difference in frequency between the static and dynamically clamped plates is not only a function of the dimensions of the resonator as suggested by equation 7.5, but also of the mode of resonance. In terms of Figure 7.3 this would mean that the two curves have to be made coincident by movement along both axis. Therefore equation 7.5 should be written as

$$\frac{1}{\sqrt{\Omega}} = \frac{1}{\sqrt{\lambda}} \left|6(1-\sigma)\right|^{\frac{1}{4}} \left|\left(\frac{a}{h} + Q\right) + P\sqrt{\lambda}\left|6(1-\sigma)\right|^{-\frac{1}{4}}\right| \qquad 7.7$$

where P and Q are constant, and may be determined from the values of k obtained for the two experiments, by solving the following simultaneous equations

$$Q + P\sqrt{\lambda_n}\left|6(1-\sigma)\right|^{-\frac{1}{4}} = k_n \qquad 7.8$$

$\lambda_1 = 3.49$ $\qquad$ $k_1 = 0.68$ $\qquad$ (first experiment)

and

$\lambda_2 = 21.76$ $\qquad$ $k_2 = 1.14$ $\qquad$ (second experiment)

For a value of σ=0.29 P and Q have the values 0.236 and 0.373 respectively. Hence for dynamically clamped plates the natural frequencies can be obtained from equations 7.6 and 7.8. In particular for σ=0.29

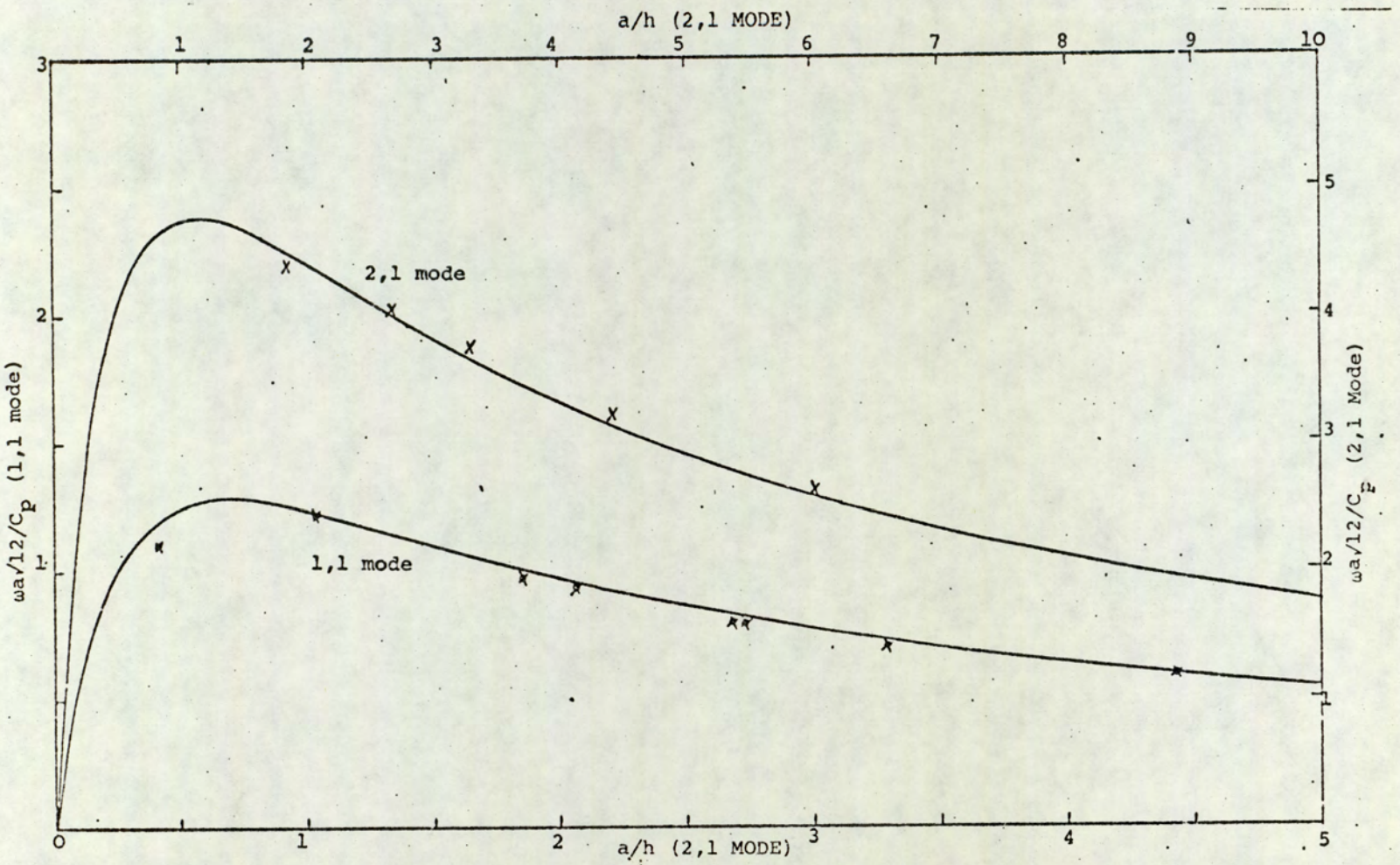

Fig. 7.4 Frequency curves obtained using equations 7.9 and 7.10 for the 1,1 and 2,1 modes in the tuning fork type resonator. Indicated points are experimental results given in tables 7.1, 7.2 and 7.3. Top and right hand scale for 2,1 mode. Bottom and left hand scale for 1,1 mode.

$$\omega = \lambda h C_p / \sqrt{12}\ (a + kh)^2 \qquad 7.9$$

where

$$k = 0.373 + 0.164\ \sqrt{\lambda} \qquad 7.10$$

Figure 7.4 shows a plot of the factor $\omega a\sqrt{12}/C_p$ versus a/h, as obatined from equations 7.9 and 7.10 and experiment, for the 1,1 and 2,1 modes so far considered.

The 1,1 and 2,1 modes are affected very little by the ratio a/b, this is in fact common to all modes containing no nodal lines at right angles to the clamped edge. If equations 7.9 and 7.10 are applied to another mode and in particular one without the symmetry displayed by the 1,1 and 2,1 modes the extent to which they may be used could be determined. The lowest anti-symmetric mode is the 1,2 mode, this has one nodal line at right angles to the calmped edge. Its λ value varies from 3.85 for a/b = 0.2 to 17.988 at a/b = 2.5. Two experiments were carried out on this mode, one in which a/b remained constant and h varied, this would produce a curve similar to those already plotted since λ and hence k would be constant, and one in which h was held constant and a/b varied.

Table 7.4 gives results of the experiments.

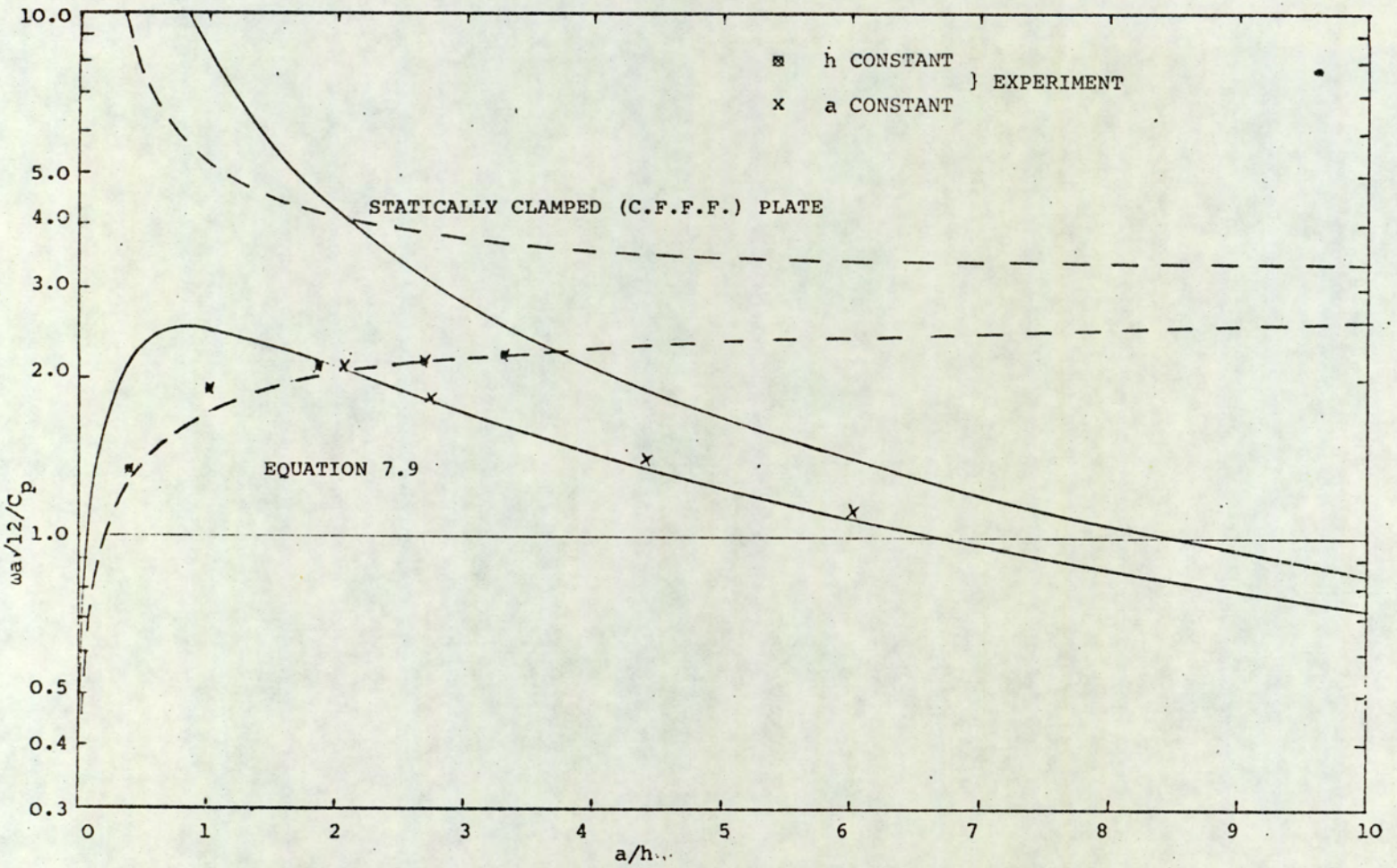

Fig. 7.5 Frequency curves for 1,2 mode in tuning fork type resonator. Indicated points are experimental results given in table 7.4. (——): a constant; (---): h constant. The curve for the statically clamped plate was obtained from equation 7.3

Frequency KHz	h cm	b cm	a cm	a/h	$\omega a\sqrt{12}/C_p$
27.506	0.616	1.27	2.032	3.299	2.24
33.161	0.616	1.27	1.651	2.68	2.195
46.126	0.616	1.27	1.143	1.856	2.113
75.044	0.616	1.27	0.635	1.031	1.910
132.45	0.616	1.27	0.254	0.412	1.349
41.937	0.616	1.27	1.27	2.062	2.135
36.469	0.465	1.27	1.27	2.731	1.857
28.047	0.287	1.27	1.27	4.425	1.428
22.097	0.211	1.27	1.27	6.020	1.125

Table 7.4 Experimental results for mild steel tuning forks in 1,2 mode.

The results of table 7.4 and those of equations 7.9 and 7.10 are plotted in figure 7.5. Points for the theoretical curve were obtained using λ values given by references (69) and (49), remembering that a/h is related to $\lambda(a/b)$ by $a/h = (b/h)(a/b)$ for h constant.

Figure 7.5 also shows curves for the same mode in a C.F.F.F. plate. A logrithmic scale has been used to enable all four curves to be presented. The results for the anti-symmetric mode are remarkably good, since both the

constants of equation 7.10, which was used to obtain the curve, were arrived at independently. Comparison with the curves for a statically clamped plate indicate how well equation 7.9 represents the dynamic situation. At a = 2h, for example, where the modified equation is seen to be still quite accurate, the difference between the two sets of curves is 100%.

The effect of Poisson's ratio on the foregoing solutions is small as can be seen by the results obtained for Aluminium and Copper tuning forks, shown in Table 7.5. Investigations carried out by Leissa on the effect of σ upon the frequency parameter λ show that the sensitivity is very much a function of the ratio a/b and mode. However, in the range of σ for the more common materials, say 0.25 to 0.35 the error is probably less than 4% by using the centre value.

It is obvious from the curves that unlike the statically clamped plates the dynamic structure reaches a maximum frequency as h is increased. The maximum value can be obtained by differentiation of equation 7.9 to give

$$\frac{\partial \omega}{\partial h} = \frac{\lambda C_p}{\sqrt{12}(a + kh)^2} \left| \frac{a - kh}{a + kh} \right| \qquad 7.11$$

from which it is seen that ω is a maximum when a = kh, the maximum frequency is given by

$$\omega = \frac{\lambda C_p}{4\sqrt{12}ak} \qquad 7.12$$

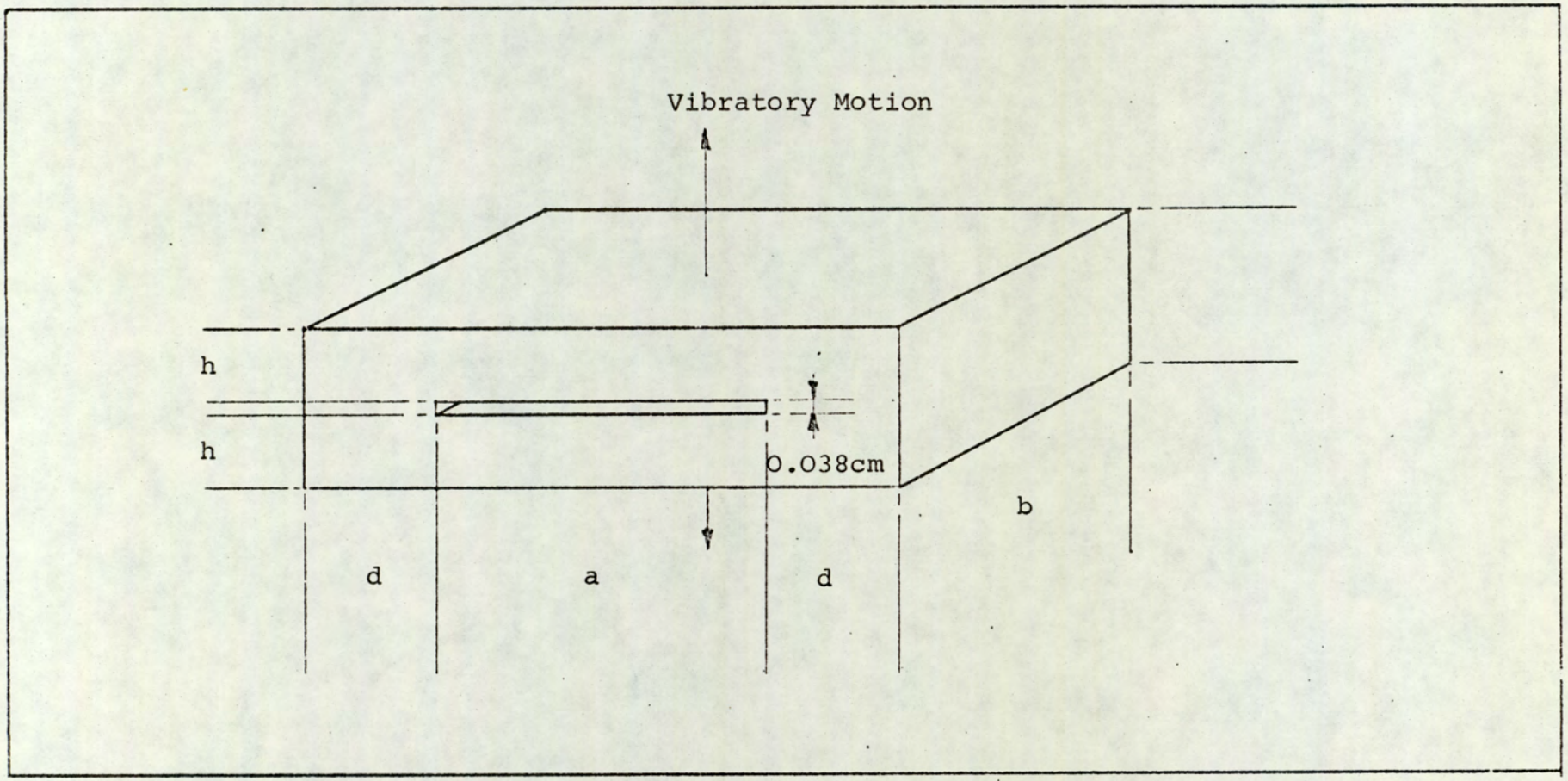

Fig. 7.6 Dynamically clamped (C.F.C.F.) arrangement

or

$$\frac{\omega a\sqrt{12}}{C_p} = \frac{\lambda}{4k} \qquad 7.13$$

where k has the value shown in equation 7.10. The right hand side of equation 7.13 then becomes totally a function of λ, hence the anti-symmetric modes have a maximum only when a/b is constant.

7.3 Dynamically Clamped (C.F.C.F.) Plates

The geometry for the resonator is shown in Figure 7.6. In effect the structure is made up of two tuning forks end to end, for the experiments however, the complete system was machined from the solid. Because of the problems of manufacture, the possiblity of carrying out experiments on the lines just discussed, were not contemplated, therefore experiments were aimed at obtaining practical results to test the usefulness of the equations, obtained in the previous section, when applied to this geometry.

The equations for the tuning fork were obtained by deriving an expression for the experimental curve in Figure 7.3. This was achieved by modifying the theoretical equation to make the two plots coincident. It was found that the required condition could only be met if the curve were translated along both axis, one representing an apparent increase in a/h and the other an apparent decrease in frequency. Two assumptions will be made for the resonator under consideration. Firstly, the relationship between dynamic and static clamping for the

C.F.C.F. plate is the same as for the C.F.F.F. plate (i.e. Figure 7.3). Secondly the apparent increase in a/h is double that of the tuning fork, because of the two clamped boundaries that exist. From the first assumption therefore,

$$\omega = \lambda h C_p / \sqrt{12}\ (a + kh)^2 \qquad 7.14$$

and from the second

$$k = 2(0.373) + 0.164\ \sqrt{\lambda} \qquad 7.15$$

Table 7.5 gives the results of experiments carried out on a mild steel specimen together with calculated results using the above equations for the same dimensions.

Mode	a/b	λ	f(C.F.C.F. plate)	f(exp) KHz	f(theory) KHz
1,1	1.35	22.21	13.51	10.125	10.216
1,2	1.35	29.31	17.83	13.428	13.219
2,1	1.35	61.33	37.32	26.077	25.883
2,2	1.35	71.73	43.65	30.608	29.758
2,3	1.35	122.76	74.7	47.885	47.697

Table 7.5 Comparison of measured frequencies with calculated, from equations 7.14 and 7.15 and equation for C.F.C.F. plate. Plate dimensions h = 0.4 cm, a = 4.046 cm, d = 2.0 cm and C_p = 5420 m/s.

The agreement between results are good, the maximum error

Material	σ	a cm	C_p m/s	1,1 mode		1,2 mode		2,2 mode	
				f KHz	$\omega a\sqrt{12}/C_p$	f KHz	$\omega a\sqrt{12}/C_p$	f KHz	$\omega a\sqrt{12}/C_p$
M/S	0.29	1.143	5,420	21.276	0.977	46.127	2.117	130.983	6.012
Aluminium	0.34	1.27	5,410	18.338	0.937	40.086	2.048	116.718	5.964
Copper	0.34	1.27	3,900	13.339	0.945	29.56	2.095	85.854	6.085

Table 7.5 Experimental results for tuning forks having h=0.616cm and b=1.27cm.

being 3% for the 2,2 mode. Of course the experimental values are likely to be high rather than low, this being one of the characterisitics of the measuring technique, but since the constants of equation 7.15 were evaluated using the same set of experimental conditions the net difference in results, created by this, should be small. The values of the constant themselves may not be optimum, as only more experiments will tell, but the sensitivity of frequency to changes of k show that the values must be reasonably close. For example differentiation of equation 7.1 with respect to k gives

$$\frac{\partial\omega}{\omega} = - \frac{\partial k}{k} \, 2k/(a/h + k) \qquad 7.16$$

Therefore the sensitivity of frequency to changes of k is a function of both k and a/h, which means that the lower modes are least effected. Also as a/h becomes large the sensitivity gets less, which is to be expected, since if the plate is extremely long the type of clamping will be of little consequence, and if extremely thin the clamping will approach that of the static situation. Considering mode 2,3 of table 7.5, which will be the most sensitive to changes of k, the percentage change in ω is given by

$$\frac{\partial\omega}{\omega} = -0.4 \quad \frac{\partial k}{k} \qquad 7.17$$

Hence a 5% change in k will result in a 2% change in ω or

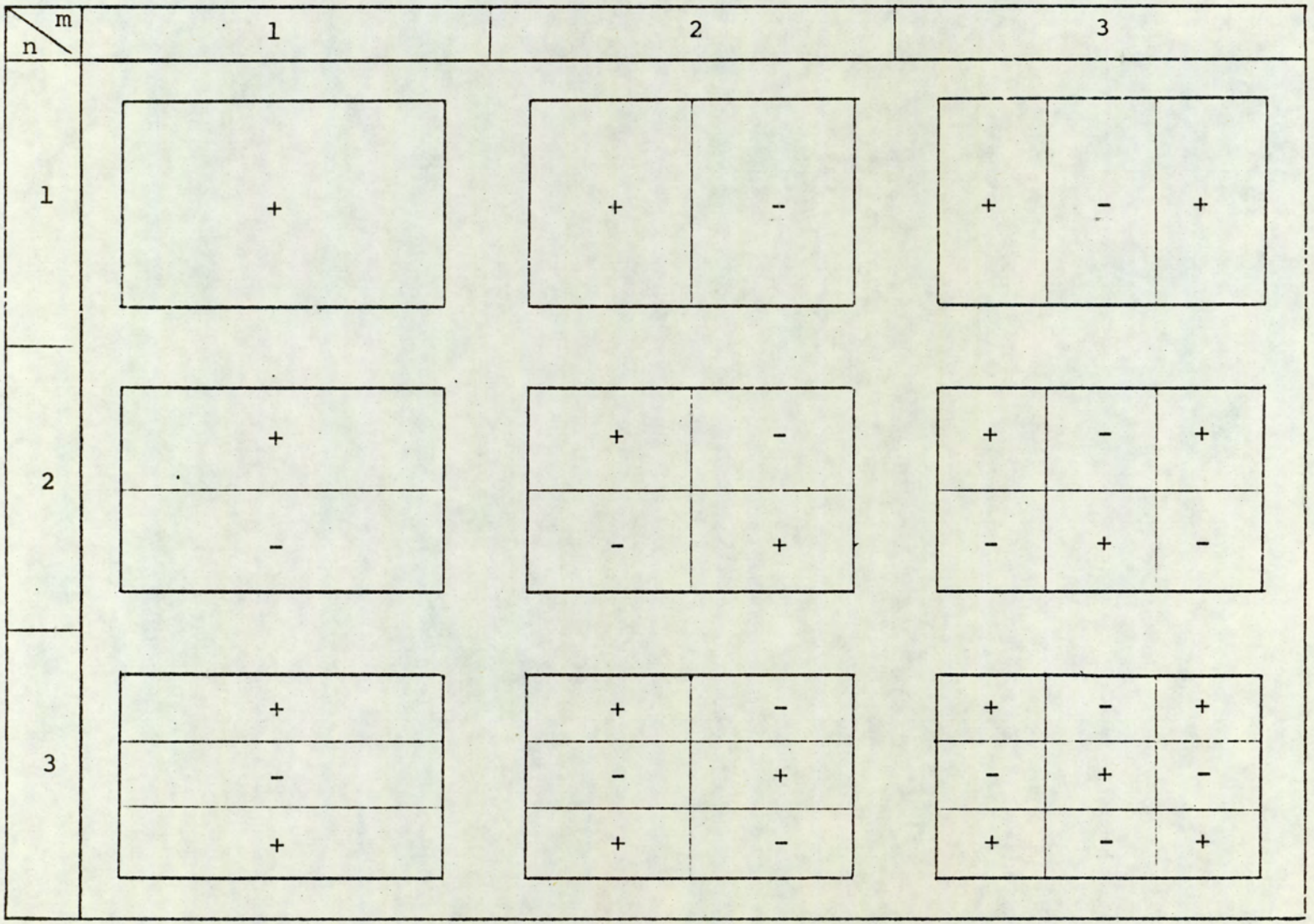

Fig. 7.7 Displacement patterns for m,n modes. Clamped edges are considered to be at the left and right hand sides of each sketch.

0.373 → 0.391

0.164 → 0.172

47.697 → 46.648

Finally, the maximum sensitivity, according to equation 7.16, will occur when a/h = 0, however equation 7.14 is probably only reliable up to the point a/h = k leaving the maximum dependence of ω at

$$\frac{\partial\omega}{\omega} = -\frac{\partial k}{k}$$

Other results relating to experiments of this section are shown in Table 7.6 together with associated calculated results. The significance of the mode numbering i.e. 1,1 and 1,2 etc. is shown in chart form in Figure 7.7.

Mode	a/b	λ	f(C.F.C.F. plate) KHz	f(exp) KHz	f(Theory) KHz
1,1	1.84	22.2	13.53	9.95	10.229
2,1	1.84	61.3	37.3	25.83	25.872
3,1	1.84	120.6	73.38	47.34	46.829
1,2	1.84	34.5	21.00	15.40	15.37
2,2	1.84	79.9	48.62	33.95	32.734
3,2	1.84	142.4	86.65	55.74	53.956
1,3	1.84	96.9	58.96	42.00	38.76
3,3	1.84	214.3	130.39	79.53	75.86

Table 7.6 Measured and calculated frequencies of mild steel specimen h = 0.4 cm, a = 4.046 cm, d = 2.0 cm and C_p = 5420 m/s.

7.4 Comments

The empirical equation derived offers an easy means of obtaining, if not accurate, approximate values for the natural modes of vibration for the structures considered. In terms of percentages the maximum discrepancy between experimental and calculated results was 7.7% for the 1,3 mode table 7.6. The majority of the results showed an error of less than 3%. It is thought that the large errors in the last two modes of table 7.6, i.e. 1,3(7.7%) and 3,3 (4.6%) is due to interpolation of λ between a/b = 2 and 1.67. As already discussed modes posessing nodal lines at right angles to the clamped edges are very sensitive to changes in the ratio a/b, the more nodes the greater the sensitivity as can be seen by the changes of λ for the above two values of a/b.

a/b = 2.0	$\lambda(1,3)$ = 109.2	$\lambda(3,3)$ = 227.6
a/b = 1.67	$\lambda(1,3)$ = 82.5	$\lambda(3,3)$ = 196.9

The range of a/h to which equation 7.9 may be applied will depend mainly upon the mode of vibration, and the accuracy of the computed values of λ. In the upper limit, as the tine approaches the dimensions of a reed, equation 7.9 reduces to that of 7.3, providing $k \ll a/h$. The validity of the equation for small values of a/h is predominantly dependant upon the accuracy of λ. For the modes considered, theory and experiment were found to depart

noticeable for $a/h<k$. This departure is obviously brought about by the limitation of the thin plate theory used to compute the values of λ. In conclusion therefore the lower limit, in the absence of more representative values of λ, must be considered to lie in the region of $a/h \doteq k$.

APPENDICES

APPENDIX A.2.3

Equation 2.20 can be written as

$$C^2_d \nabla\Delta - 2C^2_s \nabla \times \bar{\omega} = \ddot{\bar{u}} \qquad \text{A.1}$$

where ∇ is the vector operator "del". The dilatation Δ is the divergence of the displacement vector $\bar{u}$ written as $\nabla.\bar{u}$. In terms of displacement the rotational vector $\bar{\omega}$ is expressed as half the curl of $\bar{u}$ or in symbolic form as $\frac{1}{2}\nabla \times \bar{u}$. Performing these operations on equation 2.21 gives

$$\nabla.\bar{u} = \nabla.\nabla\phi + \nabla.\nabla \times \bar{H} \qquad \text{A.2}$$

Since $\nabla.\nabla \times \bar{H} = 0$ we have

$$\nabla.\bar{u} = \nabla^2\phi \qquad \text{A.3}$$

also $\frac{1}{2}\nabla \times \bar{u} = \frac{1}{2}\nabla \times \nabla\phi + \frac{1}{2}\nabla \times \nabla \times \bar{H}$

using the fact that $\nabla \times \nabla\phi = 0$ and $\nabla.\bar{H} = 0$.

$$\tfrac{1}{2}\nabla \times \bar{u} = -\tfrac{1}{2}\nabla^2\bar{H} \qquad \text{A.4}$$

Substituting A.3, A.4 and 2.21 in A1 gives

$$\nabla(C^2_d\nabla^2\phi - \ddot{\phi}) + \nabla \times (C^2_s\nabla^2\bar{H} - \ddot{\bar{H}}) = 0 \qquad \text{A.5}$$

This equation is satisfied if each bracketed term vanishes, requiring therefore that

$$C^2_d\nabla^2\phi = \ddot{\phi}$$

and $C^2_s\nabla^2\bar{H} = \ddot{\bar{H}}$

i.e. equations 2.22 and 2.23.

APPENDIX A.2.4

The determinant 2.33 is written as

$$\begin{vmatrix} a_{11} & a_{12} & a_{13} \\ a_{21} & a_{22} & a_{23} \\ a_{31} & a_{32} & a_{33} \end{vmatrix} = 0$$

where

$$a_{11} = (n^2 - 1 - \Omega^2/2 + \gamma^2 a^2) J_n(ha)$$

$$a_{12} = (n^2 - 1 - k^2 a^2) J_n(ka)$$

$$a_{13} = 2(n^2 - 1)(kaJ_{n-1}(ka) - nJ_n(ka)) - k^2 a^2 J_n(ka)$$

$$a_{21} = haJ_{n-1}(ha) - (n + 1) J_n(ha)$$

$$a_{22} = kaJ_{n-1}(ka) - (n + 1) J_n(ka)$$

$$a_{23} = (2n^2 + 2n - k^2 a^2) J_n(ka) - 2kaJ_{n-1}(ka)$$

$$a_{31} = haJ_{n-1}(ha) - nJ_n(ha)$$

$$a_{32} = (1 - (\Omega^2/2\gamma^2 a^2))(kaJ_{n-1}(ka) - nJ_n(ka))$$

$$a_{33} = n^2 J_n(ka)$$

APPENDIX A 3.2

The rotational vector $\bar{\omega}$ is half the curl of the displacement vector $\bar{u}$ or

$$2\,\bar{\omega} = \nabla x \bar{u} \qquad \text{A3.2.1}$$

Expanding the righthand side of this expression gives

$$2\,\bar{\omega} = i\omega_r + j\omega_\theta + k\omega_z$$

where

$$\omega_r = \left(\frac{1}{r}\frac{\partial u_z}{\partial \theta} - \frac{\partial u_\theta}{\partial z}\right)$$

$$\omega_\theta = \left(\frac{\partial u_r}{\partial z} - \frac{\partial u_z}{\partial r}\right)$$

$$\omega_z = \left(\frac{1}{r}\frac{\partial}{\partial r} ru_\theta - \frac{1}{r}\frac{\partial u_r}{\partial \theta}\right)$$

Therefore if $u_r = u_\theta = 0$ and $u_z \neq f(r,\theta)$

$$\bar{\omega} = 0.$$

APPENDIX 5.1.1

MODE / σ	F(2,1)	F(3,1)	F(4,1)	F(5,1)	F(6,1)	F(7,1)	F(8,1)
0.00	2.33618	3.54520	4.57078	5.52881	6.45681	7.36901	8.27184
0.01	2.33667	3.54802	4.57665	5.53756	6.46824	7.38298	8.28823
0.02	2.33710	3.55079	4.58241	5.54623	6.47959	7.39685	8.30451
0.03	2.33755	3.55353	4.58813	5.55481	6.49084	7.41062	8.32069
0.04	2,33799	3.55623	4.59378	5.56331	6.50200	7.42429	8.33675
0.05	2.33845	3.55889	4.59936	5.57172	6.51306	7.43785	8.35271
0.06	2.33887	3.56152	4.60487	5.58005	6.52402	7.45130	8.36855
0.07	2.33930	3.56411	4.61031	5.58829	6.53480	7.46465	8.38428
0.08	2.33973	3.56666	4.61568	5.59644	6.54566	7.47789	8.39988
0.09	2.34015	3.56917	4.62100	5.60451	6.55632	7.49102	8.41537
0.10	2.34056	3.57165	4.62625	5.61249	6.56688	7.50403	8.43074
0.11	2.34097	3.57410	4.63143	5.62038	6.57735	7.51694	8.44598
0.12	2.34138	3.57651	4.63654	5.62818	6.58770	7.52957	8.46109
0.13	2.34178	3.57888	4.64159	5.63590	6.59796	7.54239	8.47608
0.14	2.34217	3.58123	4.64657	5.64353	6.60811	7.55494	8.49094
0.15	2.34257	3.58354	4.65149	5.65108	6.61816	7.56738	8.50566
0.16	2.34295	3.58581	4.65635	5.65853	6.62810	7.57969	8.52026
0.17	2.34334	3.58806	4.66114	5.66590	6.63794	7.59189	8.53472
0.18	2.34371	3.59027	4.66587	5.67318	6.64767	7.60396	8.54905
0.19	2.34409	3.59246	4.67054	5.68038	6.65730	7.61592	8.56324
0.20	2.34446	3.59461	4.67514	5.68749	6.6682	7.62775	8.57730
0.21	2.34482	3.59673	4.67969	5.69451	6.67624	7.63946	8.59122
0.22	2.34519	3.59882	4.68417	5.70145	6.68555	7.65105	8.60501
0.23	2.34554	3.60088	4.68860	5.70831	6.69476	7.66251	8.61865
0.24	2.34590	3.60292	4.69296	5.71508	6.70386	7.67386	8.63216
0.25	2.34625	3.60492	4.69727	5.72176	6.71285	7.68508	8.64553
0.26	2.34659	3.60690	4.70152	5.72837	6.72175	7.69618	8.65876
0.27	2.34694	3.60885	4.70571	5.73489	6.73054	7.70716	8.67186
0.28	2.34727	3.61078	4.70984	5.74132	6.73922	7.71801	8.68481
0.29	2.34761	3.61267	4.71392	5.74781	6.74781	7.72875	8.69763
0.30	2.34794	3.61455	4.71795	5.75629	6.75629	7.73936	8.71031
0.31	2.34827	3.61639	4.72192	5.76015	6.76467	7.74985	8.72285
0.32	2.34859	3.61821	4.72583	5.76627	6.77295	7.76023	8,73525
0.33	2.36892	3.62001	4.72970	5.77231	6.78112	7.77048	8.74752
0.34	2.34925	3.62178	4.73351	5.77827	6.78920	7.78062	8.75965
0.35	2.34955	3.62353	4.73727	5.78416	6.79719	7.79064	8.77165
0.36	2.34986	3.62525	4.74093	5.78997	6.80507	7.80054	8.78351
0.37	2.35017	3.62695	4.74464	5.79570	6.81286	7.81032	8.79523
0.38	2.35047	3.62865	4.74825	5.80137	6.82055	7.81999	8.80683
0.39	2.35077	3.63029	4.75181	5.80695	6.82815	7.82955	8.81829
0.40	2.35107	3.63192	4.75532	5.81247	6.83565	7.83899	8.82962

Table of Ω_c values for a solid rod. $\Omega_c = \omega a / C_s$

APPENDIX 5.1.1

MODE σ	F(2,1)	F(3,1)	F(4,1)	F(5,1)	F(6,1)	F(7,1)	F(8,1)
0.00	2.33620	3.54522	4.57080	5.52883	0.45683	7.36903	8.27186
0.01	2.33665	3.54801	4.57659	5.53749	0.46815	7.38286	8.28809
0.02	2.33710	3.55070	4.58221	5.54591	6.47917	7.39633	8.30389
0.03	2.33753	3.55331	4.58765	5.55408	6.48988	7.40944	8.31930
0.04	2.33794	3.55584	4.59293	5.56202	6.50031	7.42221	8.33431
0.05	2.33835	3.55828	4.59805	5.56974	6.51046	7.43465	8.34894
0.06	2.33874	3.56065	4.60302	5.57725	6.52033	7.44677	8.36320
0.07	2.33912	3.56294	4.60785	5.38456	6.52995	7.45857	8.37711
0.08	2.33949	3.56517	4.61253	5.59164	6.53931	7.47008	8.39067
0.09	2.33985	3.56733	4.31708	5.59854	6.54842	7.48129	8.40389
0.10	2.34020	3.56942	4.62150	5.60525	6.56730	7.49223	8.41679
0.11	2.34054	3.57145	4.62580	5.61179	6.56596	7.50289	8.42938
0.12	2.34087	3.57342	4.62998	5.61815	6.57439	7.51328	8.44165
0.13	2.34120	3.57534	4.63404	5.62435	6.58260	7.52342	8.45364
0.14	2.34151	5.57720	4.63799	5.63038	6.59061	7.53331	8.46533
0.15	2.34182	5.57901	4.64183	5.63626	6.59842	7.54296	8.47675
0.16	2.34211	3.58077	4.64557	5.64198	6.60604	7.55238	8.48789
0.17	2.34240	3.58248	4.64921	5.64756	6.61347	7.56157	8.49878
0.18	2.34269	3.58414	4.65276	5.65300	6.62072	7.57054	8.50941
0.19	2.34296	3.58576	4.65621	5.65830	6.62779	7.57930	8.51970
0.20	2.34323	3.58734	4.65957	5.66348	6.63469	7.58786	8.52994
0.21	2.34349	3.58887	4.66285	5.66852	6.64143	7.59621	8.53985
0.22	2.34375	3.59037	4.66605	5.67344	6.64801	7.60438	8.54954
0.23	2.34400	3.59182	4.66916	5.67825	6.65444	7.81236	8.55901
0.24	2.34424	3.59324	4.67220	5.68294	6.66071	7.62015	8.56827
0.25	2.34448	3.59463	4.67517	5.68751	6.66684	7.62777	8.57732
0.26	2.34471	3.59598	4.67806	5.69198	6.67284	7.63522	8.58618
0.27	2.34494	3.59730	4.68088	5.69635	6.67869	7.64251	8.59484
0.28	2.34516	3.59858	4.68364	5.70061	6.68441	7.64963	8.60331
0.29	2.34538	3.59984	4.68633	5.70478	6.69001	7.65660	8.61161
0.30	2.34559	3.60107	4.68896	5.70886	6.69348	7.66341	8.61977
0.31	2.54581	3.60226	4.69152	5.71284	6.70084	7.67009	8.62766
0.32	2.34601	3.60343	4.69403	5.71673	6.70607	7.67661	8.63544
0.33	2.34621	3.60457	4.69649	5.72054	6.71120	7.68300	8.64305
0.34	2.34640	3.60569	4.69888	5.72426	6.71621	7.68926	8.65061
0.35	2.34659	3.60678	4.70123	5.72790	6.72112	7.69539	8.65781
0.36	2.34678	3.60785	4.70352	5.73147	6.72592	7.70139	8.66497
0.37	2.34696	3.60889	4.70576	5.73496	6.73063	7.70726	8.67198
0.38	2.34714	3.60991	4.70796	5.73837	6.73523	7.71302	8.67885
0.39	2.34732	3.61091	4.71010	5.74172	6.73974	7.71866	8.88558
0.40	2.34749	3.61189	4.71221	5.74499	6.74417	7.72419	8.69218

Table of Ω_D values for disc. $\Omega_D = \omega a/C_s$

BIBLIOGRAPHY

1. L. Pochhammer, "Uber die Fortpflanzungsgeschwindigkeiten Kleiner Schwingungen in Einem Unbegrenzten Isotropen Kreiszylinder", J. Reine Angear. Math. 81, 324-336 (1876).

2. C. Chree, "The Equations of an Isotropic Elastic Solid in Polar and Cylindrical Coordinate, their Solutions and Applications", Trans. Cambridge Phil. Soc. 14, 250-369 (1889).

3. D. Bancroft, "The Velocity of Longitudinal Waves in Cylindrical Bars", Phys. Rev. 59, 588-593 (1941).

4. G. E. Hudson, "Dispersion of Elastic Waves in Solid Cylinders", Phys. Rev. 63, 46-51 (1943).

5. A. N. Holden, "Longitudinal Modes of Elastic Waves in Isotropic Cylinders and Slabs", Bell. Sys. Tech. J. 30, 956-969 (1951).

6. M. Onoe, "A Study of the Branches of the Velocity - Dispersion Equations of Elastic Plates and Rods", Report of Joint Committee on Ultrasonics of the Institute of Electrical Communication Engineers and the Acoustical Society of Japan, (1955).

7. J. Adem, "On the Axially-Symmetric Steady Wave Propagation in Elastic Circular Rods", Quart. Appl. Math. 12, 261-275 (1954).

8. M. Onoe, H. D. McNiven, and R. D. Mindlin, "Dispersion

of Axially Symmetric Waves in Elastic Rods", J. Appl. Mech. 29, 729-734 (1962).

9. J. Zemanek, JR., "An Experimental and Theoretical Investigation of Elastic Wave Propagation in a Cylinder", J.A.S.A. 51, 265-283 (1972).

10. A. E. H. Love, "A Treatise on the Mathematical Theory of Elasticity",(Cambridge Univ. Press. 1927).

11. T. R. Meeker, and A. H. Meitzler, "Guided Wave Propagation in Elongated Cylinders and Plates", in Physical Acoustics, W. P. Mason, Ed. (Academic, New York, 1964) Vol 1.

12. H. N. Abramson, H. J. Plass, and E. A. Ripperger, "Stress Wave Propagation in Rods and Beams", Advances in Applied Mechanics, 5, 111-194 (1958).

13. H. J. McSkimin, "Propagation of Longitudinal Waves and Shear Waves in Cylindrical Rods at High Frequencies", J.A.S.A. 28, 484-494 (1956).

14. R.D. Mindlin, and H. D. McNiven, "Axially Symmetric Waves in Elastic Rods", Trans. of the A.S.M.E. (Series E), 27, 145-151 (1960).

15. J. Zemanek, JR., and I. Rudnick, "Attenuation and Dispersion of Elastic Waves in a Cylindrical Bar", 33, 1283-1288 (1961).

16. C. L. Dym, "Some New Results for the Vibrations of Circular Cylinders", J. of Sound & Vibrations, 29, 189-205 (1973).

17. S. N. Rasband, "Resonant Vibrations of Free Cylinders and Disks", J.A.S.A., 57, 899-905 (1975).

18. R. Kumar, and R. W. B. Stephens, "Dispersion of Flexural Waves in Cylindrical Shells," Proc. R. Soc. Lond. A., 329, 283-297 (1972).

19. H. D. McNiven, "Extensional Waves in a Semi-Infinite Elastic Rod", J.A.S.A., 33, 23-27 (1961).

20. R. K. Kaul, and J. J. McCoy, "Propagation of Axisymmetric Waves in a Circular Semiinfinite Elastic Rod", J.A.S.A. 36, 653-660 (1964).

21. H. Kolsky, "Stress Waves in Solids", (Dover, 1963).

22. I. E. Campbell, and E. M. Sherwood, "High Temperature Materials and Technology", (Wiley, 1967).

23. W. Voigt, Ann. d. phys., 47, 671 (1892).

24. P. M. Morse, and H. Feshbach, "Methods of Theoretical Physics", Part 1 p. 52, (McGraw-Hill, New York, 1953).

25. A. H. Meitzler, "Mode Coupling Occurring in the Propagation of Elastic Pulses in Wires", J.A.S.A., 33, 435-445 (1961).

26. A. H. Meitzler, "Backward-Wave Transmission of Stress Pulses in Elastic Cylinders and Plates", J.A.S.A., 38, 835-842 (1965).

27. H. Lamb, "On Waves in an Elastic Plate", Proc. Roy. Soc. A., 93, 114-128 (1917).

28. A. E. Armenakas, D. C.Gazis, and G. Herrman, "Free Vibrations of Circular Cylindrical Shells", (Pergamon Press Inc. 1969).

29. H. F. Pollard, "Resonant Behaviour of an Acoustic Transmission Line", Austral, J. Phys. 15,513-526 (1962).

30. J. C. K. Sharp, "A Theoretical and Experimental Investigation into the Spectra of Selected Resonators", (Ph.D. Thesis, Department of Electrical Engineering, Univ. of Aston in Birmingham, 1974).

31. J. F. W. Bell, B. P. Doyle, and B. S. Smith, "An Instrument for the Measurement of Acoustic Pulse Velocity and Attenuation in a Solid Probe", J.Sc.Inst., 43, 28 (1966)

32. J. F. W. Bell, "A Solid Acoustic Thermometer", Ultrasonics, 6, 11-14 (1968).

33. K. F. Graff, "Wave Motion in Elastic Solids", (Oxford Univ. Press, 1975).

34. J. M. Pelmore, "Internal Friction and High Temperature Measurements on Refractory Materials", (Ph.D. Thesis Department of Electrical Engineering, Univ. of Aston In Birmingham, 1975).

35. J. C. Snowdon, "Longitudinal Vibrations of Internally Damped Rods", J.A.S.A.,36, 502-510 (1964).

36. J. C. Snowdon, "Response of a Simply Clamped Beam to Vibratory Forces and Moments", J.A.S.A.,36, 495-501 (1964).

37. J. C. Snowdon, "Response of Internally Damped Beams to Sinusoidal Vibration," J.A.S.A., 38,271-281(1965).

38. J. C. Snowdon, "Forced Vibration of Internally Damped Circular Plates with Supported and Free Boundaries", J.A.S.A., 47, 882-891 (1970).

39. E. J. Skudrzyk, "Vibrations of a System with a Finite or an Infinite Number of Resonances", J.A.S.A., 30, 1140-1152 (1958).

40. E. J. Skudrzyk, B. R. Kautz, and D.C. Greene, "Vibration of, and Bending-Wave Propagation in Plates", J.A.S.A. 33, 36-45 (1961).

41. D. A. Thomas, "Characteristics Impedances for Flexure Waves in Thin Plates", J.A.S.A., 30,220-221(1958).

42. R. C. Jones, "The Driving-Point Impedance of an Infinite Solid Plate", J.A.S.A.,17, 334-336 (1946).

43. N. W. McLachlan, "Theory of Vibrations", (Dover Pub.Inc., 1951).

44. J. C. Snowdon, "Vibration and Shock in Damped Mechanical Systems", (WIley & Sons, Inc., 1968).

45. L. E. Kinsler, and A. R. Frey, "Fundamentals of Acoustics", (Wiley & Sons, Inc. 1950).

46. C. R. Wylie, "Advanced Engineering Mathematics", (McGraw Hill, 1951).

47. S. Timoshenko, "Vibration Problems in Engineering ", (Van Nostrand Co., Inc., 1928).

48. N. W. McLachlan, "Bessel Functions for Engineers", (Oxford Univ. Press, 1934).

49. A. W. Leissa, "Vibration of Plates", N.A.S.A. SP-160.

50. J. Oliver, "Elastic Wave Dispersion in a Cylindrical Rod by a Wide-Band Short-Duration Pulse Technique", J.A.S.A., 29, 189-194 (1957).

51. See Reference (19).

52. H. D. McNiven, and D.C. Perry, "Axially Symmetric Waves in Finite, Elastic Rods", J.A.S.A.,34, 433-437, (1962).

53. G. W. McMahon, "Experimetnal Study of the Vibrations of Solid, Isotropic, Elastic Cylinders", J.A.S.A., 36, 85-92, (1964).

54. R. E. Booker and F. H. Sagar, "Velocity Dispersion of the Lowest-Order Longitudinal Mode in Finite Rods of Circular Cross Section", J.A.S.A., 49, 1491-1498 (1971).

55. M. Onoe, "Contour Vibrations of Isotropic Circular Plates," J.A.S.A.,28, 1158-1162 (1956).

56. J. F. W. Bell, and J. C. K. Sharp,"The Precision Measurement of the Elastic Constants of Isotrpoic Solids over Wide Temperature Ranges", Rev.Int.Htes. Temp.et.Refnact,

12, 40-43 (1975).

57. Lord Rayleigh, "On the Free Vibrations of an Infinite Plate of Homogeneous Isotropic Elastic Matter", Proc.Lond.Math.Soc.,20, 225-234 (1889).

58. H. Lamb, "On the Flexure of an Elastic Plate", Proc. Lond.Math.Soc., 21, 85 (1889).

59. R. D. Mindlin, and E.A. Fox, "Vibrations of Waves in Elastic Bars of Rectangular Cross Section", Trans. of the A.S.M.E. (Series E),27, 152-158 (1960).

60. E. A. G. Shaw, "On the Resonant Vibrations of Thick Barium Titanate Disks", J.A.S.A.,28,38-50 (1956).

61. R. D. Mindlin , and M. A. Medick, "Extensional Vibrations of Elastic Plates," Trans. of the A.S.M.E.,26, 561-569 (1959).

62. D. C. Gazis, and R. D. Mindlin, "Extensional Vibrations and Waves in a Circular Disk and a Semi-Infinite Plate", Trans. of the A.S.M.E., 541-547 (1960).

63. M. Onoe, "Contour Vibrations of Thin Rectangular Plates", J.A.S.A., 30, 1159-1162 (1958).

64. P. J. Torvik, "Reflection of Wave Trains in Semi-Infinite Plates", J.A.S.A., 41, 346-353 (1967).

65. O. E. Jones, "Longitudinal Strain Pulse Propagation in Wide Rectangular Bars", Parts 1 and 2, Trans.of the A.S.M.E., 51-69 (1963).

66. W. L. Pilant, "The Propagation of Elastic Waves in Thin Plates", (Ph.D. Thesis, Univ. of Calif. at Los Angeles, Los Angeles 1960).

67. T. N. Seth, "Ultrasonic Pyrometer for Industrial Applications", (Ph.D. Thesis, Department of Electrical Engineering, Univ. of Aston in Birmingham, 1974).

68. A. A. Fathimani, "The Automation of Resonant Thermometer Probe Measurements", (Ph.D. Thesis, Department of Electrical Engineering, Univ of Aston in Birmingham, 1976).

69. A. W. Leissa, "The Free Vibration of Rectangular Plates", J. of Sound & Vib., 31, 257-293 (1973).

70. D. Young, "Vibration of Rectangular Plates by the Ritz Method", J. of Applied Mechanics, 17, 448-453 (1950).